Some Studies on PMUs for Event Detection and Stability in Power Systems

Ph. D. Thesis

AJEET KUMAR SINGH

ID No. 2014REE9044

DEPARTMENT OF ELECTRICAL ENGINEERING

MALAVIYA NATIONAL INSTITUTE OF TECHNOLOGY JAIPUR

July 2019

Some Studies on PMUs for Event Detection and Stability in Power Systems

Submitted in

fulfillment of the requirements for the degree of

Doctor of Philosophy

by

Ajeet Kumar Singh

ID: 2014REE9044

Under the Supervision of

Prof. Manoj Fozdar

DEPARTMENT OF ELECTRICAL ENGINEERING

MALAVIYA NATIONAL INSTITUTE OF TECHNOLOGY JAIPUR

July 2019

Declaration

I, **Ajeet Kumar Singh** declare that this thesis titled, ***"Some Studies on PMUs for Event Detection and Stability in Power Systems"*** and work presented in it, is my own. I confirm that:

- This work was done wholly or mainly while in candidature for a research degree at this university.
- Where any part of this thesis has previously been submitted for a degree or any other qualification at this university or any other institution, this has been clearly stated.
- Where I have consulted the published work of others, this is always clearly attributed.
- Where I have quoted from the work of others, the source is always given. With the exception of such quotations, this thesis is entirely my own work.
- I have acknowledged all main sources of help.
- Where the thesis is based on work done by myself, jointly with others, I have made clear exactly what was done by others and what I have contributed myself.

Date:

Ajeet Kumar Singh

(2014REE9044)

Certificate

This is to certify that the thesis entitled ***"Some Studies on PMUs for Event Detection and Stability in Power Systems"*** being submitted by ***Ajeet Kumar Singh (ID: 2014REE9044)*** is a bonafide research work carried out under my supervision and guidance in fulfillment of the requirement for the award of the degree of **Doctor of Philosophy** in the Department of Electrical Engineering, Malaviya National Institute of Technology Jaipur, India. The matter embodied in this thesis is original and has not been submitted to any other University or Institute for the award of any other degree.

Place:

Date:

Prof. Manoj Fozdar

Department of Electrical Engineering
Malaviya National Institute of Technology Jaipur

Dedicated with

reverence to

my parents

Acknowledgements

It is my pleasure and privilege to appreciate those who have played the larger role in the completion of my thesis with their encouragement and support.

First and foremost, I take this opportunity to express sincere gratitude to my research supervisor, Prof. Manoj Fozdar, for his guidance and support during the progression of this thesis. I am beholden to him for his faith in my capabilities during adversities. He provided me with moral and emotional support when I was going through a rough patch. His rich experience of both research and life shared with me is something I will always treasure. I will cherish his fellowship and remain indebted to him forever.

I would like to thank my DREC members: Prof. Rajesh Kumar, Dr. Nikhil Gupta, and Dr. Kusum Verma for their invaluable comments. Their inputs opened the door to new possibilities and provided guidelines for continuing the work documented in this thesis.

I am also grateful to Prof. Udaykumar R. Yaragatti, Director, MNIT Jaipur, for his unfailing assistance in providing infrastructure and computation facilities required for research. Thanks are also due to Prof. Rajesh Kumar, Head of the Department, and Prof. Harpal Tiwari, Convener, DPGC for extending all possible support to research scholars of the department in pursuing their Ph. D.

A very special gratitude goes out to Dr. Reetu Singh and Dr. Shailendra Pratap Singh for their help and coorporation. Thanks to all institute staff who have associated with me in this quest.

This acknowledgment remains incomplete unless I mention my seniors, friends and fellow research scholars who have supported me along the way. I am grateful to my seniors Dr. Narayanan K. and Dr. Shahbaz Ahmed Siddiqui for proofreading my research articles and their advice on proceeding further. I am obliged to Dr. Manoj Kumawat, Dr. Nand Kishor Meena, Dr. Saurabh Ratra, Mr. Pranda Prasanta Gupta, and Mr. Rayees Ahmad Thokar for creating a delightful and supportive atmosphere. It was great sharing laboratory with all of them for four long years that seem to have passed in the blink of an eye. My heartfelt regards to Mr. Satyendra Singh for taking my academic responsibilities upon himself while I was pursuing this research. With a special mention to Mr. Pradeep Singh, I will always remember the night-long discussions with him on all spheres ranging from technical to social issues. His inquisitiveness and conversance broadened my horizons as well. I will always look at him as a true and dependable friend. I am also grateful to

Mr. Vikram Singh, Dr. Venu Sangwan, Dr. Abhilash Kumar Gupta, Ms. Akanksha Shukla, Ms. Ankita Tripathi, Mr. Sunny Nashier, Mr. Jitender Nashier, and Mr. Vikas Nashier for making my stay in Jaipur feel like home away from home. ad to endure many inconveniences during the course of writing this book. I also express thanks to other research scholars of the department, not mentioned here, for their support in countless ways when this work was in progress. Special thanks to Ms. Anjali Singh, who makes my days brighter.

And finally, last but by no means least, I convey my regards to my parents: because I owe it all to them. Thanks beyond words!

Ajeet Kumar Singh

Abstract

The electrical power system is an enlarging infrastructure with a continuously growing demand for energy. Thus, regional grids are being interconnected for power exchange, and renewable generation is being integrated to serve the load demand. However, the growing intricacy increases the possibility of contingencies and severity of its outcome. Increasing penetration of asynchronous renewable generation decreases the overall inertia of the system, thereby, reducing its resilience to withstand major events. Additionally, the mounting stress on the electric grid due to deregulation further increases its vulnerability to instability. In an integrated power system, an event such as loss of generation or short-circuit fault affects rotor angle separation of generators, bus voltages, and frequency of the system, which can incite a sequence of unpredictable cascading failures subject to the tolerance of the system. Therefore, efficient monitoring and emergency control schemes are necessary for maintaining power system stability.

The operation and control of the power system are being revitalized due to the assimilation of information and communication technology in its real-time monitoring. A situational awareness framework for assessing the performance of the system allows the operators to undertake informed decisions promptly to maintain the system security and integrity. The development of Phasor Measurement Units (PMUs) is the driving force behind the real-time monitoring. PMUs measure various power system parameters such as voltage, current, and frequency, etc. This measurement set, known as *'Synchrophasor measurements'* or simply *'Synchrophasors'* is time-stamped by utilizing Global Positioning System (GPS) satellites which ensure the synchronization accuracy of 1μs. Measurements are taken at a rate of 30-120 samples per second and sent to the Phasor Data Concentrators (PDCs) installed at the central control location. The high temporal resolution of PMUs allows accurate tracking of the changing dynamics of the system which was previously unattainable with the conventional monitoring system of Supervisory Control And Data Acquisition (SCADA). This complete infrastructure comprising of PMUs, communication channels, and data storage for monitoring and control of a large power system has been termed as Wide-Area Monitoring System (WAMS).

The first step in the development of WAMS is the selection of suitable locations in the grid for installation of PMUs. With a huge amount of capital associated with PMU installation, utilities are looking for a suitable placement strategy that minimizes the investment but ensures a complete observability of the system. This work proposes a method for optimal placement of PMUs considering system configuration and its attributes during the planning

phase of PMU deployment. Each bus of the system is assessed on four diverse attributes, and a consolidated *'degree of criticality'* is determined. A modified objective function which incorporates values of the degree of criticality of buses is developed. As budgetary restrictions on utilities may not allow installation PMUs even at optimal locations in a single phase, multi-horizon deployment of PMUs is also addressed. The proposed approach is tested on IEEE 14-bus, IEEE 30-bus, New England (NE) 39-bus, IEEE 57-bus and IEEE 118-bus systems and compared with some existing methods.

Power systems suffer from unforeseen events, e.g., short-circuit faults, generator outage, etc. which endanger its security. Therefore, early detection of events and the information about its location and characteristics is vital to preserve system integrity. The PMU assisted surveillance of power system can render unparalleled insights in the state of the system. Synchrophasor measurements from the installed PMUs are utilized for the automatic diagnosis of power system events. A new index for early detection of events and its geographical localization is proposed. A supervised learning-based event classification module is proposed for real-time identification of the events. The discontinuities generated in voltage and frequency measurements due to events are adequately localized in the wavelet domain. Therefore, the discrete wavelet transform is used for the detection and localization of events. Wavelet transform has been extended to establish coherency of generators by determining the instantaneous phase difference between their rotor angles. The effectiveness of the proposed approach is demonstrated on the NE-39 bus test system.

An event anywhere in the system will influence the power transfer capability of the transmission corridor and confront the stability of the system. The aim of the proposed work is to identify such events at the earliest utilizing supervised learning based classification modules and initiate the suitable emergency control action. The imbalances of active and reactive power in the aftermath of an event have been utilized to predict the stability of the system. A new formulation has been presented for estimation of reactive power imbalance. An event predicted as unstable is counteracted by prompt load-shedding. Conventionally, load-shedding is based on frequency or voltage information independently which reduces the effect of load shedding. In this thesis, a new load-shedding procedure has been proposed considering both active and reactive power available in the system. The proposed scheme is tested on NE-39 bus system and the results of the load-shedding have been compared with two existing load-shedding schemes.

The proposed work is an effective scheme for situational awareness, stability assessment and emergency control of electrical grids. It envisions an intelligent and regenerative grid

capable of enduring significant events efficiently. At the end of the thesis, the future scope of the research work is discussed.

Contents

List of Tables

List of Figures

Abbreviations

PMU	**P**hasor **M**easurement **U**nit
SCADA	**S**upervisory **C**ontrol **A**nd **D**ata **A**cquisition
RTU	**R**emote **T**erminal **U**nits
RMS	**R**oot **M**ean **S**quare
SE	**S**tate **E**stimator
EEC	**E**stimation **E**rror **C**ovariance
WLS	**W**eighted **L**east **S**quare
OPP	**O**ptimal **P**MU **P**lacement
GPS	**G**lobal **P**ositioning **S**ystem
PDC	**P**hasor **D**ata **C**oncentrators
WAMS	**W**ide **A**rea **M**onitoring **S**ystems
FNET	**F**requency Monitoring **NET**work
ROCOF	**R**ate **O**f **C**hange **O**f **F**requency
ILP	**I**nteger **L**inear **P**rogramming
BIP	**B**inary **I**nteger **P**rogramming
SORI	**S**ystem **O**bservability **R**edundancy **I**ndex
BOI	**B**us **O**bservability **I**ndex
TOPSIS	**T**echnique for **O**rder of **P**reference by **S**imilarity to **I**deal **S**olution
MCDM	**M**ulti-**C**riteria **D**ecision **M**aking
NDM	**N**ormalized **D**ecision **M**atrix
CPF	**C**ontinuation **P**ower **F**low
GA	**G**enetic **A**lgorithm
FFT	**F**ast **F**ourier **T**ransform

RR	**R**ecurrence **R**ate
PCA	**P**rincipal **C**omponent **A**nalysis
AI	**A**rtificial **I**ntelligence
ANN	**A**rtificial **N**eural **N**etwork
NN	**N**eural **N**etworks
DT	**D**ecision **T**ree
DSA	**D**ynamic **S**ecurity **A**ssessment
FCT	**F**ault **C**learing **T**ime
UFLS	**U**nder-**F**requency **L**oad **S**hedding
UVLS	**U**nder-**V**oltage **L**oad **S**hedding
API	**A**ctive **P**ower **I**mbalance
RPI	**R**eactive **P**ower **I**mbalance
PSA	**P**redictive **S**tability **A**ssessment
SFR	**S**ystem **F**requency **R**esponse
VAR	**V**olt-**A**mpere **R**eactive
PF	**P**ower **F**actor
FACTS	**F**lexible **A**lternating **C**urrent **T**ransmission **S**ystem
HVDC	**H**igh-**V**oltage **D**irect **C**urrent
FVSI	**F**ast **V**oltage **S**tability **I**ndex
SVC	**S**tatic **V**AR **C**ompensator
STATCOM	**Stat**ic Synchronous **COM**pensator
TVR	**T**ertiary **V**oltage **R**egulators
FCT	**F**ault **C**learing **T**ime
WT	**W**avelet **T**ransform
CWT	**C**ontinous **W**avelet **T**ransform
DWT	**D**iscrete **W**avelet **T**ransform
XWT	Cross **(X)** **W**avelet **T**ransform
VCPI	**V**oltage **C**ollapse **P**roximity **I**ndicator
VID	**V**oltage **I**nstability **D**etection
VSM	**V**oltage **S**tability **M**argin
RPR	**R**eactive **P**ower **R**eserve

AVR	**A**utomatic **V**oltage **R**egulator
VSLBI	**V**oltage **S**tability **L**oad **B**us **I**ndex
MVEE	**M**inimum **V**olume **E**nclosing **E**llipsoid
SVM	**S**upport **V**ector **M**achine
DSVM	**D**endrogram Based **S**upport **V**ector **M**achine
RBF	**R**adial **B**asis **F**unction
STFT	**S**hort-**T**erm **F**ourier **T**ransform
MAD	**M**edian **A**bsolute **D**eviation
WC	**W**avelet **C**oefficients
WCSS	**W**ithin-**C**luster **S**um of **S**quares
COI	**C**enter **O**f **I**nertia
COIn	**C**one **O**f **In**fluence
PDM	**P**hase **D**ifference **M**atrix
CT	**C**urrent **T**ransformers
PT	**P**otential **T**ransformers
SD	**S**tandard **D**eviation
NE	**N**ew **E**ngland
IEEE	**I**nstitute of **E**lectrical and **E**lectronics **E**ngineers
CIGRE	**C**onseil **I**nternational des **G**rands **R**éseaux **É**lectriques
NERC	**N**orth **A**merican **R**eliability **C**orporation
WECC	**W**estern **E**lectricity **C**oordination **C**ouncil

Symbols

$C_{R,i}$	Redundancy Criteria Score
$C_{G,i}$	Generation Bus Criteria Score
$C_{L,i}$	Line Contingency Criteria Score
$C_{Q,i}$	Reactive Power Loss Criterion Score
N_B	Total number of buses
N_G	Total number of generators
N_L	Total number of load buses
A	Binary Connectivity Matrix
Y_{bus}	Bus Admittance Matrix
λ^{max}	Maximum loading limit
Λ^{+}	Ideal solution
Λ^{-}	Negative-ideal solution
Υ_i^*	Degree of Criticality of the i^{th} bus
$x(t)$	Continuous time signal
$\psi_{a,b}$	Mother Wavelet at scale a and position b
$\psi_{m,n}$	Dyadic grid mother wavelet at level m and position n
$\phi_{m,n}$	Scaling function
$T_{m,n}$	Wavelet detail coefficients
$S_{m,n}$	Wavelet approximation coefficients
L	Length of a signal
E	Signal energy
E_m	Signal energy corresponding to details in level m
$R^{(J,l)}[t]$	Proposed index for event detection at t^{th} instant; J $\in \{V, F\}$

ζ_V	Threshold value of the event detection index for voltage
ζ_F	Threshold value of the event detection index for frequency
ϑ^{Fl}	Threshold value of Fault Suspicion Criterion
B^{Fl}	Suspected Fault Bus
D_E	Energy Dispersion
υ_A	Average Frequency
$f_m^{'}$	Pseudo-frequency in m^{th} decomposition level
H_{log}	Log Energy Entropy
p_n	Energy probability distribution of wavelet coefficients
X	Measurement sequence of voltage or frequency
Z_j	Z-score of the j^{th} feature
μ_F	Mean of feature vector
σ_F	Standard deviation of feature vector
α_z	Feature vector
β_z	Predefined class label
w	Vector of coefficients in SVM
b	Bias term in SVM
ξ	Error term in SVM
C	Penalty constant in SVM
K	Kernel function
s	Number of classes
f_c	Frequency at the COI
H_l	Inertia constant of the l^{th} generator
f_l	Frequency of the l^{th} generator
B^{Ev}	Suspected Event Bus
ΔP	Active Power Imbalance
ΔQ	Reactive Power Imbalance
ΔS	Apparent Power Imbalance
f_n	Nominal frequency of the system
$\cos\ \Psi$	Power factor of apparent power imbalance
$\cos\ \phi_l^{L_0}$	Power factor of load at l^{th} load bus

$P_l^{L_0}$	Initial active component of load at l^{th} load bus
$Q_l^{L_0}$	Initial reactive component of load at l^{th} load bus
P^{Shed}	Amount of active power load to shed

Chapter 1

Introduction

The increasing demand for electricity has compelled the utilities to interconnect regional grids together and integrate renewable energy resources to the main grids. Thus, modern power systems are large dynamic systems having many complicated interconnections with adjoining networks. This has made the operation and control of the power system more complex. The intermittency of renewable resources and uncertainties in operating conditions directly affect the dynamics of the power system. Unlike conventional synchronous generators which can resist event-driven frequency oscillations because of their inertia, asynchronous renewable energy generators such as wind, micro/mini hydro, etc. supplement no inertia to the grid. Therefore, increasing penetration of renewables lowers the resilience of the grid to endure major events. Environmental restrictions on power system expansion, market pressure for the cost-efficient supply, enlarging urban infrastructure, and increased power demand; drives the operators to run the power system under stressed conditions leaving narrow margins of stability. Any disturbance under such circumstances can prove to be fatal and cause the system to lose operating equilibrium. Numerous widespread blackouts observed throughout the globe testify that lack of situational awareness and efficient schemes to counteract instability stemming from a disturbance can cause catastrophic failure [1]. These blackouts directly result in socio-economic deprivation. India suffered two such severe power outages on 30^{th} and 31^{st} July 2012 successively. Often considered as the largest power outage in the history, counting the number of people affected, 31^{st} July blackout resulted in loss of about 48,000 MW of load and deprived 620 million Indian residents of electricity [2]. Investigations suggest that both the disturbances were initiated by tripping of a bulk power carrier single circuit transmission line. The heavy active power flow and reactive power loss resulted in low

voltage and high current in the line. This was misinterpreted as a line fault by a distance relay, and it tripped the line on zone-3 of Main-II protection. It proved to be the first in a cascade of dominoes and afterward, numerous lines tripped on load encroachment and power swings, eventually leading to complete collapse of the grid leaving only small islands of generation and load in operation [3].

Some recommendations of the report of the enquiry committee on 2012 Indian blackouts are as under:

1. Deployment of Wide Area Monitoring Systems (WAMS)
2. Intelligent relays to distinguish between load encroachment and faults
3. Exploration of applications of synchrophasor measurements from PMUs for protection systems
4. Improve the visibility and situational awareness of the system
5. Analyse the system behaviour under different network status/tripping of lines/outage of generators.
6. Possibility of voltage collapse prediction

It is observed from these recommendations that situational awareness about various events taking place in the grid and prediction of its consequences is a pressing concern. The necessity of developing more efficient and robust monitoring control schemes to capture even the small deviation of the system from the normal operating state and to develop efficient emergency control schemes is the motivation of the proposed work.

An effective monitoring scheme of the power system is indispensable for its proper operation and control. Conventionally, power system has been monitored using SCADA since the 1970s. SCADA measurement set includes Root Mean Square (RMS) values of power flows, power injections, voltages and line currents which are non-linear functions of system state *viz.* voltage and angle at each bus. These measurements are periodically obtained from Remote Terminal Units (RTUs) installed in substations. These data are then analyzed by a computer program called State Estimator (SE) which estimates the state of the power system. State vector of the power system comprises of voltage magnitude and angle of all busbars in the system. Traditional SEs used iterative Weighted Least Square (WLS) SE technique which utilized first-order Taylor's series expansion to convert non-linear equations into linear form. However, SCADA suffers from low sampling rate

and low accuracy. During fast disturbances, dynamics of the power system change very rapidly in the fraction of a second. Also, the data obtained from SCADA is unsynchronized, and phase angles of busbar voltages are not measured directly. Thus, SCADA is not an effective strategy for real-time monitoring of power system.

The outset of PMUs is a breakthrough in wide area monitoring of electrical power systems. The idea of representing alternating currents and voltages by the mathematical form of phasors was first conceived by Charles Proteus Steinmetz in 1893. Phasors represent amplitude, angular frequency and the initial phase of a sinusoidal function. The invention of PMU is credited to Phadke and Thorp [4] at Virginia Tech., Blacksburg, USA in the early 1980s. A PMU installed at a bus is capable of measuring following parameters:

1. Voltage phasor of that bus,
2. Current phasors of all the lines directly connected to that bus,
3. Local frequency, and
4. Rate Of Change Of Frequency (ROCOF).

PMUs can also be modified to measure harmonics, positive, negative and zero sequence quantities. Their *'Synchrophasor measurements'* or *'Synchrophasors'* directly indicates the state of the system and state estimator associated with PMUs in linear and doesn't require any iteration based solution. These fast and accurate readings enable the operator to track dynamics of the system in real-time. Some potential applications of synchrophasors have been discussed below:

1. Improved situational awareness [5, 6],
2. Optimization of transmission corridor [7, 8],
3. Improved state-estimation [9, 10],
4. Load shedding and other load control techniques such as demand response mechanisms to manage a power system [11, 12],
5. Increase the reliability of the power grid by detecting faults early, allowing isolation of healthy system, and the prevention of power outages [13, 14],
6. Network model validation [15, 16],

7. Monitoring of electromechanical dynamics, such as inertial response [17, 18], and inter-area oscillation [19–21].

However, it is not possible to install a PMU at every bus of the system due to high cost related to PMUs and required infrastructure. Since the voltage at one end of a line and current flowing through it can be measured through PMUs, the voltage at another end of the line can also be calculated by utilizing known line parameters. Thus, a PMU placed at a bus makes that bus, as well as all adjacent buses, observable. Clearly, installation of PMUs at each bus in a power system is not required. Thus, site selection for PMU placement needs to be addressed rationally. The Optimal PMU Placement (OPP) problem revolves around minimizing the number of PMU installed while maintaining the complete observability of the system.

Power blackouts witnessed all over the globe have shown that power systems suffer from unforeseen disturbances or events which endanger its security. Any event, as small as mal-operation of a relay, may lead to cascading collapse of the entire grid. Common events in a power system include unintentional line trips, faults in transmission lines, unintentional load shedding, unintentional generator tripping, unintentional islanding, and a capacitor or reactor outage. Such events may be reflected in adjacent grids as well, which is unacceptable in the era of competitive electricity markets. Several instances of relay mal-operations and hidden failures have been observed and attributed to blackouts in the past. Although relay trip status is transmitted to the control centers, the current monitoring setup lacks the amenities to authenticate operation of relays and other protective devices in real time. An event anywhere in the system will influence the power transfer capability of the transmission corridor and confront the stability of the system. Promptly mitigating such disturbances can prevent the system from probable grid collapse. With aging infrastructure, increasing intricacy of the network and mounting stress on the grid due to deregulation, it will not be possible to rely solely on relays in the near future. An oversight support framework to validate every maneuver of protective devices in the grid, and an efficient plan for emergency control of the power system is indispensable for its appropriate operation and control. Any event in the system will leave a signature response in WAMS. The objective of event analysis is to extract such signatures and map them to their corresponding events.

An event can confront both frequency as well as voltage stability of the system. Frequency instability results in a gradual decline of frequency or sustained frequency swings while voltage instability is identified as the progressive decline of voltage magnitudes in significant parts of the power system. Both instabilities result in load rejection, loss of

transmission lines and even loss of synchronism among alternators [22]. While frequency stability can be easily monitored by measuring the frequency at the *Center of Inertia (COI)* [23], the real-time assessment of voltage stability is a challenging task due to the participation of various equipment such as generators, transmission lines, shunt capacitors, etc. in both reactive power generation and consumption. The estimate of reactive power imbalance in the system is a measure of voltage instability. As the operators run the power system closer to its stability limits for deriving maximum financial profit, it is necessary to develop indices which can forewarn the operator about impending instability. The information of arising instability will allow early activation of remedial measures. Load shedding is an emergency control required to maintain stability of system against critical events. Both deterministic and adaptive load shedding are triggered when either frequency or voltage violates a pre-determined threshold. However, reactive power is generally not considered in load shedding problem. Thus, new avenues can be explored for detecting impending stability and enhanced load shedding considering reactive power.

This thesis is divided into 6 chapters. In Chapter 1, the motivation of this thesis has been discussed and a brief introduction to the research work carried out has been provided.

Chapter 2 provides an insight into the state-of-the-art optimal PMU placement and its applications in wide area monitoring and control of power systems. A detailed literature survey of the existing methods of optimal PMU placement, event detection techniques, stability assessment, and emergency control along with the limitations of these existing methods has been presented.

Chapter 3 discusses the optimal location for PMU installation for complete power system observability. The proposed approach traces the crucial buses in the network and prioritizes them for PMU installation.

Chapter 4 presents a real-time event diagnosis approach for improved situational awareness in power systems using synchrophasor measurements available from PMUs. A new method for detecting and localizing events from real-time PMU measurements has been presented. An event classifier module has been proposed for identifying the event type. The coherent groups of generators are also identified from the rotor angles oscillating after an event.

Chapter 5 proposes a scheme for real-time monitoring and protection of stability of the power system after an unanticipated event that endanger the frequency or voltage stability of the system. A new load shedding formulation is presented considering both active and reactive power imbalances, incorporating constraints of capacitor removal.

In Chapter 6, major contributions, conclusions and future scope of the proposed research work are discussed.

Chapter 2

Literature Survey

Large-scale blackouts in the recent past have stimulated worldwide deployment of PMUs [24]. The installation of PMUs in electric grids can give a quantum leap to standards of wide area monitoring. Unlike traditional SCADA based monitoring, which has a slow scan rate, PMUs capture measurements as fast as one phasor measurement per cycle of the system frequency. This helps the operator to track power system dynamics in real-time. As deployment of PMUs is still in a primitive stage, an extensive scope for research is available in the development of schemes competent of improving situational awareness and emergency control. The prime objective of this research is to harness the benefits of PMUs in power system event detection, predictive instability assessment and mitigation.

In this chapter, state-of-the-art on deployment of PMUs in power system networks and its applications in wide area event detection, stability assessment and emergency control has been discussed.

2.1 Optimal PMU Placement

Optimal locations for PMU installation for complete power system observability has been a topic of research for power system academicians and researchers since PMUs came into existence. It aims at determining the minimum number of PMUs and/or minimizing the investment associated with PMU installation and their locations such that each bus of the network is observed by atleast one PMU or the network is topologically observable. The OPP is inherently an *NP*-complete problem with a solution space of 2^{N_B} potential combinations for an N_B-bus electric power system [25]. Baldwin *et al.* [26] provided the

pioneer solution to OPP problem by implementing a dual search algorithm comprising of a modified bisecting search and simulated annealing. Bisecting search iteratively finds the minimum number of PMUs for complete observability. Later, simulated annealing minimizes the number of unobserved buses keeping the number of PMUs constant. Results concluded that about one-fourth to one-third of the system buses needed to be equipped with PMUs for complete observability. Milosevic *et al.* [27] proposed a non-dominated sorting genetic algorithm for achieving optimal solution to two conflicting objectives simultaneously: minimization of number of PMUs and maximization of measurement redundancy. Bei *et al.* [28], Abbasy *et al.* [29] and Gou [30] proposed an Integer Linear Programming (ILP) framework for OPP solution with and without the presence of conventional measurements and zero-injection buses. Nuqui *et al.* [31] introduced a novel concept of *'depth of unobservability'*. Optimal location of PMUs was found using tree search technique and spanning tree of the power system graph. It further extended the problem to unavailability of communication facilities in the network and phased installation of PMUs. Chakrabarti *et al.* [32] suggested integer quadratic programming for minimizing the number of PMUs and maximizing the measurement redundancy. The proposed PMU configuration was capable of ensuring complete observability of the system even under outage of a single transmission line or a single PMU ($N-1$ contingency). A study on probability of outages of various WAMS components (e.g. transmission lines, communication links, CTs, PTs, PMUs etc.) is performed by Aminifar *et al.* [33, 34]. A *Probability of Observability Index* for each bus and a *System Observability Redundancy Index (SORI)* are proposed and used in selection of best solution among multiple solutions with same installation cost resulting from ILP solution in [34]. In [33] average probability of observability is maximized in each horizon of multi-horizon establishment of PMUs. Selection of best solution from multiple ILP solutions based on minimization of state Estimation Error Covariance (EEC) is proposed by Tai *et al.* [35]. Theodorakatos *et al.* [36] used quadratic programming approach with non-linear constraints and proved that it gives same number of PMUs as the Binary Integer Programming (BIP) method. Chakrabarti *et al.* [37] utilized a binary exhaustive search for determining minimum number of PMUs considering single branch outages. A methodology for selecting best solution from the set of final solution was also proposed. Dua *et al.* [38] advocated a two stage 'master-slave' ILP. Stage 1 finds the minimum number of PMUs while Stage 2 detects the best solution on the basis of two formulated indices, *Bus Observability Index (BOI)* and *System Observability Redundancy Index (SORI)*. BOI of a bus is the number of PMUs observing it, and SORI is the sum of all BOI for the system in the given PMU configuration. Stage 1 provides multiple solutions with same cost for optimal PMU placement. Thereafter, in Stage 2, the solution set which maximizes

SORI is selected as the best PMU configuration. Optimal multistage deployment of PMUs using ILP approach is also reported in [33], [39], [40] and [41]. Gou [42] and Esmaili *et al.* [43] formulated ILP and mixed-integer linear programming respectively for optimal PMU placement incorporating already installed conventional power flows and injection measurements. Roy *et al.* [44] and Alvarez [45] proposed a heuristic approach for optimal site selection. An ILP based PMU installation method for complete observability even in case of controlled island of the system is presented by Huang *et al.* [46]. Quantification of benefits of deploying PMUs against capital investment is done in [47]. A pragmatic approach to placement of PMUs with limited number of channels is presented in [48], [49] and [50]. However, these all methods were only focused on minimizing the number of PMUs and failed to take dynamics of power system into account. There may be some buses or lines which are crucial and heavily govern transient or dynamic stability of the power system depending upon system configuration. Such buses should be kept under constant supervision of a PMU directly as failure to monitor such buses can lead to catastrophic results. Sodhi *et al.* [51] proposed an ILP approach including voltage stability based contingency ranking of buses. Thukaram *et al.* [52] suggested critical buses on the basis of transient stability analysis for PMU placement. Gomez *et al.* [53] identified critical buses/area based on inter-area and intra-area oscillations. Placement of more PMUs at bus with higher sensitivity of node voltage with respect to line parameters to effectively monitor disturbances is proposed in [54]. A multi-criteria selection on critical buses is also available in [39], [41] and [55]. Other techniques employed in solution of OPP problem include iterated local search [56], quadratic minimization subject to non-linear observability constraints [57], binary particle swarm optimization [58], Tabu search [59], recursive Tabu search [60], non-dominated sorting differential algorithm [61], fuzzified artificial bee colony algorithm [62], greedy algorithm [63].

2.2 Event Detection and Localization

Real-time detection of events can enable the operator to initiate appropriate remedial actions and preserve the integrity of the system. Large imbalance between power demand and supply generate frequency variations around the rated value. Thus, it is straightforward to visually detect large, and sudden imbalances in generation and load by monitoring frequency; however, information related to events such as transmission line reclosing and trips and other equipment trips is not readily available. But, such events leave their signature in PMU data which can be extracted and much research is devoted to this feature extraction. North American Reliability Corporation (NERC) published standards based

on magnitude of voltage, frequency, and ROCOF for detection of events in Western Electricity Coordination Council (WECC) system [64]. However, studies have reported that only few events have been recorded by these standards [14]. Some more responsive techniques based on the divergence of the voltage in the moving window and the estimation of power spectral density to screen PMU data for possible events are proposed in [65]. However, their performance is system dependent and susceptible to the threshold values selected. An energy function of cumulative magnetic and potential energy contained in loads, transmission lines, and generators is proposed for detection of events in [66]. It has been demonstrated that energy functions of loads, transmission lines and generator are sensitive to corresponding disturbances. However, it requires dynamic internal state of generators which are directly immeasurable and need the implementation of complex filters for their estimation. The backward difference derivatives of voltage and frequency are applied for the detection of events in [67, 68]. However, these criteria are vulnerable to false triggering whenever measurements are polluted with noise. If the input signal is constant or steadily varying but corrupted by high-frequency noise, the entire value of its derivative is of variation of noise. The computation of derivatives over longer time frames can overcome their susceptivity to incorrect triggering. However, the derivatives calculated upon longer periods may omit an event particularly if it occurs between the two extremities of the frame [69]. Other signal processing methods deployed for event detection are Principal Component Analysis (PCA) [70], Wavelet transform [71, 72], and Kalman filtering [73].

The variance is considered a more reliable indicator of events than the rate of change. Event detection by observing the size of the error ellipsoid between the variances of frequencies measured at two distant locations, along their first principal component is proposed in [74]. The method has certain limitations, primarily for coherent buses where frequencies hold a tendency to swing together even after the disturbances. The detection and location of events through the variance of rotor speed of one representative machine from all coherent set of generators is proposed in [75,76]. However, the coherency of the generators is varying *i.e.* a set of generators oscillating together after a contingency may not necessarily oscillate together for different contingency. Also, squaring the difference from the mean value of the frequency in the measurement window to calculate the variance eliminates positive and negative values and hence hinder in classifying events as frequency rise or dip. Therefore, this approach offers limited applications. A multidimensional Minimum Volume Enclosing Ellipsoid (MVEE) which accommodates a stream of PMU measurements is proposed for detection of events in [71] and coupled with multiclass Decision Tree classifier in [77] for their real-time classification. The geometrical attributes of MVEE such as size, change

in size, and center are used in the feature vector as input to the classifier. However, the number of features is significantly high and hence, the classifier requires extensive training data set following the *'curse of dimensionality'*.

The information of the location of disturbances allows activating corrective schemes e.g. load shedding, actuation of reactive power reserves, and controlled islanding. Any significant event in the power system triggers perturbations in frequencies which traverse the entire grid as electromechanical waves at a measurable speed [78]. Majority of contemporary monitoring setup exploit these perturbations to localize events in terrestrial boundaries. A wide area frequency based event location using Internet Based Frequency Monitoring Network (FNET) is proposed by Tao [79]. The frequency disturbance recorders dispersed in the network determine *'wave-front arrival time'* at different locations [80]. The product of the propagation time of the wave and the speed of the wave is then applied to trace the locus of disturbance. This method is based on the underlying assumption that the wave propagation speed is invariable. However, practically the wave propagation speed shows a significant variation in the range 100 to 1000 miles/sec. depending upon network configuration and surrounding conditions [81]. An additional discrepancy between actual location and determined location is generated due to the inconsistency between geographic distance and electrical distance.

2.3 Frequency and Voltage Stability Assessment

Power transfer capability of a system is restricted by rotor angle stability as well as thermal loading limits of the transmission line [82]. However, expanding infrastructure, increasing load demands, change in energy portfolio, increased penetration of renewable energy resources etc. are prime factors which force utilities to operate power systems under stressed conditions making it more vulnerable to instability. In this thesis, event-driven frequency and voltage stability have been discussed. Frequency instability is an outcome of imbalance between active power generation and active load demand. Voltage instability is caused by insufficient generation of reactive power by reactive power resources and/or incompetence of transmission lines to transfer reactive power to the load bus. Events like element outages (transmission line tripping, generator outage, capacitor outage etc.) can propel the system towards both frequency and/or voltage instability. Frequency instability is conventionally monitored using ROCOF at the COI. However, real-time voltage stability assessment is more complex because of non-linear nature of power system which becomes more and more noticeable when stress on the system is increased [83]. Several indices have been proposed

for assessment and anticipation of voltage stability. The conventional P-V and Q-V curves are extensively used as a tool to study voltage stability and for determination of maximum permissible loading. To generate these curves, large numbers of repetitive load-flow solutions are required. Thus, these methods are time consuming, computationally inefficient and not fit for real-time assessment. Also, Jacobian of the Newton-Raphson load flow becomes singular at steady state voltage stability limit (Bifurcation Point) and getting a convergence becomes improbable. In such situations, Continuation Power Flow (CPF) formulated by Ajjarapu and Christy [84] is used. Several other methods such as modal analysis [85], L-index [86], bifurcation theory [87], energy function methods [88], Fast Voltage Stability Index (FVSI) [89], Voltage Collapse Proximity Indicator (VCPI) [90], etc., have been proposed in the literature. The uniqueness of static voltage stability irrespective of the adopted technique is proved in [91]. Static indices such as L-index [86], extended L-index [92], Voltage Collapse Proximity Index (VCPI) [90] and L_{mn} [93] are suitable for long-term (e.g. slow load increase) voltage stability assessment. Such indices fail to convergence to their limiting values in large-disturbance voltage instability. Similarly, indices based on static load flow methods lose their efficacy when used in the dynamic analysis because of interaction between several control actions such as generator excitation limits and prime mover controls. Furthermore, these indices do not provide explicit information about the deficiency of reactive power following an event. The reactive power deficit has been calculated by assuming the power factor of generation and total load to be equal in [94]; which is generally not correct as other sources also contribute to generating reactive power. The amount of reactive power reserve (RPR) available from generators, synchronous condensers and static VAR compensators can be used as a signal of system stress. Bruno and Ajjarapu [95] developed a multi-linear regression model to establish a relationship between RPR and Voltage Stability Margin (VSM). It was observed that relationship between RPR and VSM can be linear or quadratic subject to operating range.

Machine learning and data mining are emerging tools in dynamic security assessment (DSA) of power systems. Computer based algorithms are trained offline through experimental data, simulation, or knowledge of the system operator and deployed in control center for online monitoring. These can be trained with any logical power system attribute such as active/reactive power flow, voltage magnitude, phase angles etc. For their effective performance, they need to be trained with as much data and scenarios as possible. Such algorithms are called Artificial Intelligence (AI) techniques. Measurements collected from PMUs dispersed throughout the network are gathered at a central location where system voltage security assessment is performed by AI techniques. Kamalasadan *et al.* [96] postulated application of Artificial Neural Network (ANN). Feed forward neural network

is trained with real power, reactive power and voltage phasor of all generator and load buses. Output vector of the neural network is L-index values for all buses for normal and contingent cases. Being fast and devoid of complex mathematical calculations, Decision Trees (DTs) are an adequate choice for machine learning based applications. Prompt response by DTs gives ample time to operators to take preventive action in case system is adjudged to be insecure. Khatib *et al.* [97] correlated voltage security and reactive power flow in transmission lines and bus angle difference and use them as attributes to train DTs. Diao *et al.* [98, 99] advocated DTs for online voltage security monitoring. Past operating condition data was collected and used to forecast operating condition data for the next 24 hours. Voltage security analysis was performed on the forecasted data and DT is trained for the next day. On the following day, DT is updated on hourly basis to incorporate newly predicted operating conditions. A supervised learning based method using bus voltages as input features for determining the probability of generators hitting their over-excitation limits is presented in [100] for voltage stability monitoring.

Voltage instability is coupled with combined maximum power transfer capability of transmission and generation systems. Therefore, significant amount of literature focusing on maximum power transfer condition or impedance matching is available. Real-time identification of Thevenin's parameters based on synchrophasor measurements are proposed in [101–104]. Using similar approach, a new index namely Voltage Stability Load Bus Index (VSLBI), defined as the ratio of load bus voltage and voltage across transmission impedance, is proposed by Milosevic [105]. Thevenin's parameters were calculated using a sliding window of discrete data samples by using a parameter identification algorithm such as Least Square or the Recursive Least Square. Although, voltage instability is characterized by low voltages in considerable part of power system, voltage magnitude is a poor indicator of voltage instability [106], [107]. Hence, protection system based on monitoring of merely bus voltage magnitude is ineffective. Vu *et al.* proposed estimation of Thevenin's equivalent of generation and transmission systems as seen by a load bus using recursive least-square identification method on continuous local measurements for Voltage Instability Detection (VID). However, load power-factor and non-linear nature of power system was ignored. A similar approach is presented by Julian *et al.* [108] with proximity to maximum load expressed in terms of power margin. Vournas and Cutsem [109] proposed a voltage stability index using Tellegen's theorem and adjoint networks for local voltage stability monitoring. A new index for voltage stability margin by measuring rate of change of apparent power with respect to load admittance (dS/dY) considering load power factor is presented in [107], [110]. As a power system reaches in the proximity of voltage collapse, reactive power transferred to the load starts decreasing because transmission lines itself

become a reactive power consumer. Based on this approach, Verbic and Gubina [111] proposed S Difference Criterion by measuring time derivative of apparent power at the receiving end of the transmission line. However, an adequate emergency control should assure both frequency and voltage stability following an event. Also, most of the existing stability indices lack anticipation. Therefore, there is a need to develop schemes which can predict the stability of the system after an event.

2.4 Emergency Control: Load Shedding

Preventive actions must be taken forthwith after the system is found to be insecure. Under-Frequency Load Shedding (UFLS) and Under-Voltage Load Shedding (UVLS) are most extensively exercised countermeasures to sustain the stable operation. These methods are activated when frequency or voltage violates a predefined threshold. UFLS sheds fixed quantum of the load from predefined locations, irrespective of the magnitude and nature of the event which may have an adverse impact on voltage [112]. Similarly, UVLS is a local operation and does not necessarily restore the frequency. Both schemes operate autonomously, and are inefficient in administering combined instability [94] as voltage/M-VAR and angle/MW problems are inseparable for a system operating at its physical limits [113]. Moreover, both UFLS and UVLS are inadequate for maintaining rotor angle stability, which necessitates immediate remedial action.

Adaptive UFLS has been proposed to overcome the deterministic nature of UFLS in [23, 114]. A heuristic method for optimal load shedding which restores frequency and also minimizes frequency overshoot/undershoot is presented in [115]. A discrete load shedding scheme based on ROCOF for self-healing is presented in [116]. However, these extended methods still are only frequency dependent. An adaptive UFLS at load buses after an event is presented in [117, 118]. It is a unified approach against frequency and voltage instability by calculating disturbance power from ROCOF. Buses were ranked according to voltage dips at respective buses and higher ranked buses were selected for load curtailment. However, it requires parameters to violate a pre-determined system-specific threshold and hence can be initiated only after a time delay. A similar approach based on the selection of the load shedding location by the magnitude of bus voltages and their static voltage stability VQ margins is presented in [119]. However, it doesn't consider the contribution of reactive power injected by controllable resources. A unified load shedding plan based on frequency and a local voltage stability index using Thevenin equivalent of the system as seen from the load bus is proposed in [120]. The method is unsuitable for dynamic

voltage stability analysis as *(i)* Thevenin equivalent is only an approximate model of the network and does not indicate rapid changes in the system states; *(ii)* for the estimation of Thevenin equivalent, voltage and impedance must remain constant over the measurement window. A scheme that prioritizes buses for load shedding on basis of ROCOF and rate of change of voltage is suggested in [121]. The minimization of total load shedding cost for maintaining transient stability is performed in [122]. Leonardi *et al.* [8] determined sensitivity of RPR with respect to each of active power generation, shunt compensation and active and reactive load shedding. A convex quadratic objective function comprising of weighted sum of squares of each control action to determine minimum amount of control required is formulated. It is subjected to minimum RPR, minimum VSM, voltage limits at buses, constant power factor and load shedding constraints.

2.5 Critical Review

Widespread blackouts experienced throughout the globe in the recent past, testify that there is still a dearth of proficient schemes for situational awareness and emergency control in the power system. Optimally installed PMUs in the network can enable enhanced real-time assessment of power system dynamics. However, most of the existing methods focus exclusively on minimizing the number of PMUs to ensure topological observability. This results in a random distribution of PMUs across the grid. However, the PMUs installed at critical locations can provide vital information of the system health at the remote control center [52]. Therefore, a suitable strategy should be devised for selection for optimal locations for PMU installation considering criticality of buses. Additionally, OPP has a non-unique solution, *i.e.*, it offers multiple solutions with the same number of PMUs. Hence, methods for selecting the best alternative among these optimal solutions, taking into consideration different criteria, have to be developed. The average overall cost per PMU (cost for procurement, installation, and commissioning) ranged from $40,000 to $180,000 (2014) [123]. Therefore, most of the utilities can't install PMUs at all buses (or even at optimal locations) in a single time horizon. Thus, a suitable approach for multi-horizon deployment of PMUs needs to be developed. The synchrophasor measurements obtained from PMUs can be utilized in event analysis for increased situational awareness.

The proliferation of PMUs coupled with data mining and signal processing techniques provide a potential solution to the identification of events and predict its consequences. A comprehensive scheme which identifies events and is also able to find its location can serve as a supervisory framework for events occurring in the power system. The developed

scheme should be capable of classifying the type of event and quantify the magnitude of the event in real-time also, so that effective control measures can be devised to limit the consequence of disturbances.

Traditionally, the power system has been monitored through static stability indices. However, deregulation, increased penetration of distributed generation and the growing number of interconnections have mounted stress on the power system. Thus, with increasing complexity, it is necessary to develop faster approaches to anticipate instability from the initial response of the system to an event. It is found from the literature survey, that most of the voltage stability assessment approaches are only suitable for static analysis as they fail to reach their expected values in dynamic scenarios. Further, they do not provide explicit information about the deficiency of reactive power following an event. Additionally, critical events also pose a threat to frequency stability. However, a combined study of voltage and frequency stability is limited. Therefore, there is a need to evolve predictive methods to recognize impending frequency and voltage instability accurately.

An event generally perturbs the equilibrium of both active and reactive power in an operating power system. However, reactive power is generally not considered in load shedding, which leads to improper load shedding distribution. Hence, adaptive load shedding schemes need to be developed based on the knowledge of both active and reactive power deficits caused by an event. Shunt capacitors may also be installed in the grid for reactive power support. After load shedding, the capacitor output should also be adjusted in accordance with the newer load schedule; otherwise, overvoltages are observed in the system. Hence, capacitor regulation must be considered along with load shedding.

2.6 Research Objectives Attempted

In the light of literature survey, problems associated with the existing methods of PMU placement, event analysis and its impact on stability and emergency control are identified and the research objectives for the present work are framed as follows:

1. To develop an effective scheme for optimal PMU placement taking dynamics of the system into consideration.
2. To develop a suitable strategy for multistage deployment of PMUs.
3. To analyze different power system events and implement analytics for detecting and locating events through PMU data.

4. To develop a suitable scheme for early detection of imminent frequency and voltage instability under critical events using wide-area synchrophasor measurements.

5. To device suitable plan of action for prompt load shedding considering the balance of both active and reactive powers.

In this chapter, a detailed literature survey of the existing methods of optimal PMU placement, event detection techniques, stability assessment, and emergency control along with the limitations of these existing methods has been presented.

In the next chapter, the optimal placement of PMUs considering critical buses has been presented and compared with some existing schemes.

Chapter 3

Strategic PMU Placement

3.1 Introduction

The outset of PMUs was a breakthrough in the surveillance of electrical power systems. A PMU installed at a bus measures its voltage phasor, frequency, ROCOF and current phasors of all transmission lines connected to it [4]. Since voltage phasor at one end of the line and current flowing through it are known; the voltage at another end of the line can be estimated by utilizing line parameters. Thus, a PMU observes the bus where it is installed and all adjacent buses. Apparently, PMUs located optimally in the system can make the system completely observable. The Optimal PMU Placement (OPP) problem is concerned about minimizing the number of PMUs required while preserving the complete observability of the system.

As discussed in Chapter 2, many optimization algorithms have been suggested in the literature for finding the optimal locations for PMU placement for complete power system observability. Most of these methods aim to achieve topological observability only. However, a severe situation may be encountered because of instability stemming from vulnerable buses such as angle instability at generators or voltage instability arising at reactive power deficit buses, etc. Therefore, it is essential to monitor these buses using PMUs continuously. This chapter recommends a strategic planning before PMU deployment. A comprehensive investigation of system topology is conducted, and each placement site is evaluated by quantifying four attributes; namely, redundancy of measurements, rotor angle and frequency monitoring of generator buses, reactive power deficiency, and maximum loading limit under line outage contingency. An overall score of criticality of the bus and, subsequently its rank is evaluated through the Technique for Order of Preference by

Similarity to Ideal Solution (TOPSIS). In this method, Euclidean Distance of all the alternatives from the theoretical ideal and the theoretical negative ideal solution is computed, and relative proximity of a particular alternative to the ideal solution is taken as a measure of criticality of a bus. Buses with higher *'degree of criticality'* are provided greater weight in the problem formulation. The problem is expressed in binary integer programming model as the maximization of aggregate criticality of the entire network. The resultant PMU configuration covers more critical buses with the same number of PMUs as proposed in the available literature [37], [45], and [124]. This further eliminates the issue of the non-unique solution generated by conventional ILP.

3.2 Proposed Optimal PMU Placement Problem Formulation

Any plausible contingency, including, but not limited to, line outage, generator outage can lead to the instability in the system. The voltage, and frequency of the buses and rotor angles of machines can be severely disturbed if not taken care of timely. Under such conditions, an adequate monitoring scheme must be available to track down the cause of the stemming instability and report it to the operator for timely initiation of the corrective measures if the need arises. The PMUs installed at critical locations can provide vital information of the system health at the remote control center. In the present work, four attributes are utilized for quantifying the severity of each candidate bus in the network. The considered attributes are: *(a)* redundancy of measurements, *(b)* rotor angle and frequency monitoring of generator buses, *(c)* reactive power deficiency, and *(d)* maximum loading limit under line outage contingency. Each bus is scored on these attributes and a consolidated degree of criticality is computed employing TOPSIS. Finally, buses are prioritized on the basis of the criticality for potential locations for PMU installation.

3.2.1 Evaluation of the Attributes at Each Bus

The four attributes considered in the present work are evaluated for each bus, and a composite score is calculated to adjudge its suitability for PMU placement. The buses having better scores for all the attributes are considered to be better locations for PMU installation. The four attributes and their assessment are demonstrated below:

1. **Increased Redundancy of Measurements**

   In any power system, several buses have a higher number of connections to other adjacent buses. Such buses are a better choice for PMU installation as they increase redundancy which is essential for the determination of the unique system state and bad data detection [124]. For instance, a PMU installed at a radial bus observes two buses exclusively. However, a PMU placed at a bus directly connected to a radial bus, monitors more than two buses and, consequently, is a better site for PMU installation. In this work, connectivity of the buses to their adjacent buses is used to prioritize them, and each bus is scored equal to the number of lines emerging from that bus. Thus, a Redundancy Criteria Score ($C_{R,i}$) is calculated for the i^{th} bus in an N_B-bus system as follows:

$$C_{R,i} = \sum_{j=1}^{N_B} A_{ij} - 1 \tag{3.1}$$

   where A is a graph theory based binary connectivity matrix as explained below [28].

$$A_{i,j} = \begin{cases} 1 & \text{if } i = j \\ 1 & \text{if bus } i \text{ and bus } j \text{ are directly connected} \\ 0 & \text{otherwise} \end{cases} \tag{3.2}$$

2. **Rotor Angle and Frequency Monitoring of Generator Buses**

   Angular stability and frequency stability issues can stem from any generator outage followed by the loss of synchronism among generators resulting in a cascading black-out. Moreover, the reactances of the generator change from their effective values during the transient state following a disturbance, which introduces an inconsistency between the rotor angle of the alternator and its terminal voltage angle. A PMU installed at a generator bus produces fast and accurate measurements which facilitate the estimation of rotor angle of the generator [125]. Thus considering these issues, it is suggested that all generator buses are suitable locations for keeping under constant supervision of a PMU. Therefore, a Generation Bus Criteria Score ($C_{G,i}$) is calculated for the i^{th} bus in an N_B-bus system as follows:

$$C_{G,i} = \begin{cases} 1 & \text{if } i^{th} \text{ bus is a generator bus} \\ 0 & \text{otherwise} \end{cases} \tag{3.3}$$

All generator buses have been scored equally to keep the computation simple. However, generator buses may also be scored in accordance with their generation capacity, the inertia of connected generator, load demand served, participation in damping low-frequency oscillations and so forth.

3. **Maximum Loading Limit under Line Outage Contingency**
   A transmission line outage can push the system towards instability. For a secure operation of the system, the operator must ensure that system can supply the present load for each possible line outage contingency; a condition acknowledged as $N-1$ contingency stability criterion. In the proposed work, CPF [84] is utilized to assess maximum loading limit λ^{max} under the impact of each line outage contingency. If contingency evaluation results in $\lambda^{max} < 1$, where 1 signifies the current loading level, then stable operation under such a line outage is not possible. Hence, the installation of PMU on buses connecting such lines is paramount. Therefore, a Line Contingency Criteria Score ($C_{L,i}$) is expressed for the i^{th} bus in an N_B-bus system as follows:

$$C_{L,i} = min\left[\lambda_{i-j}^{max} \times \Gamma\right];\ j = 1, 2, ...N_B,\ j \neq i \tag{3.4}$$

$$\Gamma = \begin{cases} 1 & \text{if } i^{th} \text{ and } j^{th} \text{ bus are connected} \\ 0 & \text{otherwise} \end{cases} \tag{3.5}$$

   where $\lambda_{i-j}^{\max}$ is the maximum loadability limit in case of the outage of transmission line connecting i^{th} and j^{th} bus.

4. **Reactive Power Deficiency**
   Although voltage stability is correlated to load dynamics [82], transmission and generation systems play significant roles. Voltage instability originates when loads attempt to withdraw power beyond the combined transfer capability of transmission and generation [126]. In a modern power system, it mostly results from an insufficient generation of reactive power, the incompetence of transmission lines to deliver required reactive power to the load bus, or both. Hence, buses with reactive power deficiency are a viable option for monitoring using a PMU. The method proposed in [127] is used to determine deficit or surplus reactive power available at all load buses. Every bus is assigned score equal to reactive power deficiency at that bus, the procedure for determining the reactive power deficiency at each bus is summarized as follows:

   Step 1: For a power system with N_G generator and N_L load buses, arrange steady

state generator bus current injection I_G and load bus current injection I_L equations as follows:

$$[I_G] = [Y_{GG}][V_G] + [Y_{GL}][V_L] \tag{3.6}$$

$$[I_L] = [Y_{LG}][V_G] + [Y_{LL}][V_L] \tag{3.7}$$

where $[Y_{GG}]$, $[Y_{GL}]$, $[Y_{LG}]$ and $[Y_{LL}]$ are submatrices of reshuffled bus admittance matrix Y_{bus}.

Step 2: Each generator is modeled as equivalent shunt admittance $Y_{G,j}$ as follows:

$$Y_{G,j} = \frac{1}{V_{G,j}}\left(-\frac{S_{G,j}}{V_{G,j}}\right)^* \tag{3.8}$$

where $S_{G,j}$ and $V_{G,j}$ are apparent power and bus voltage of j^{th} generator respectively. Equivalent shunt admittances of each generator are added to corresponding diagonal elements of bus admittance matrix which is repartitioned as in Step 1 to obtain $[Y'_{GG}]$, $[Y'_{GL}]$, $[Y'_{LG}]$ and $[Y'_{LL}]$.

Step 3: Following (3.6), voltages of generator buses are formulated as a linear function of voltages of load buses as follows:

$$[V_G] = -[Y'_{GG}]^{-1}[Y_{GL}][V_L] = [Y^B_{GL}][V_L] \tag{3.9}$$

Step 4: Eliminating V_L from (3.6) using (3.7) and substituting V_G from (3.9), generator bus injection current can be expressed as:

$$[I_G] = -\left([Y_{GG}] - \frac{[Y_{GL}][Y_{LG}]}{[Y_{LL}]}\right)[Y^B_{GL}][V_L] + \frac{[Y_{GL}]}{[Y_{LL}]}[I_L] \tag{3.10}$$

Step 5: V_G, V_L, and I_L are modified to form diagonal matrices. The reactive power contribution of all generators can be formulated as:

$$[Q_{gen}]_{G\times L} = \Im\left([V_G]_{G\times G}\,[I_G]^*_{G\times L}\right) \tag{3.11}$$

$$= \Im\left([V_G]_{G\times G}\left(-\left([Y_{GG}] - \frac{[Y_{GL}][Y_{LG}]}{[Y_{LL}]}\right)[Y^B_{GL}][V_L]_{L\times L} + \frac{[Y_{GL}]}{[Y_{LL}]}[I_L]_{L\times L}\right)\right)^* \tag{3.12}$$

TABLE 3.1: Decision matrix

Bus No.	Criterion Score of i^{th} bus			
i	$C_{R,i}$	$C_{G,i}$	$C_{L,i}$	$C_{Q,i}$
1	M_{11}	M_{12}	M_{13}	M_{14}
2	M_{21}	M_{22}	M_{23}	M_{24}
:	:	:	:	:
N_B	M_{N_B1}	M_{N_B2}	M_{N_B3}	M_{N_B4}

STEP 6: The reactive power loss assigned to each load bus i can be estimated as:

$$Q_{loss,i} = \sum_{j=1}^{N_G} Q_{gen(j,i)} - Q_{L,i} \tag{3.13}$$

where $Q_{L,i}$ is the reactive power load demand at i^{th} bus. Finally, the Reactive Power Loss Criterion Score ($C_{Q,i}$) can be computed for the i^{th} bus as follows:

$$C_{Q,i} = \begin{cases} Q_{loss,i} & \text{if } Q_{loss,i} > 0 \\ 0 & \text{otherwise} \end{cases} \tag{3.14}$$

Buses having surplus reactive power are not considered for PMU installation and, hence, assigned zero score.

3.2.2 Quantification of the Consolidated Degree of Criticality of Buses

Multiple criteria scores evaluated in the preceding section are incommensurable. In this work, TOPSIS is used to process these numerical values. TOPSIS is a Multi-Criteria Decision Making (MCDM) approach applied to select the best alternative when dealing with manifold, and usually, contradictory criteria. It is based on the notion that the accepted alternative should have the minimum Euclidean distance to the ideal solution, and the maximum Euclidean distance to the negative-ideal solution [128]. The steps for implementing TOPSIS are summarized as follows:

STEP 1: A decision matrix is constructed comprising of the scores of four attributes of each bus as shown in Table 3.1.

STEP 2: The decision matrix is normalized to transform diverse attribute dimensions into dimensionless numerals. Each element r_{ij} of the Normalized Decision Matrix (NDM)

is calculated by dividing individual score in the decision matrix by l^2-norm of all the scores in a particular attribute, as stated below:

$$r_{ij} = \frac{M_{ij}}{\sqrt{\sum_{i=1}^{N_B} M_{ij}^2}} \tag{3.15}$$

where $j \in \{1, 2, 3, 4\}$ for an N_B-bus power system.

Step 3: As utilities can have varied hierarchy of priorities among the four attributes, a set of weights $W = (w_1, w_2, w_3, w_4)$ as decided by the utility is incorporated in the decision matrix to form the weighted normalized decision matrix ν. Each element of ν is defined as follows:

$$v_{ij} = w_j * r_{ij} \tag{3.16}$$

A weighted normalized decision matrix substantiates the preferences of the decision maker on various criteria. This work considers $w_1 = w_2 = w_3 = w_4 = 1$. However, other suitable values may also be selected without the loss of generality.

Step 4: Next, ideal (Λ^+) and (Λ^-) negative-ideal solutions are decided. The ideal solution is a hypothetical solution containing the best value for each attribute while the negative-ideal is a hypothetical solution comprising of worst value of each attribute among all alternatives.

$$\Lambda^+ = \left\{ \left(\max v_{ij} | \, j \in J\right), \left(\min v_{ij} | \, j \in J'\right), i \in 1, 2...N_B \right\} \tag{3.17}$$

$$\Lambda^- = \left\{ \left(\min v_{ij} | \, j \in J\right), \left(\max v_{ij} | \, j \in J'\right), i \in 1, 2...N_B \right\} \tag{3.18}$$

where J is related to criteria to be maximized and J' is related with criteria to be minimized. In a power system, buses with higher redundancy score ($C_{R,i}$), availability of generator ($C_{G,i}$), higher reactive power loss ($C_{Q,i}$), but lower maximum loading limit under $N-1$ contingency ($C_{L,i}$), should be preferred for installing PMUs. Accordingly,

$$\begin{aligned} \Lambda^+ &= \{\max(v_{i1}), \ \max(v_{i2}), \ \min(v_{i3}), \ \max(v_{i4})\}, \quad i \in 1, 2...N_B \\ &= \{v_1^+, \ v_2^+, \ v_3^+, \ v_4^+\} \end{aligned} \tag{3.19}$$

and

$$\begin{aligned} \Lambda^- &= \{\min(v_{i1}), \ \min(v_{i2}), \ \max(v_{i3}), \ \min(v_{i4})\}, \quad i \in 1, 2...N_B \\ &= \{v_1^-, \ v_2^-, \ v_3^-, \ v_4^-\} \end{aligned} \tag{3.20}$$

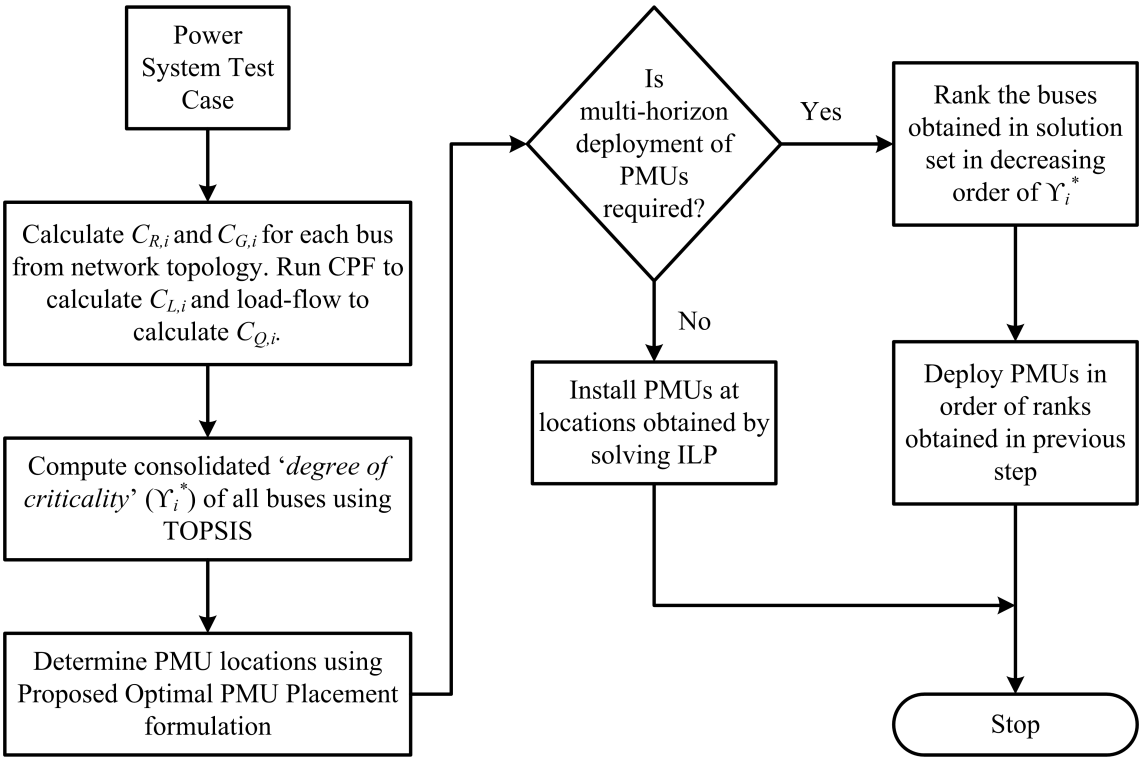

FIGURE 3.1: Flowchart of the proposed optimal PMU placment formulation

STEP 5: In this step, Euclidean Distance from each alternative to the ideal solution and the negative-ideal solution is determined.

$$S_i^+ = \sqrt{\sum_{j=1}^{4} (v_{ij} - v_j^+)^2}, \quad i = 1, 2..N_B \tag{3.21}$$

$$S_i^- = \sqrt{\sum_{j=1}^{4} (v_{ij} - v_j^-)^2}, \quad i = 1, 2..N_B \tag{3.22}$$

STEP 6: Finally, the relative proximity of an alternative to the ideal solution Λ^+ is determined as follows:

$$\Upsilon_i^* = \frac{S_i^-}{S_i^+ + S_i^-}, \quad i = 1, 2...N_B \tag{3.23}$$

where $0 \leq \Upsilon_i^* \leq 1, \forall\, i$ is a consolidated degree of criticality of the i^{th} bus. The bus with the highest value of Υ_i^* has minimum Euclidean distance to the ideal solution and maximum Euclidean distance to the non-ideal solution. Buses arranged in decreasing order of Υ_i^* indicate the most suitable and least suitable alternative, respectively, for PMU installation. The flowchart of the complete proposed methodology is shown in Fig. 3.1.

3.2.3 Optimal PMU Placement Problem Formulation Considering Degree of Criticality

The objective of the proposed scheme is to minimize the total number of PMUs in the system while ensuring complete power system observability such that most of the PMUs remain concentrated at critical buses. For an N_B-bus power system, the problem is formulated as integer linear programming with binary decision variables as follows:

$$\min \sum_{i=1}^{N_B} (1 - \Upsilon_i^*)\, x_i \tag{3.24}$$

subject to the following constraints of connectivity of buses:

$$A.[x_1 \;\; x_2 \;\; . \;\; . \;\; x_{N_B} \;]^T \geq 1 \tag{3.25}$$

where A is the binary connectivity matrix defined in Section 3.2.1 and $x_i \in \{0, 1\}\,,\ \forall\ i$ is the PMU placement variable defined as:

$$x_i = \begin{cases} 1 & \text{if PMU is installed at } i^{th} \text{ bus} \\ 0 & \text{if PMU is not installed at } i^{th} \text{ bus} \end{cases} \tag{3.26}$$

Minimizing $\sum_{i=1}^{N_B} (1 - \Upsilon_i^*)$ is equivalent to maximizing the total sum of the degree of criticality in the network. Connectivity constraints in (3.25) guarantee that at least one PMU observes every bus in the network. A higher redundancy also can be achieved, such as at least 2 PMUs observe each bus, by substituting 2 in the right-hand side of (3.25).

3.3 Simulation and Results

The effectiveness of the proposed methodology is examined on IEEE 14-bus, 30-bus, NE 39-bus, 57-bus and 118-bus test systems. The single line diagrams and elaborate system data for each of these networks is available in [129,130]. For more realistic results a distributed slack bus model [131] was utilized, and all the generators contributed equally to the system power losses. The reactive power loss ($Q_{loss,i}$) at each load bus are determined at peak loaded condition retaining a spinning reserve of 10 %.

TABLE 3.2: Decision matrix of IEEE 14-bus system

Bus No. i	Criterion Score of i^{th} bus				Degree of Criticality
	$C_{R,i}$	$C_{G,i}$	$C_{L,i}$	$C_{Q,i}$	Υ_i^*
1	2	1	0.9955	0	0.4212
2	4	1	0.9955	0	0.4423
3	2	0	1.3024	0	0.0885
4	5	0	1.5980	0.2020	0.2820
5	4	0	1.3081	0.9255	0.5832
6	4	0	1.3081	0	0.1856
7	3	0	1.5038	0.1587	0.1838
8	1	0	1.6929	0	0.0092
9	4	0	1.5038	0.0487	0.1887
10	2	0	1.7507	0.0163	0.0680
11	2	0	1.7507	0	0.0661
12	2	0	1.7582	0	0.0661
13	3	0	1.6758	0	0.1259
14	2	0	1.6632	0.0306	0.0726

TABLE 3.3: Optimal location of PMUs for IEEE 14 bus system

No. of PMUs Required	PMU Locations	PMU Installation %
4	2, 6, 7, 9	28.57 %

3.3.1 Test results of the proposed method on IEEE-14 bus test system

IEEE 14-bus is a small network consisting of 20 transmission lines, 2 alternators connected to buses 1, 2, whereas 3 synchronous condensers are installed at buses 3, 6, 8, and a shunt capacitor connected to bus 9. The decision matrix obtained for this system is presented in Table 3.2. The transmission line connecting buses 1-2 transfers 63.79% of the total load demand under peak loading condition. $N-1$ Contingency analysis using CPF shows that maximum loading limit ($\lambda^{\max}$) drops below 1 in the event of line 1-2 outage, indicating instability of the system under the given contingency. Hence, both buses 1 and 2 have $C_{L,i} = \lambda_{1-2}^{\max} = 0.9955$. An ample number of generators in this system provide abundant reactive power reserves and allow sufficient voltage control capability. As buses 11, 12, 13 are lightly loaded; there is surplus reactive power available at these buses additionally. Hence, buses 1, 2, 3, 6, 8, 11, 12, and 13 have $C_{Q,i} = 0$ as given in (3.14). It can be observed from the table, that the buses numbered 1, 2, 4, 5, 6, 7 and 9 have a high consolidated score of criticality as compared to other buses indicating potential PMU placement sites. Table 3.3 shows the optimal location and minimum number of PMUs required for complete observability of the system. PMU installation percentage which denotes ratio between the number of PMUs and the number of system buses is also calculated. As evident from the

table, 4 PMUs located at buses 2, 6, 7 and 9 are required for complete observability of the system. However, as utilities prefer the installation of PMUs in a multi-horizon manner in a large system due to financial limitations, therefore the bus in the obtained solution set with a highest degree of criticality (Υ_i^*) in the decision matrix must be equipped with the PMU first and so on. As observed from Table 3.2, for multi-horizon PMU placement, bus 2 is to be installed with PMU first, followed by bus 9, 6 and 7.

TABLE 3.4: Decision matrix for IEEE-30 bus system

Bus No. i	Criterion Score of i^{th} bus				Degree of Criticality
	$C_{R,i}$	$C_{G,i}$	$C_{L,i}$	$C_{Q,i}$	Υ_i^*
1	2	1	0.9211	0	0.4403
2	4	1	0.9211	0	0.4558
3	2	0	1.2358	0.8560	0.5275
4	4	0	1.2438	0.4949	0.3926
5	2	0	1.1407	0	0.0649
6	7	0	1.3915	0	0.2429
7	2	0	1.3925	0	0.0516
8	2	0	1.5018	0	0.0492
9	3	0	1.4099	0.1114	0.1342
10	6	0	1.4099	0.0027	0.2110
11	1	0	1.4810	0	0.0068
12	5	0	1.2932	0.0066	0.1774
13	1	0	1.4740	0	0.0076
14	2	0	1.5381	0.0123	0.0504
15	4	0	1.5036	0.0175	0.1384
16	2	0	1.5367	0.0072	0.0495
17	2	0	1.5416	0.0223	0.0529
18	2	0	1.5371	0.0082	0.0497
19	2	0	1.5320	0.0267	0.0543
20	2	0	1.5144	0.0058	0.0495
21	2	0	1.5233	0.0488	0.0644
22	3	0	1.5307	0	0.0944
23	2	0	1.5334	0.0089	0.0498
24	3	0	1.5307	0.0262	0.0980
25	3	0	0.6845	0	0.1267
26	1	0	0.6845	0.0135	0.0903
27	4	0	1.2639	0.0000	0.1392
28	3	0	1.2639	0	0.0987
29	2	0	1.4913	0.0084	0.0500
30	2	0	1.4567	0.0403	0.0608

TABLE 3.5: Optimal location of PMUs for IEEE 30 bus system

No. of PMUs Required	PMU Location	PMU Installation %
10	2, 3, 6, 9, 10, 12, 15, 19, 25, 27	30 %

3.3.2 Test results of the proposed method on IEEE-30 bus test system

IEEE 30-bus consists of 41 transmission lines, 2 alternators connected to buses 1, 2 whereas 4 synchronous condensers are installed at buses 5, 8, 11 and 13. The shunt capacitors are connected to bus 10 and 14. Decision matrix obtained for this system is presented in Table 3.4. The transmission line connecting buses 1-2 is a bulk power carrier line, individually transferring 64.73 % of the total load demand under peak loading condition. $N-1$ Contingency analysis using CPF reveals that maximum loading limit ($\lambda^{\max}$) drops below 1 in the event of line 1-2 outage, indicating that stable operation under this contingency is not possible. Hence, both buses 1 and 2 have $C_{L,i} = \lambda^{\max}_{1-2} = 0.9211$. The buses 6, 9, 11, 13, 22, 25, 27 and 28 do not have any load connected to them while bus 7 has surplus reactive power available. Therefore, buses 1, 2, 5, 6, 7, 8, 9, 11, 13, 22, 25, 27 and 28 have $C_{Q,i} = 0$ as given in (3.14).

Table 3.5 shows the minimum number of PMUs required for complete observability and their optimal locations. It can be observed that only 30 % of the total buses require PMUs installation and PMUs located at buses 2, 3, 6, 9, 10, 12, 15, 19, 25 and 27 completely observe the system.

3.3.3 Test results of the proposed method on NE 39-bus, IEEE 57-bus, and IEEE 118-bus test systems

The proposed methodology is tested further on NE 39-bus, IEEE 57-bus, and IEEE 118-bus networks to validate its efficacy. The decision matrices associated with these systems are presented in Table 3.6, Table 3.7 and Table 3.8 respectively. Simulation results for the minimum number of PMUs and their optimal locations are summarized in Table 3.9 and compared with 3 existing techniques proposed in [37], [45], and [124]. Table 3.9 shows the number of PMUs reported by the proposed method is consistent with other methods; however, a difference in optimal locations can be observed. Large networks can have a significant number of alternative PMU configurations which allow complete observability with the same number of PMUs. Most of the methods proposed earlier rely on the selection of PMU configuration which maximizes the redundancy in the system. The proposed method selects the configuration which has more PMUs on critical buses.

TABLE 3.6: Decision matrix for NE-39 bus system

Bus No. i	Criterion Score of i^{th} bus				Degree of Criticality
	$C_{R,i}$	$C_{G,i}$	$C_{L,i}$	$C_{Q,i}$	Υ_i^*
1	2	0	1.2213	0	0.0731
2	4	0	0	0	0.2898
3	3	0	1.1259	0.6761	0.2428
4	3	0	1.1259	1.5185	0.4355
5	3	0	1.1763	0	0.1388
6	4	0	0	0	0.2898
7	2	0	1.0989	2.7662	0.6128
8	3	0	1.0846	1.7594	0.4873
9	2	0	1.0846	0	0.0811
10	3	0	0	0	0.2635
11	3	0	1.1428	0	0.1398
12	2	0	1.2455	0.1592	0.0875
13	3	0	1.1966	0	0.1383
14	3	0	1.1824	0	0.1386
15	2	0	1.1084	0.9157	0.2728
16	5	0	0.3458	0.7181	0.3717
17	3	0	1.2258	0	0.1378
18	2	0	1.2308	0.3824	0.1338
19	3	0	0	0	0.2635
20	2	0	0	0.9406	0.3678
21	2	0	1.192	0.5565	0.1778
22	3	0	0	0	0.2635
23	3	0	0	0	0.2635
24	2	0	1.2323	0.6044	0.1892
25	3	0	0	0	0.2635
26	4	0	1.222	0.2734	0.2165
27	2	0	1.222	0.7	0.2139
28	2	0	1.2335	0.3383	0.1235
29	3	0	0	0	0.2635
30	1	1	0	0	0.3571
31	1	1	0	0	0.3571
32	1	1	0	0	0.3571
33	1	1	0	0	0.3571

34	1	1	0	0	0.3571
35	1	1	0	0	0.3571
36	1	1	0	0	0.3571
37	1	1	0	0	0.3571
38	1	1	0	0	0.3571
39	2	1	1.1297	0	0.3086

It can be observed from the table, that inclusion of the degree of criticality in the objective function by the proposed technique causes more critical buses to be directly observed by the PMUs. Table 3.9 shows that certain PMU locations are common among the proposed method and other methods. However, the advantage of the proposed method can be observed in dissimilar PMU locations. The proposed methodology proposes buses 11, 32, 33, 37 as suitable buses for PMU placement in NE-39 bus system. Bus 11 offers high redundancy $C_{R,11} = 3$ (only two other buses 6 and 16 have greater redundancy ($C_{R,6} = C_{R,16} = 4$) than bus 11). Similarly, buses 32, 33 and 37 are generator buses and monitoring such buses directly is essential as loss of generator at any of these buses will instigate power imbalance and risk the stability of the system. Similarly in IEEE 118 bus system, buses 10, 36, 87 and 91 in the solution set are generator buses, bus 30 is a high redundancy bus $C_{R,30} = 4$ and buses 44 and 47 are reactive power deficit and undergo rapid voltage decline on load increase. Thus, the solution set obtained using the proposed approach encompasses more critical buses than other methods. As the number of PMUs is increased to achieve higher redundancy of measurements, the proposed approach concentrates even more PMUs on critical buses, which shows the effectiveness of the presented scheme.

Table 3.7: Decision matrix for IEEE-57 bus system

Bus No. i	Criterion Score of i^{th} bus				Degree of Criticality
	$C_{R,i}$	$C_{G,i}$	$C_{L,i}$	$C_{Q,i}$	Υ_i^*
1	4	1	1.4723	0	0.3457
2	2	0	1.4723	0	0.0409
3	3	1	1.5558	0	0.3399
4	4	0	1.5558	0	0.1091
5	2	0	1.6286	0	0.0388
6	4	0	1.5475	0	0.1092
7	3	0	1.1128	0.7821	0.6483
8	3	1	1.0951	0	0.3421

9	6	0	1.0951	0	0.1738
10	3	0	1.5665	0	0.0753
11	4	0	1.6093	0	0.1089
12	5	1	1.5706	0	0.3519
13	6	0	1.5706	0	0.1698
14	3	0	1.5654	0.0091	0.0765
15	5	0	1.4921	0	0.1409
16	2	0	1.6013	0.0604	0.0768
17	2	0	1.5807	0.1558	0.1724
18	2	0	1.6241	0.0355	0.0552
19	2	0	1.6316	0.0064	0.0396
20	2	0	1.6388	0.0053	0.0394
21	2	0	1.641	0	0.0388
22	3	0	1.5536	0	0.0754
23	2	0	1.5536	0.0131	0.0422
24	3	0	1.5452	0	0.0754
25	2	0	1.0268	0.0194	0.065
26	2	0	1.5895	0	0.039
27	2	0	1.4902	0.0123	0.043
28	2	0	1.3934	0.0056	0.0439
29	3	0	1.1128	0.0144	0.0869
30	2	0	1.0268	0.0163	0.0639
31	2	0	1.3698	0.0303	0.0556
32	3	0	1.057	0.0078	0.0875
33	1	0	1.057	0.0186	0.0501
34	2	0	1.0643	0	0.0586
35	2	0	0	0.0171	0.1265
36	3	0	0	0	0.1369
37	3	0	1.1907	0	0.0822
38	5	0	1.1907	0.0304	0.1504
39	2	0	1.6357	0	0.0388
40	2	0	1.6402	0	0.0388
41	4	0	1.6084	0.0124	0.1108
42	2	0	1.6084	0.0221	0.0461
43	2	0	1.6093	0.0019	0.039
44	2	0	1.5839	0.0189	0.0445

45	2	0	1.5839	0	0.039
46	2	0	1.565	0	0.0392
47	2	0	1.565	0.0566	0.0735
48	3	0	1.6162	0	0.0751
49	4	0	1.5923	0.0344	0.1172
50	2	0	1.625	0.0405	0.0592
51	2	0	1.5665	0.0167	0.0436
52	2	0	1.3697	0.0071	0.045
53	2	0	1.5843	0.0301	0.0514
54	2	0	1.6089	0.0045	0.0393
55	2	0	1.4193	0	0.0424
56	4	0	1.6325	0.0225	0.1131
57	2	0	1.6357	0.0218	0.0459

TABLE 3.8: Decision matrix for IEEE-118 bus system

Bus No. i	Criterion Score of i^{th} bus				Degree of Criticality
	$C_{R,i}$	$C_{G,i}$	$C_{L,i}$	$C_{Q,i}$	Υ_i^*
1	2	0	2.0725	0	0.0289
2	2	0	2.0801	0	0.0288
3	3	0	2.042	0	0.0564
4	2	0	1.996	0	0.0295
5	5	0	1.2722	0.5632	0.1384
6	2	0	2.0785	0	0.0288
7	2	0	2.1142	0	0.0288
8	3	0	0.3428	0	0.1012
9	2	0	0	0.8475	0.1525
10	1	1	0	0	0.2218
11	4	0	2.0463	0	0.0825
12	7	1	0	0	0.2587
13	2	0	2.0463	0	0.029
14	2	0	2.1207	0	0.0288
15	5	0	2.0583	0	0.1074
16	2	0	2.1044	0	0.0288
17	6	0	1.99	0	0.1312
18	2	0	2.0715	0	0.0289

19	4	0	2.1162	0	0.0824
20	2	0	2.098	0	0.0288
21	2	0	2.0705	0.0146	0.029
22	2	0	2.0399	0.0084	0.0291
23	4	0	2.0399	0.9276	0.1463
24	3	0	2.0728	0	0.0563
25	3	1	2.0441	0	0.2122
26	2	1	1.9421	0	0.208
27	4	0	2.0441	0	0.0825
28	2	0	2.1128	0	0.0288
29	2	0	2.1164	0	0.0288
30	4	0	1.9421	0.9699	0.151
31	3	1	2.1102	0	0.2121
32	5	0	2.0765	0	0.1074
33	2	0	2.1109	0	0.0288
34	4	0	2.0666	0	0.0825
35	2	0	2.1147	0	0.0288
36	2	0	2.1167	0	0.0288
37	6	0	1.6571	0	0.1328
38	3	0	1.6571	0	0.0607
39	2	0	2.0882	0	0.0288
40	4	0	2.0882	0	0.0824
41	2	0	2.1073	0	0.0288
42	3	0	2.0209	0	0.0565
43	2	0	2.0666	0.0075	0.0289
44	2	0	2.0684	0.0197	0.0291
45	3	0	2.0436	0	0.0564
46	3	1	2.0436	0	0.2122
47	3	0	2.0992	2.6059	0.3351
48	2	0	2.1091	0	0.0288
49	9	1	2.0209	0	0.268
50	2	0	2.1138	0	0.0288
51	3	0	2.1082	0	0.0562
52	2	0	2.1172	0.0164	0.0289
53	2	0	2.1096	0	0.0288
54	5	1	2.1096	0	0.2262

55	3	0	2.1101	0	0.0562
56	5	0	2.113	0	0.1073
57	2	0	2.1181	0	0.0288
58	2	0	2.1176	0	0.0288
59	6	1	2.0142	0	0.2355
60	3	0	2.1124	0	0.0562
61	4	1	2.1075	0	0.2183
62	4	0	2.1182	0	0.0824
63	2	0	2.0089	0	0.0293
64	3	0	1.9113	0	0.0572
65	4	1	1.6589	0	0.2195
66	4	1	2.0783	0	0.2184
67	2	0	2.1186	0.0245	0.029
68	4	0	0	7.2118	0.7646
69	6	1	1.9059	0	0.2358
70	5	0	1.9754	0	0.1076
71	3	0	0.0001	0	0.1139
72	2	0	2.1113	0	0.0288
73	1	0	0.0001	0	0.101
74	2	0	2.0954	0	0.0288
75	5	0	1.5824	3.0883	0.4076
76	2	0	1.7845	0	0.0335
77	6	0	1.7845	0	0.132
78	2	0	2.1187	0	0.0288
79	2	0	2.1169	0	0.0288
80	7	1	2.1056	0	0.2456
81	2	0	2.1034	0	0.0288
82	3	0	2.1188	0	0.0562
83	3	0	2.1184	0	0.0562
84	2	0	2.1184	0	0.0288
85	5	0	0.3421	0	0.1339
86	2	0	0	0	0.1047
87	1	1	0	0	0.2218
88	2	0	2.1159	0.1359	0.0339
89	4	1	2.0821	0	0.2184
90	2	0	2.1194	0	0.0288

91	2	0	2.119	0	0.0288
92	6	0	2.0821	0	0.131
93	2	0	2.1185	0	0.0288
94	5	0	2.1184	0.1815	0.1115
95	2	0	2.1184	0.054	0.0297
96	5	0	2.1192	0	0.1073
97	2	0	2.1195	0	0.0288
98	2	0	2.1131	0.004	0.0288
99	2	0	2.1184	0	0.0288
100	8	1	1.6484	0	0.2576
101	2	0	2.1186	0.1149	0.0326
102	2	0	2.1181	0	0.0288
103	4	1	1.6484	0	0.2195
104	3	0	2.0052	0	0.0565
105	5	0	2.1047	0	0.1073
106	3	0	1.9591	0	0.0568
107	2	0	2.1047	0	0.0288
108	2	0	2.119	0	0.0288
109	2	0	2.119	0	0.0288
110	4	0	0	0	0.1272
111	1	1	0	0	0.2218
112	1	0	0	0	0.101
113	2	0	2.0496	0	0.029
114	2	0	2.1191	0	0.0288
115	2	0	2.1162	0	0.0288
116	1	0	0	0	0.101
117	1	0	0	0.0101	0.1011
118	2	0	1.5824	0	0.0396

TABLE 3.9: Comparison of optimal PMU locations obtained by proposed methodology with available techniques

Test system	No. of PMUs required for complete observability	PMU installation %	Optimal PMU locations				
			Common PMU location	Proposed methodology	Chakrabarti and Kyriakides [37]	Alvarez *et al.* [45]	Roy *et al.* [124]
NE 39-bus	13	33.33 %	2, 6, 9, 14, 17, 20, 22, 23, 29	11, 32, 33, 37	10, 11, 19, 25	NA	10, 12, 19, 25
IEEE 57-bus	17	29.82 %	1, 4, 9, 32, 36, 38, 41	7, 15, 20, 24, 25, 28, 47, 50, 53, 57	NA	7, 15, 19, 22, 25, 27, 47, 51, 53, 57	20, 24, 27, 29, 30, 39, 45, 46, 51, 54
IEEE 118-bus	32	27.12 %	5, 12, 17, 21, 23, 49, 56, 62, 68, 71, 75, 77, 80, 85, 94, 105, 110	3, 10, 15, 28, 30, 36, 40, 44, 47, 52, 64, 87, 91, 101, 115	NA	3, 9, 15, 25, 29, 34, 37, 40, 45, 52, 64, 86, 90, 102, 115	1, 9, 13, 26, 28, 34, 37, 41, 45, 53, 63, 86, 90, 101, 114

3.4 Summary

The major finding of this chapter are summarized below:

1. This chapter presented a methodology for determining the minimum number of PMUs and their optimal locations for complete topological observability of the system considering critical buses. Four different attributes; namely redundancy of measurements, rotor angle, and frequency monitoring of generator buses, reactive power deficiency, and maximum loading limit under transmission line outage contingency are considered for selecting a bus for PMU installation.

2. Each attribute is evaluated for all the buses in the system and a consolidated score, referred as the degree of criticality, is determined using TOPSIS.

3. The optimal PMU placement problem is formulated as a binary integer linear programming problem.

4. The bus with the high degree of criticality is assigned more weight for PMU installation in the optimization problem.

5. The results verify that the majority of PMU locations are at the buses having a high degree of criticality.

6. The proposed scheme is also compared with the three existing methods for PMU placement. The resultant PMU configuration has an equal number of PMUs as reported by other methods but different PMU locations.

7. The multi-horizon deployment of PMUs is also addressed for utilities with limited financial resources.

Next chapter deals with development of machine learning based modules for real-time analysis of events using the synchrophasor measurements obtained from PMUs.

Chapter 4

Real-time Event Detection and Classification

4.1 Introduction

Several accounts of power outages have been determined to be either initiated or accelerated by relay maloperations and hidden failures. Although control centers receive the response of protective devices in the form of relay trip status and circuit breaker flags, an additional layer of security can be added by identification of events from the real-time PMU signals. In this chapter, an event analysis framework has been proposed utilizing wide-area synchrophasor measurements received from PMUs. The purpose of the framework is to automatically identify an event occurring in the system and validate the response of relays and other protective equipment to the event.

A three-phase fault is the most critical event that occurs in a power system in operation. It subjects the generator to mechanical stress and excessively high-temperatures exceeding the operating limits, that deteriorate its mechanical strength and insulation. A more severe fault may result in rotor angle instability, sudden loss of transmission-lines, oscillations in the rotor, vigorous machine vibrations and even breakdown. Low-inertia generators, such as mini-hydro, micro-turbines, are most affected by these disturbances. Thus, timely detection and clearance of faults is indispensable to safeguard the stability of the system.

From a critical review of the literature presented in Chapter 2, it is observed that there is a pressing need for the development of a comprehensive scheme which not only detects events

but is also able to find its location. The developed scheme should be capable of classifying the type of event and quantify the magnitude of the event in real-time also so that effective control measures can be devised to limit the consequence of disturbances. Therefore in this chapter, a new unified scheme is proposed for detection of events, their localization, and classification by analyzing both voltage and frequency waveforms. Simultaneous analysis of both voltage and frequency ensures that both active and reactive power events are detected due to the existence of a strong coupling between frequency and active power; and voltage and reactive power. The signal energy has been used to recognize an event and identify its location. For event classification, a supervised learning based approach has been proposed. A dataset with various events has been first simulated, and labelled with its respective class. It is randomly shuffled and divided into the training and testing sets with 60 % and 40 % cases respectively. A multi-class Support Vector Machine (SVM) classifier is trained using appropriate features extracted from the training dataset, while the testing dataset remains unseen to the classifier. SVM algorithm automatically infers the mapping function from the input features to the output class. After it is trained, its performance is validated on the testing dataset. However, non-stationary dynamic nature of the power system is its intrinsic characteristic. As a consequence, the measurement signals like rotor angle, rotor speed, frequency, and voltage after a disturbance perturbs the system are also non-stationary. Therefore, in this work, the wavelet transform has been used to interpret these signals.

4.2 Wavelet Transform (WT)

Wavelet Transform is an excellent tool for investigating signals of non-stationary, aperiodic, and abrupt nature. It renders superior temporal as well as frequency resolution. It finds its applicability in diverse spheres such as noise cancellation, data compression, pattern recognition, seismic signal analysis, etc. It resolves the signal of interest into *'wavelets'* which are dilated and translated variants of the *'mother wavelet* ($\psi_{a,b}$)*'* [132]. A mother wavelet at scale a and position b is defined as:

$$\psi_{a,b}(t) = \frac{1}{\sqrt{a}}\psi\left(\frac{t-b}{a}\right) \tag{4.1}$$

where a and b are called *dilation parameter* and *translation parameter* respectively. It is squeezed or dilated and translated to and fro along the length of the signal. WT is the convolution of a input continuous-time signal $x(t)$ with the scaled variants of mother

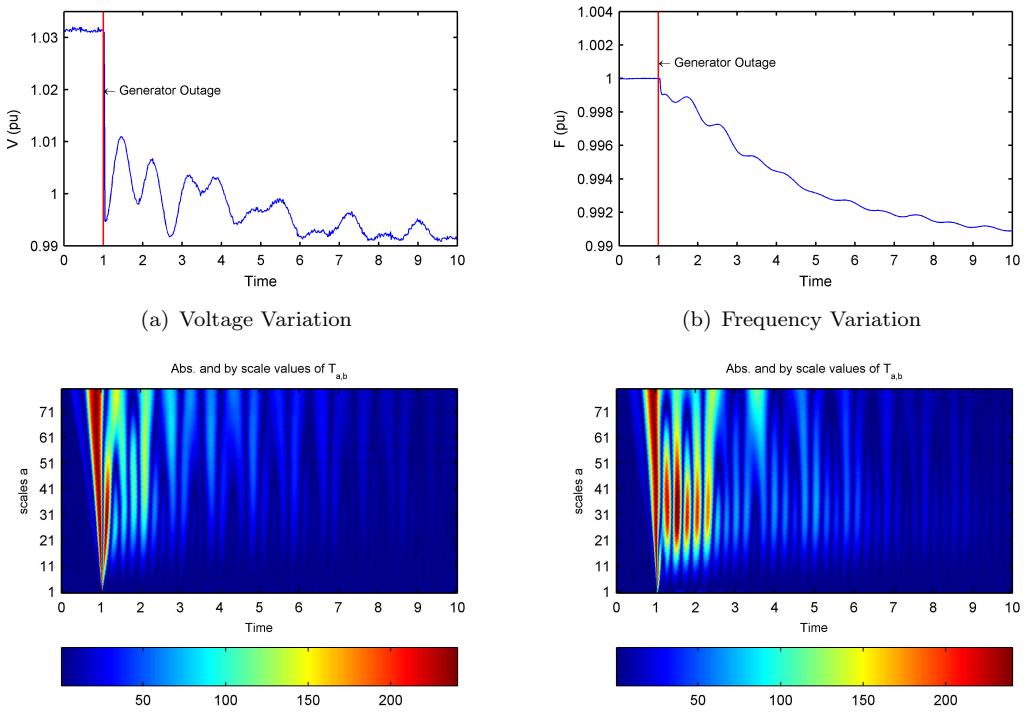

(a) Voltage Variation

(b) Frequency Variation

(c) Plot of WCs of voltage

(d) Plot of WCs of frequency

FIGURE 4.1: Time-frequency plots of generator outage at bus 31

wavelet. Mathematically,

$$T_{a,b} = \frac{1}{\sqrt{a}} \int_{-\infty}^{\infty} x(t)\psi\left(\frac{t-b}{a}\right)dt \tag{4.2}$$

where $T_{a,b}$ are termed as *detail coefficients* or directly *wavelet coefficients (WCs)*. The values of $T_{a,b}$ quantify the correlation between the mother wavelet and a local segment of the signal. These coefficients show proportionally higher magnitude at a particular scale indicating the existence of a strong frequency component. The dilation and contraction of the mother wavelet govern its characteristic frequency. WCs show proportionally higher magnitude at particular scales and time indicating the existence of a strong frequency component as can be observed in Fig. 4.1 in case of outage of generator 2 in NE 39 bus system. Fig. 4.1(a) and 4.1(b) show voltage and frequency variation at bus 31 after the outage of the generator. Both voltage and frequency are observed to oscillate at approximately 1 Hz. The corresponding plots of WCs for continuous values of a and b normalized by maximum absolute value of the coefficient at each scale using 'db2' mother wavelet are shown in Fig. 4.1(c) and Fig. 4.1(d). These plots are known as *Continuous Wavelet Transform (CWT)* plots. It is observed that WCs delineate abrupt discontinuities

and oscillations present in both voltage and frequency waveforms. The discontinuities result in large absolute values of WCs concentrated at the time of generator outage. Also, WCs adequately localize oscillations present in the input signal at particular scales. It is observed that abrupt discontinuities in signals result in large absolute values of wavelet coefficients concentrated in a narrow region centered at the time of generator outage. The perimeter of this region is called the *Cone of Influence (COIn)*. The event of generator outage is more precisely localized at lower scales where the wavelet is less dilated than at higher scales inside the cone of influence. The transform plot also shows the large value of coefficients at intermediate scales inferring that wavelet size at these scales approximates the waveform.

4.2.1 Discrete Wavelet Transform (DWT)

CWT translates and dilates the mother wavelet over the entire signal for continuous values of a and b. Consequently, it generates substantial quantity of redundant information. Hence, DWT is favored due to more efficient and simpler practical implementation. In DWT, both a and b are discrete values exclusively; $a = a_0^m$ and $b = nb_0a_0^m$; $m, n \in \mathbb{Z}$. For typical values of $a_0 = 2$ and $b_0 = 1$, a dyadic grid mother wavelet $\psi_{m,n}(t)$ and its scaling function $\phi_{m,n}(t)$ are described as:

$$\psi_{m,n}(t) = 2^{-m/2}\psi(2^{-m}t - n) \tag{4.3}$$

$$\phi_{m,n}(t) = 2^{-m/2}\phi(2^{-m}t - n) \tag{4.4}$$

The detail and approximation coefficients are obtained by convolution of $x(t)$ with mother wavelet and scaling function respectively as stated in (4.5) and (4.6):

$$T_{m,n} = \int_{-\infty}^{\infty} x(t)\frac{1}{2^{m/2}}\psi(2^{-m}t - n)dt \tag{4.5}$$

$$S_{m,n} = \int_{-\infty}^{\infty} x(t)\frac{1}{2^{m/2}}\phi(2^{-m}t - n)dt \tag{4.6}$$

The detail coefficients $T_{m,n}$ characterize the sudden changes or high frequency components present in the signal. Conversely, approximation coefficients $S_{m,n}$ describe the trend of the signal or the low frequency component [133]. Both approximation and detail components reconstructed from approximation and detail coefficients of a signal at a specific level are downsampled by a factor of 2, and the approximation are utilized for further decomposition. The process is repeated until the required level of detail coefficients is obtained [134, 135].

4.2.2 Cross Wavelet Transform (XWT)

Non-stationary nature of power system signals hinders their phase estimation using simple methods such as Cross-correlation and Fourier transform. Therefore, the instantaneous phase of oscillating signals has been estimated using Cross-Wavelet transform. The XWT of two signals $x(t)$ and $y(t)$ is defined as:

$$T_{a,b}^{x,y} = T_{a,b}^{x} T_{a,b}^{y*} \tag{4.7}$$

The modulus of XWT, $\left|T_{a,b}^{x,y}\right|$, is cross wavelet power while its complex argument, $\varsigma_a = \arg(T_{a,b}^{x,y})$, is instantaneous relative phase difference between $x(t)$ and $y(t)$.

4.3 Event Detection and Classification

Normally, power system functions in a quasi-static state. However, the unexpected occurrence of an event initiates power imbalance in the system, which is reflected as an abrupt variation in voltage and frequency measurements recorded by PMUs. This imbalance is corrected by governor action and excitation control, which take up to 2 s to participate in stabilizing the system. The voltage and frequency waveforms during this period are deemed as the natural response of the power system to the event. The post-disturbance waveforms of voltage and frequency associated with the similar type of events exhibit very similar characteristics in both time and frequency domain [136]. It illustrates that sufficient information for detection and classification of events is available in the waveform. But, the absence of fundamental frequency in the event signals hinder their frequency representation by simple Fourier Transform [69]. Short-Term Fourier Transform (STFT) which requires sectionalizing the signal and applying the conventional Fourier Transform on individual section is another procedure for analysis of non-stationary signals. But, choice of a suitable window and inverse relationship between time and frequency resolution limit its applicability. Hence, the simultaneous analysis in time-frequency domain is a suitable choice. The DWT renders a better trade-off between temporal and frequency resolution, *i.e.* it offers good time resolution at high frequencies and good frequency resolution at low frequencies. Therefore, in this work, DWT is used to analyze the voltage and frequency signals received in real-time through synchrophasor measurements.

Fig. 4.2 shows the outline of the proposed event analysis approach. The real-time voltage and frequency measurements are received from PMUs. These signals are continuously

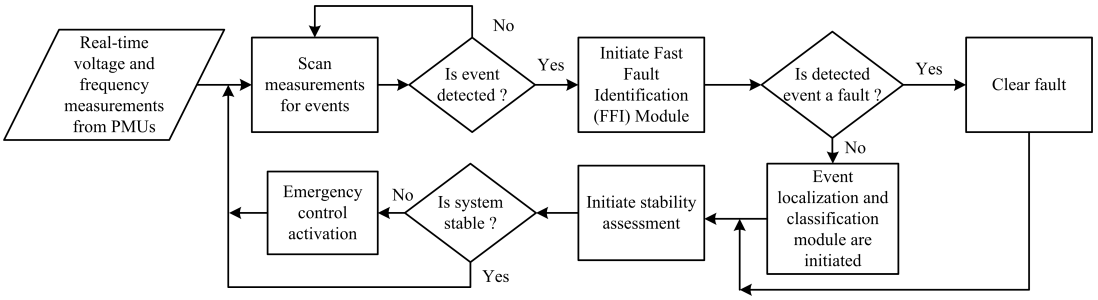

FIGURE 4.2: Flowchart of the event analysis

scanned for detecting events. Once an event is detected, it is immediately checked for being a fault. If a fault is reported, it is cleared. In the absence of fault, the event localization and classification module is initiated. Next, the impact of the event on the stability of the system is checked and remedial measures are undertaken if it leads to instability. Stability assessment and emergency control have been discussed in the next chapter.

4.3.1 Signal Energy

In this work, signal energy has been utilized to detect the occurrence of an event. It is a mensuration of intensity or magnitude of the signal. For a signal $x(t)$ of length $L = 2^M$, the signal energy is obtained as:

$$E = \int_{-\infty}^{\infty} \mid x(t) \mid^2 d(t) = (S_{M,0})^2 + \sum_{m=1}^{M} \sum_{n=0}^{N} (T_{m,n})^2 \tag{4.8}$$

where $N = 2^{M-m} - 1$ and $N + 1$ is the number of coefficients in level m. The energy corresponding to details in level m is stated as:

$$E_m = \sum_{n=0}^{N} (T_{m,n})^2 \tag{4.9}$$

It is a direct assessment of local energy in a particular frequency sub-band. At the instant of the event, the energy of voltage and frequency signals is significantly higher than its value during steady-state operation of the system.

4.3.2 Proposed Event Detection and Localization Scheme

Voltage and frequency remain almost stationary for a power system operating in equilibrium. When an event occurs, these parameters abruptly deviate from their equilibrium values. This work exploits the ability of wavelets to distinguish such abrupt transitions or *edges* from the stationary parts in the measured signal. A wavelet is a localized function and approaches to zero at a short distance from its center. Under normal operating conditions, wavelet convolutes with a virtually constant signal to give near-zero values of the integral in (4.5). As the wavelet traverses across the discontinuity present in the signal, significantly large values of WCs are obtained. The polarity and magnitude of the WCs are determined by the geometry of the wavelet used. The event detection procedure proposed in this work is based upon constant inspection of the squared detail coefficients, *i.e.*, energy corresponding to details of fixed width moving window of voltage and frequency data. Squaring the wavelet coefficients assures that the positive and negative contributions to the integral in (4.5) are not neutralized when the discontinuity coincides with the center of a symmetrical wavelet. A new index has been formulated for detection of events. It is described as the ratio of energy corresponding to detail coefficients of the present window and mean energy of 10 preceding windows. For l^{th} bus and t^{th} time instant, it is defined as:

$$R^{(J,l)}[t] = \frac{E_m^{(J,l)}[t]}{\frac{1}{10}\sum_{j=t-10}^{t} E_m^{(J,l)}[t]}; \quad J \in \{V, F\}, \forall\ l \in N_B \tag{4.10}$$

where N_B denotes the set of all buses. The average of 10 continuous cycles has been taken as it is generally used in the aggregation of continuously varying power system measurements [14, 137]. The ratio is computed for both voltages ($R^{(V,l)}$) and frequency ($R^{(F,l)}$) measurements over a 30 sample moving window with an increment of 1 sample. The size of moving window was selected according to natural frequency of oscillation of voltage and frequency after the system is perturbed by an event. If the frequency of oscillation is high, a shorter moving window size may be selected and vice-versa; such that it contains a sufficient part of voltage and frequency waveform. As observed in Fig. 4.1 (a) and (b) voltage and frequency oscillate at about 1 Hz in NE-39 bus system after outage of a generator at bus 31, *i.e.*, 1 complete cycle in 1 s. In this work, only half cycle data or 30 samples of voltage and frequency measurements have been considered for event detection as the energies of positive half cycle and negative half cycle are equivalent in sinusoidal waveforms. The occurrence of an event is indicated when either $R^{(V,l)}$ or $R^{(F,l)}$ exceeds its predefined threshold value ζ_V and ζ_F respectively anywhere in the grid at any instant

TABLE 4.1: Voltage and frequency response to various events

Event	Voltage response	Frequency response
Fault	Drastic fall	Rise
Generator outage	Fall/Rise[§]	Fall
Load rejection	Increase	Increase
Industrial load starting	Fall	Fall
Shunt capacitor outage	Drastic fall	Insignificant increase
Shunt reactor outage	Drastic rise	Insignificant decrease

[§]When synchronous generator is over-excited/under-excited

of time. The threshold values are system-specific and also depend on the wavelet family used. Under normal operating conditions:

$$R^{(V,l)} < \zeta_V \quad and \quad R^{(F,l)} < \zeta_F \tag{4.11}$$

After the detection of the occurrence of an event, it is first checked for being a short-circuit fault.

4.3.3 Fast Fault Identification Module

The Distance or Impedance Relays are commonly used as primary and backup protection against faults. However, the distance protection can incorrectly perceive heavy load as a fault due to low voltage and heavy current flow in the transmission line. This type of misinterpretation is known as *load encroachment*, and is typically observed at the beginning stage of a blackout. Therefore, a new two-step confirmation technique has been devised for prompt detection of faults and separation from all other types of events.

4.3.3.1 Fault Suspicion Criterion

A comparison of the characteristics of faults with some regular events occurring in a power system is presented in Table 4.1. It is observed that a fault leads to drastic fall in voltage while an impulsive increase in generator speed. These transient voltage and frequency responses of the power system to faults have been used in the proposed method. Due to the drastic decrease in voltage magnitude at a bus (voltage may even drop to almost zero depending upon the fault impedance), the change in voltage magnitude is used as an attribute of a fault. At bus l, the change of voltage is calculated using the backward-difference approach between real-time consecutive voltage samples obtained from PMUs.

When it declines a predefined threshold, ϑ^{Fl}, a fault is suspected. Accordingly, a Fault Suspicion Criterion is formulated as:

$$\text{Fault Suspicion Criterion: } \Delta V_l[t] = V_l[t] - V_l[t-1] < \vartheta^{Fl} \tag{4.12}$$

The threshold value ϑ^{Fl} is system specific and should be judiciously decided after exhaustive contingency analysis through offline time-domain simulation. The nearest location of the fault is determined as the bus with the maximum decrease in voltage at the time of the event. Mathematically, it is expressed as:

$$\text{Suspected Fault Bus} : B^{Fl} = \underset{l \in [1,2,..N_B]}{\arg\max} \Big(|\Delta V_l[t]| \Big) \tag{4.13}$$

where N_B is the total number of buses in the system. The reduction in voltage cannot alone serve as an effective parameter for fault recognition, because other events, such as staring of heavy industrial loads can also result in steep voltage drop. Also, the quantum of voltage dip observed at a bus depends upon fault impedance and distance from the actual fault location. Thus, a secondary check has been suggested to validate the occurrence of a fault. The power fed by a generating machine abruptly decreases to zero at the inception of fault. The turbine governor is unable to respond spontaneously due to inherent delay in the opening of steam valves, and mechanical torque exceeds electrical torque causing the generator to accelerate [138]. The rise in frequency followed by a fault is observed to be its signature response. On that premise, a supervised learning based binary SVM classification module has been proposed as an affirmative check for a fault. It is a predictive analytic tool that is first trained offline using pre-labelled data, and then implemented online to predict the state of the system based on ambient measurements. The change in magnitude of voltage and frequency have been used as two features as input to the classifier which distinguishes faults from other events. SVM finds the maximum-margin hyperplane between the *Fault* class from the *Other Event* class.

4.3.3.2 Supervised Learning Based Fast Fault Identification

In this work, supervised learning classification has been used to serve as a Fast Fault Identification (FFI) module for real-time confirmation of the occurrence of a fault. The FFI module accepts the amount of change in voltage and frequency at the *Suspected Fault Bus* as inputs and classifies the event either in *Fault* class or in *Other event* class. It is a fast and accurate tool; and can be used in conjunction with conventional distance protection scheme. When both schemes confirm a fault, it is cleared by opening the transmission

line using circuit breakers. However, in case of inconsistency between the judgement of both schemes, such as in case of load encroachment or formation of *electrical centers*, the proposed module may overrule the distance protection scheme.

If the detected event is not a fault, event localization algorithm is initiated for determining the location of the origin of the event. An event involving contingencies of reactive power apparatus do not impact system frequency significantly. However, both active as well as reactive power contingencies affect the voltage. Hence, voltage magnitude has been preferred over frequency for event localization. The proposed event localization algorithm requires a 1 s data window of voltage magnitude of each bus obtained in real-time through PMUs. The data window is composed of 30 samples of pre-event and 30 samples of post-event voltage magnitude readings. This data window is significantly small for real time use and confines the resultant voltage deviation precisely in its midpoint. The inclusion of pre-event voltage data in event localization facilitates the estimation of the relative change in the bus voltages before and after an event. The bus electrically adjoining the location of the event undergoes maximum deviation in the voltage magnitude which is apparent in the detail coefficients. The algorithm determines the energy corresponding to details of voltage magnitude for each bus as stated in (4.9). Accordingly, the bus with the highest wavelet energy is nearest to the location of the origin of the event.

4.3.4 Selection of Mother Wavelet and Decomposition Level

The discontinuities present in the input signal affect the wavelet coefficients at all levels. WCs corresponding to such discontinuities have a greater absolute magnitude than WCs corresponding to smoother features of the signal. However, the discontinuities are most accurately localized at the smallest level of wavelet decomposition because of the high-frequency components in the discontinuity. Furthermore, the event localization and classification module, proposed in this work, requires only 60 samples of PMU data. Wavelet coefficients of such short signals are also contaminated by spurious values or the edge artifacts as the number of decomposition level increases. Hence, smaller decomposition level has been considered as more suitable for wavelet decomposition. Several mother wavelet families (Daubechies 1-20 and Symlets 1-20) were also tested to check the accuracy of the classifier. After a thorough investigation, best classification results were achieved with Daubechies-2 (‘db2’) wavelet. This wavelet offers excellent performance in edge detection and transient signal analysis. Hence, ‘db2’ with decomposition level 1 is used for further analysis.

4.3.5 Proposed Feature Extraction and Dendrogram Based Support Vector Machine (DSVM) Event Classification Module

A classification module is developed for non-fault events. It aims to classify the identified event into one of the four major classes of disturbances frequently occurring in power system, *viz.* generator outage, load rejection, capacitor outage, and starting of induction motor. The classification of events is crucial to devise efficient corrective measures for maintaining the stability of the system. In the proposed scheme, the event classification is initiated after event localization algorithm. Both event localization and classification modules utilize the same data window as input.

4.3.5.1 Time-Frequency Feature Extraction

The proposed method processes voltage and frequency measurements of the bus where event is detected using DWT and extracts the features suitable for classification. These features are detailed as follows:

1. **Energy Dispersion** (D_E)**:** It measures the distribution of energy among all levels of wavelet decomposition. A signal of length 2^M, has maximum *'M'* levels of decomposition. The signal energy corresponding to each level is calculated using (4.9) and its dispersion is defined as:

$$D_E = \frac{\sigma_E^2}{\mu_E} \tag{4.14}$$

where σ_E and μ_E are standard deviation and mean of energies in each level respectively.

2. **Average Frequency** (υ_A)**:** The voltage and frequency waveforms following an event can be separated into their spectral components in each frequency sub-band corresponding to the decomposition level. The average frequency of the oscillation is calculated as:

$$\upsilon_A = \frac{\sum_{m=1}^{M} f_m^{'} \times E_m}{\sum_{m=1}^{M} E_m} \tag{4.15}$$

where $f_m^{'}$ and E_m are the associated pseudo-frequencies and energy in m^{th} decomposition level.

3. **Log Energy Entropy** (H_{log})**:** Entropy is an estimate of information contained in a signal. For wavelet coefficients at m^{th} decomposition level, it is expressed as:

$$H_{log} = \sum_{n=0}^{N} log_2(p_n)^2 \tag{4.16}$$

where p_n is the energy probability distribution of wavelet coefficients defined as:

$$p_n = \frac{(T_{m,n})^2}{E_m} \tag{4.17}$$

with the convention $log_2(0) = 0$.

4. **Median Absolute Deviation (MAD):** MAD is a robust indicator of the central tendency of a sample of univariate quantitative data. It is expressed as the median of the absolute deviations of data points from its median; *i.e.*,

$$MAD = median(\mid X_k - median(X) \mid) \tag{4.18}$$

where X is the measurement sequence in the current measurement window and $k = 1....60$. As similar events generate similar measurements sequences, the spread of data points along their median is also distinctive feature for different types of events.

Four features from voltage magnitude and four from frequency measurements are computed. Thus, the consolidated feature vector comprises a total of 8 features, *i.e.* $F \in \mathbb{R}^{1\times 8}$. Since these features are diversified, they vary over a wide range of values. In machine learning algorithms, the features in greater numeric ranges dominate those in shorter numeric ranges. Consequently, the ranges of all features are normalized so that each feature is represented proportionately. Therefore, the raw feature vector has been scaled using Z-score standardization. The Z-score of the j^{th} feature in the feature vector is determined as:

$$Z_j = \frac{F_j - \mu_F}{\sigma_F} \tag{4.19}$$

where μ_F and σ_F are mean and standard deviation of F respectively and $j = 1, 2...8$. It scales the features to have mean 0 and standard deviation 1 and eliminates the skewness in the data. This scaled feature vector is utilized as the input to the classifier which segregates the event into one of the four predefined classes.

4.3.5.2 Multi-Class Support Vector Machine Event Classification Module

SVM is a supervised learning based approach for classification problems. It classifies the data set by determining the decision boundary or *hyperplane* with the largest margin between the data points of the two classes [139]. For a given data set (α_z, β_z), $z = 1, 2, 3...N_d$,where $\alpha_z \in \mathbb{R}^n$ is the feature vector with the corresponding class label $\beta_z \in \{+1, -1\}$, the SVM is formulated as the following optimization problem [140]:

$$\min_{w,B,\xi} \frac{1}{2} w^T w + C \sum_{z=1}^{N_d} \xi_z \tag{4.20}$$

subject to

$$\beta_z(w^T \Omega(\alpha_z) + B) \geq 1 - \xi; \quad \xi \geq 0. \tag{4.21}$$

where w is the vector of coefficients, B is a bias term, ξ is the error term with penalty constant $C > 0$. The variation in parameter C adjusts the weight on the distance between the hyperplane and error points. The kernel function $K(\alpha_z, \alpha_{z'}) \equiv \Omega(\alpha_z)^T \Omega(\alpha_{z'})$ is used to project the input features into higher dimensional space and the separating hyperplane with maximum margins in higher dimensions is obtained. SVM classifier is inherently a binary classification algorithm and needs to be suitably modified to achieve multiclass classification. In this work, a Dendrogram based SVM classifier [141] has been used. It requires two steps (i) create an ascendant hierarchical cluster tree of known classes based on the smallest distance between data points (ii) link a binary SVM at each node of the tree that classifies the input sample into either of the subclasses below the node. Accordingly, *s-1* SVMs are created for classification in s-classes.

4.4 Simulation and Results

The effectiveness of the proposed methodology is demonstrated on New-England 39 bus test system. The data of dynamic models of synchronous machines and excitation systems taken in the analysis are provided in Appendix A. The dynamic simulation was performed in PSAT toolbox [142] on MATLAB R2010a platform [143] of a Windows 7 computer with a Core *i5* CPU and 4 GB of usable RAM. The system is completely observable by PMUs installed in the grid at locations suggested in Chapter 3. The reporting rate of PMUs to the centralized control center is taken as 60 samples/s. A latency of 100 ms due to the communication lag between PMUs and the central control is considered [117].

White Gaussian noise with zero mean and SNR 45 has been added to all measurements to emulate noise present in actual PMU data [144].

4.4.1 Dataset Generation

The dataset was generated by simulating five different events, namely, Generator Outage (GO), 3-phase fault (3PF), Load Rejection (LR), Capacitor Outage (CO) and Induction Motor Starting (IMS). The load in the system was varied from 85 % to 110 % of base case in step of 5 % and each event was simulated at all loading levels. The NE-39 bus system has 10 generators and 18 load buses. The dataset for class GO and LR was simulated by the abrupt rejection of each generator and load individually from the system during operation. Similarly, three phase faults, each of 8 cycles and varying fault impedance, were simulated at all zero-injection and load buses. Shunt capacitors of variable rating were placed at load bus to improve its power factor to approximately unity, and class CO data was generated by sudden elimination of the capacitor. For IMS class, a fifth-order double-cage induction motor was installed at load bus and measurements were taken at the start-up of the motor. As detailed in Table 4.2, total 558 events were created and labelled with its respective class. Synchronized voltage and frequency readings available from PMUs were recorded. Thus, the cumulative dataset was composed of 21,762 cases of events from all buses. The dataset was randomly shuffled and divided into the training and testing sets as 60 % and 40 % cases respectively.

Table 4.2: Composition of the generated dataset

Types of events	Number of events at a specific loading level
GO	10
3PF	29
LR	18
CO	18
IMS	18
Total number of events at a specific loading level	93
Number of loading level considered	6
Total number of events	$93 \times 6 = 558$
Cumulative number of cases recorded from all buses	$93 \times 6 \times 39 = 21762$

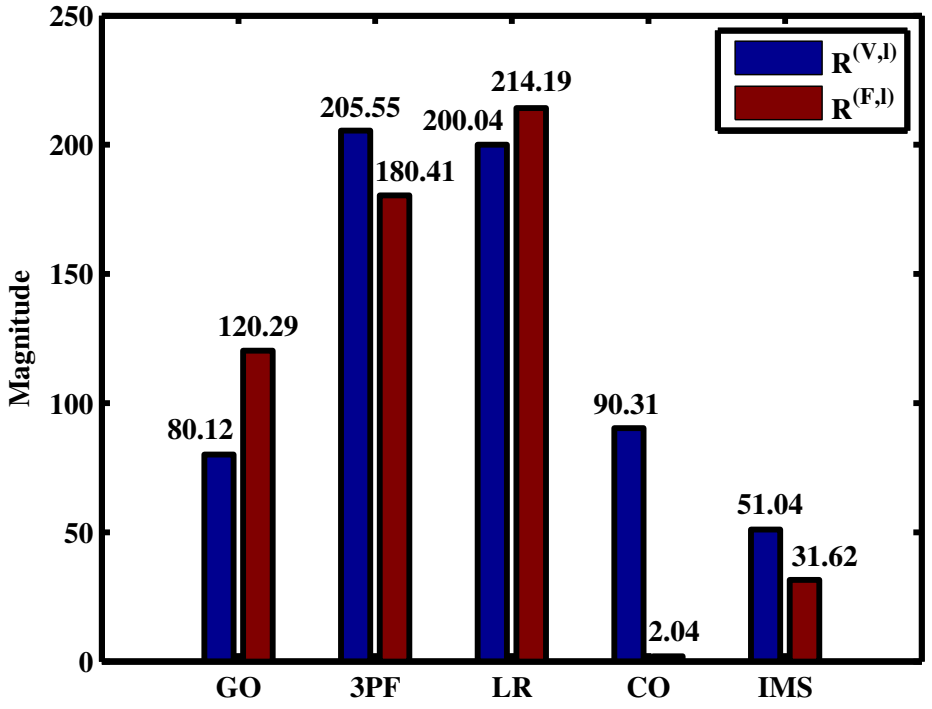

FIGURE 4.3: Selection of threshold value of $R^{(V,l)}$ and $R^{(F,l)}$

4.4.2 Selection of Threshold Values

The proposed approach requires values of three thresholds *viz.* ϑ^{Fl}, $R^{(V,l)}$ and $R^{(F,l)}$. All thresholds are system specific, and their values must be decided with caution. The maximum value of ΔV_l after a fault in the prepared dataset was selected as the threshold for Fault Suspicion Criterion. It was found to be $\vartheta^{Fl} = -0.45$ p.u. The values of other thresholds, $R^{(V,l)}$ and $R^{(F,l)}$, were selected after thorough investigation of the training dataset for lowest value of wavelet energy for each type of event. Fig. 4.3 shows the minimum values of $R^{(V,l)}$ and $R^{(F,l)}$ observed throughout the grid at the instant of event. It is observed that capacitor outage does not affect the frequency of the system significantly due to weak coupling between reactive power and frequency. The negligible value of $R^{(F,l)}$ in case of class CO is due to the noise present in the measurement. Thus, these values were neglected while selecting thresholds for $R^{(F,l)}$. Consequently, taking the minimum values in the training dataset, the threshold for $R^{(V,l)}$ and $R^{(F,l)}$ were taken to be 50 and 30 respectively.

4.4.3 Event Detection and Localization

In this section, large number of events were simulated and analyzed by employing the proposed method on voltage and frequency measurements observed from every bus. Two representative cases are presented below:

4.4.3.1 Event 1: Generator Outage at Bus 30

The synchronous generator installed at bus 30 delivering a load of 250 MW is disconnected suddenly at $t = 5\ s$ (300^{th} sample) by opening the breaker connecting the generator to the network. It causes reduction in voltage magnitude and inter-machine oscillations among other generators. The 15 s time frame of voltage and frequency oscillation at bus 30 are shown in Fig. 4.4(a) and 4.4(b) respectively. Both ratios $R^{(V,l)}$ and $R^{(F,l)}$ are continuously computed for a sliding window of 0.5 s as discussed in Section 4.3.2 and their variation with time at bus 30 is presented in Fig. 4.4(c) and 4.4(d). A sudden increase in their magnitude is observed immediately after the outage of the generator. Both ratios overreach their respective thresholds at $t = 5.0167\ s$ (301^{st} cycle) following the event. An identical increment in their values is witnessed at all remaining buses also. As $\Delta V = -0.04 > \vartheta^{Fl}$, fault is not suspected. The event localization is triggered after 0.5 s of the detection of the event. Fig. 4.4(e) shows the energies corresponding to detail coefficients at all buses computed using (4.9). It is noticed that bus 30 has the highest wavelet energy among all buses suggesting the location of the event. The impact of disturbance in the grid is also visible in the wavelet energy plot as buses electrically close to bus 30 have higher value of energy. Accordingly, bus 2 shows the greatest wavelet energy after bus 30 followed by bus 3 and 25. After localization of the event, the same data window is used to classify events. It results are presented in Section 4.4.4.

4.4.3.2 Event 2: 3-phase Fault at Bus 3

A 8 cycle 3-phase fault is simulated at bus 3 at $t = 5\ s$. The variations in voltage and frequency at bus 3 after the event are shown in Fig. 4.5(a) and 4.5(b). Fig. 4.5(c) and 4.5(d) illustrate that both $R^{(V,l)}$ and $R^{(F,l)}$ simultaneously violate their threshold limits ζ_V and ζ_F respectively in the subsequent sample after the event. The FFI module is initiated immediately after the detection of event. As Fault Suspicion Criterion is also violated ($\Delta V = -0.6$ p.u. approximately), FFI is used to confirm the occurrence of the fault. FFI module accepts the change in event bus voltage and frequency (ΔV and ΔF) as inputs

and confirms the fault. The output of the event localization algorithm is presented in Fig. 4.5(e). The wavelet energy is highest at bus 3 showing the neighborhood of the event.

The performance of the proposed indices was validated on unseen cases available in the testing dataset. Table 4.3 summarizes the results of event detection and localization when events from testing dataset were verified using the selected thresholds. It was observed that 9 events were undetectable by both $R^{(V,l)}$ or $R^{(F,l)}$ ratios while 47 cases remain undetected by $R^{(F,l)}$ independently. It was found that among these 9 undetected events, 3

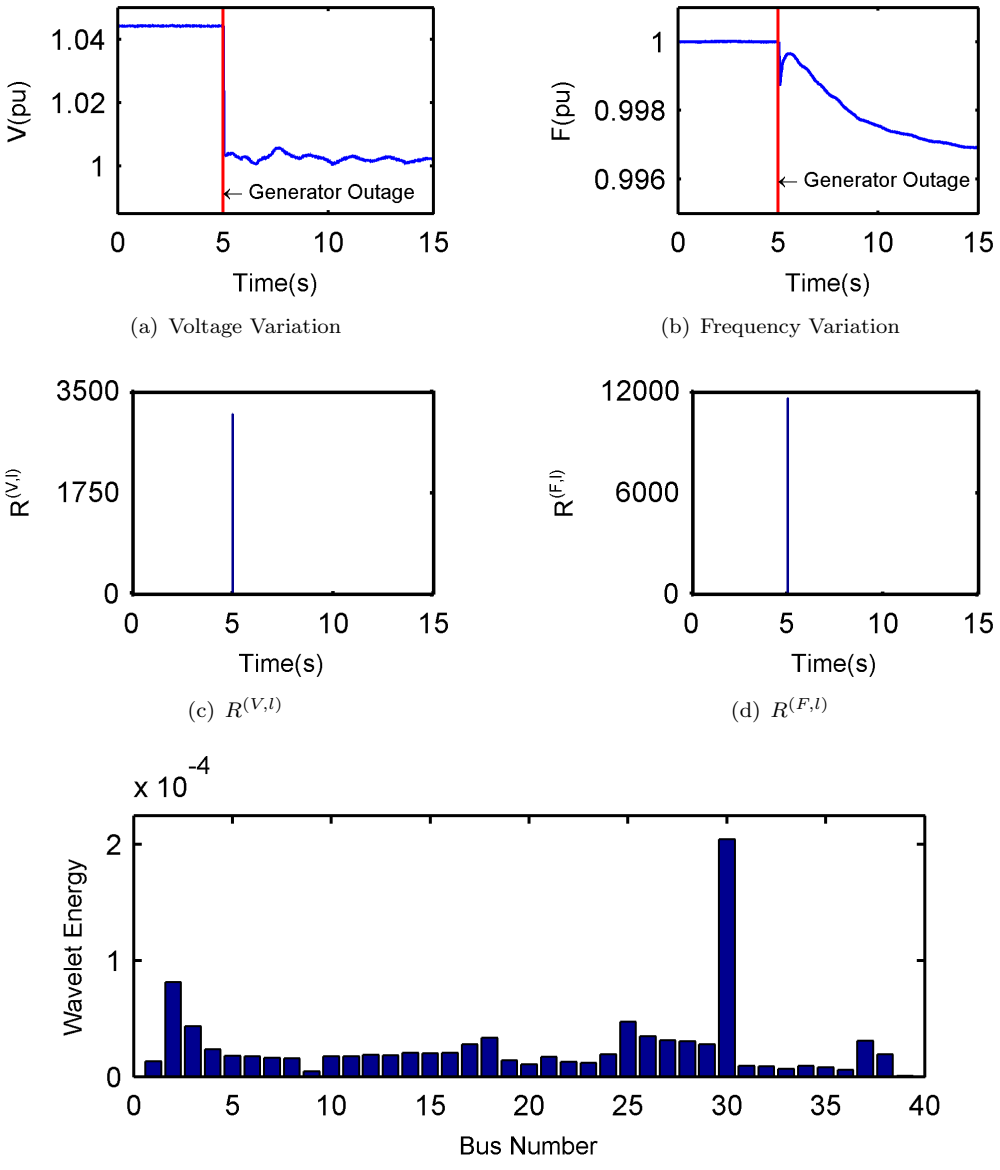

(a) Voltage Variation

(b) Frequency Variation

(c) $R^{(V,l)}$

(d) $R^{(F,l)}$

(e) Event localization results for generator outage at bus 30

FIGURE 4.4: Generator outage at bus 30

events correspond to load rejection at bus 12 at different loading conditions. The amount of load at bus 12 is considerably less (0.123 % of the total load) to generate any significant deviation in either voltage or frequency on its rejection as well it does not affect the system stability. The remaining 6 cases belong to capacitor outage at buses 3 and 29, where power factor was 0.9997 and 0.9995 respectively. Hence, the size of capacitors required to compensate their power factor to unity was relatively small. Similarly, 47 cases undetected by $R^{(F,l)}$ were of capacitor outages at different buses. Therefore, these

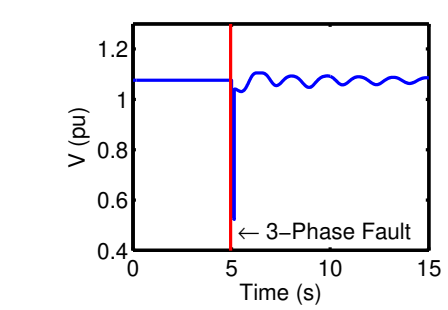

(a) Voltage variation

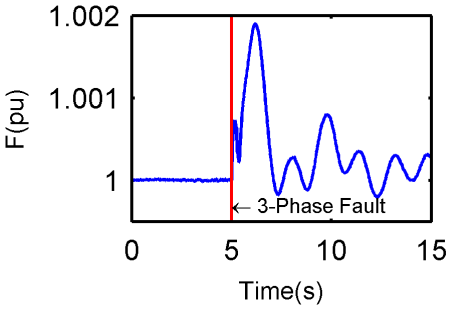

(b) Frequency variation

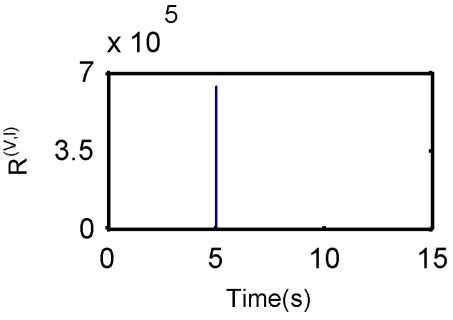

(c) $R^{(V,l)}$

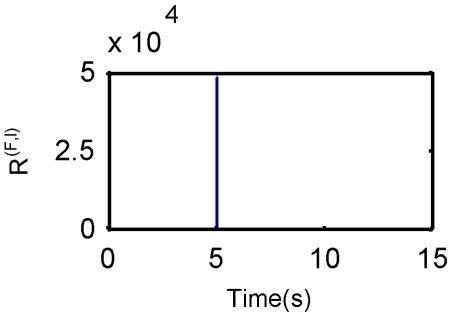

(d) $R^{(F,l)}$

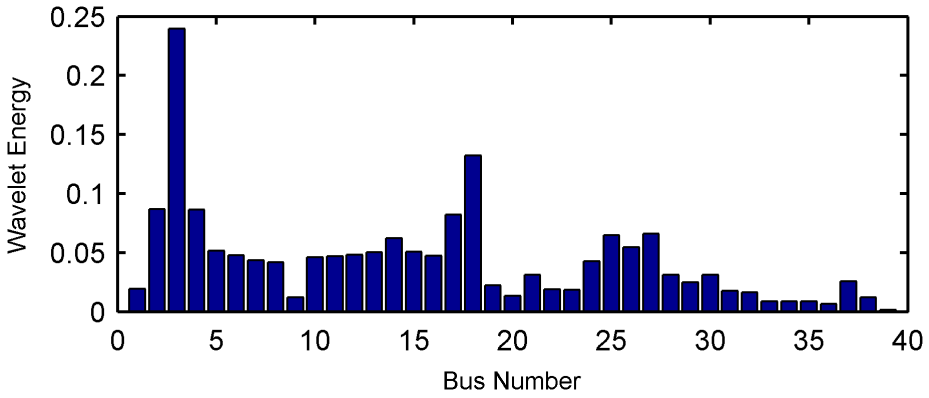

(e) Event localization results for 3-phase fault at bus 3

FIGURE 4.5: 3-phase fault at bus 3

events didn't have any noticeable effect on frequency. The event localization was tested on successfully detected events. Its accuracy was estimated to be 100 % signifying that the voltage deviation is maximum at the bus closest to the site of the event.

4.4.4 Training and Testing Event Classification Module

In this section, classification accuracy of both FFI and non-fault event classifier has been discussed. The characteristic voltage and frequency responses of a power system to faults constitute the underpinning for the proposed FFI module. The dataset is prepared for the offline training of the classifier as discussed in Section 4.4.1. The change in voltage and change in frequency at the *Suspected Fault Bus* are selected as the two features input to the classifier. Fig. 4.6 shows these features from the training dataset on x and y-axis respectively. The $*$ sign indicates data points of class *Fault*, and $+$ indicates data points of class *Other Event*. As evident from the figure, the two classes can be distinctly separated on $\Delta V - \Delta F$ plane; thus, a 'linear' kernel and hard margins are suitable for fault classification. Fig. 4.6 also shows optimal hyperplane between the two classes identified by SVM with a blue straight line. The performance of the trained classifier is validated on unseen data from the test set. Table 4.4 shows the cumulative confusion matrix of FFI module. It can be observed that the SVM classifier separates faults from other events with 100 % accuracy. The high accuracy is attributed to the existence of wide separation between the two classes because of peculiar voltage and frequency responses corresponding to fault events.

For non-fault events, features were extracted for each event case and used as input to train a DSVM classifier. Since the existence of separating margins between various classes is not known, classifier was trained with both soft and hard margins and different kernel

Table 4.3: Event detection and localization results

Total no. of events tested for event detection	226
Events correctly detected by $R^{(V,l)}$	217
Events correctly detected by $R^{(F,l)}$	179
Events correctly detected by $R^{(V,l)}$ or $R^{(F,l)}$ criteria	217
Events undetected by $R^{(V,l)}$	9
Events undetected by $R^{(F,l)}$	47
Total no. of events tested for event localization	217
Events correctly localized	217
Event inaccurately localized	0
Event detection accuracy (%)	96.01
Event localization accuracy (%)	100.00

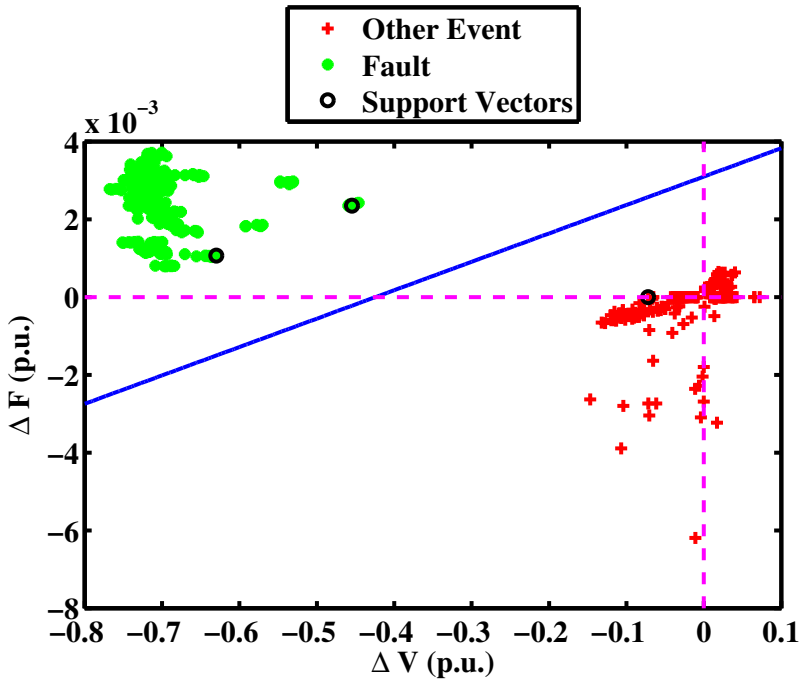

FIGURE 4.6: Decision boundary between *Fault* and *Other Event* classes for FFI module

TABLE 4.4: Confusion Matrices of Fast Fault Identification Module in NE-39 Bus Test System

	Predicted	
Actual	Fault	Other Event
Fault	1	0
Other Event	0	1
Accuracy	100 %	

functions. The linear separability between various classes facilitates efficient classification and reduces computational overhead. Thus, the classifier was first trained with a linear kernel and hard margins. The penalty term C in (4.20) provides flexibility to obtain either soft or hard margins. Hard margins enable a stricter boundary between two classes leaving lesser extent for misclassification while soft margins increases slackness in the constraint (4.21) allowing some data points to misclassify resulting in a larger margin. When trained with hard margins and linear kernel, DSVM failed to converge indicating that data are highly nonseparable [145]. Subsequently, soft margins along with linear kernel were used for training. The performance of the classifier was validated with features extracted from testing-dataset. The result of the classification is presented in the form of a confusion matrix in Table 4.5. It is observed that, it offers a mean classification accuracy of only

TABLE 4.5: Confusion Matrix of event classification with linear kernel and soft margins

	Predicted			
Actual	**GO**	**LR**	**CO**	**IMS**
GO	**0.77**	0.15	0.08	0.00
LR	0.15	**0.84**	0.00	0.01
CO	0.15	0.00	**0.85**	0.00
IMS	0.02	0.03	0.00	**0.95**
Accuracy	**85.25 %**			

TABLE 4.6: Confusion matrix of event classification with Gaussian Radial Basis function kernel and soft margins

	Predicted			
Actual	**GO**	**LR**	**CO**	**IMS**
GO	**0.95**	0.05	0.00	0.00
LR	0.06	**0.94**	0.00	0.00
CO	0.04	0.00	**0.96**	0.00
IMS	0.02	0.02	0.00	**0.96**
Accuracy	**95.25 %**			

85.25 %. The poor performance of the classifier confirms the absence of a linear separating hyperplane between the classes in lower dimensions. Non-separable features often become linearly separable after they are mapped to a high dimensional feature space. Thus, Gaussian Radial Basis Function kernel with soft margins was used for training and testing with the previous data set. Confusion matrix for the analysis is presented in Table 4.6. As observed from the table, the increased accuracy of the classifier shows that events are separable in higher dimensions. The mean accuracy of the classifier is calculated as 95.25 %.

The suitability of the presented methodology for the real-time deployment was also verified. The average time elapsed in various stages of the proposed event analysis scheme is presented in Table 4.7. The approximate time needed for the execution of event detection and localization methods was $< 10^{-4}$ s, and feature extraction and event classification required $< 10^{-2}$ s. The time consumed in the FFI module is $< 10^{-3}$ s. Therefore, a fault can be identified and cleared after two cycles of its occurrence. This latency is small for real-time situational awareness, considering that the instability generally arises after a few seconds (or even several minutes) after a critical event as observed in previous blackouts [14]. This implies that the presented approach is appropriate for diagnosis of events and functional in online polling mode of all protective devices in the grid.

TABLE 4.7: Average computation time of the proposed event analysis scheme

Stage	**Time elapsed (s)**
Event detection	$< 10^{-4}$
FFI module	$< 10^{-3}$
Waiting period	$= 5 \times 10^{-1}$
Event localization	$< 10^{-4}$
Feature extraction	$< 10^{-2}$
Event classification	$< 10^{-2}$

4.5 Coherency Identification of Generators Using Complex Wavelet Transform

In this section, a new approach for identification of coherent groups of generators in a multi-machine electrical power system has been proposed. The approach is based on the estimation of the instantaneous phase difference between oscillating rotor angles of generators after an event using XWT. Coherent groups of generators are automatically formed using k-means clustering.

Fig. 4.7 shows three pure sinusoidal signals s_1, s_2, and s_3, each of frequency 0.5 Hz and duration 10 s sampled at 100 Hz. Signals s_1 and s_2 are identical, but s_2 leads s_1 by a

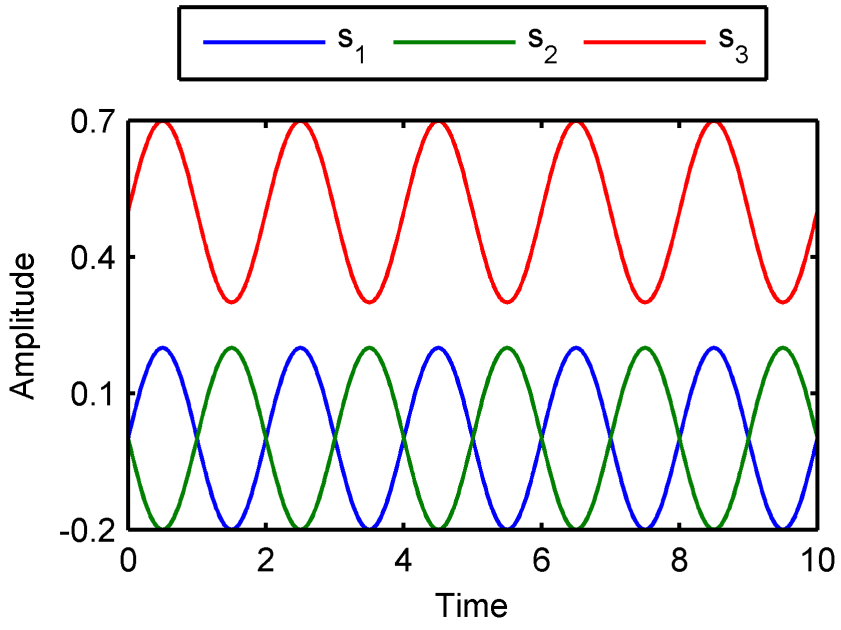

FIGURE 4.7: Three sinusoidal signals s_1, s_2 and s_3

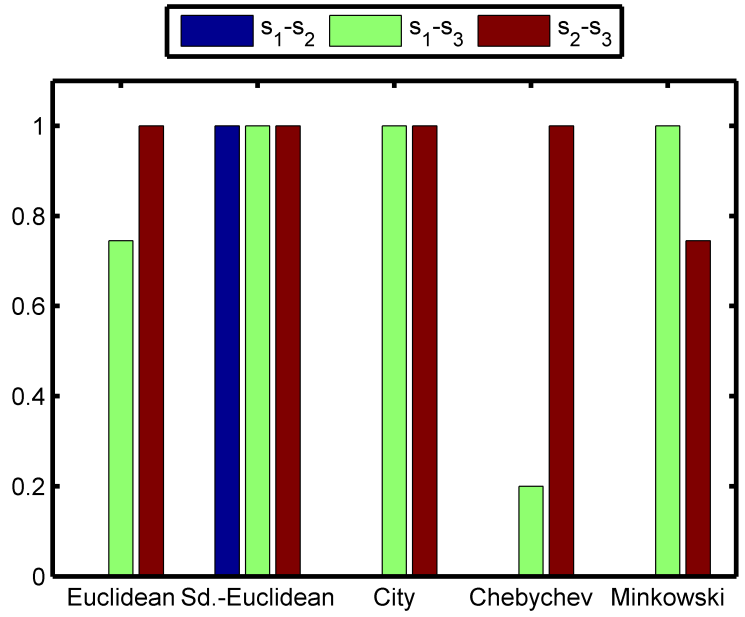

FIGURE 4.8: Normalized distances between signals s_1, s_2 and s_3

phase difference of π radians (or 180°). On the contrary, s_1 and s_3 are in phase; however, s_3 is an amplitude shifted version of s_1. Clearly, signals s_1 and s_3 are coherent while s_3 is out of phase with both s_1 and s_3. Therefore, a clustering algorithm should cluster s_1 and s_3 in one coherent group while s_3 as an independent cluster. Several standard distance measures e.g. Euclidean distance, Standardized-Euclidean distance, City distance etc. were tested to quantify the similarity among the three signals. These distances are normalized for clarity and are presented in Fig. 4.8. It is observed from the figure that in all measures, distances between s_1 and s_2 is less than the distance between s_1 and s_3. Therefore, it can be concluded that the amplitude difference has dominated phase difference between signals. Hence, a clustering algorithm will always be inclined to group s_1 and s_2 in one cluster rather than s_1 and s_3. Considering the inadequacies of these similarity measures, a new approach is suggested. A Phase Difference Matrix (PDM) based on the difference in instantaneous phase of the most dominant frequency component of two signals obtained using XWT has been developed. A new index for determination of most dominant frequency component is also suggested. PDM transforms the difference in instantaneous phase among N_G generators in a $N_G \times N_G$ dimensional space where coherent generators are in relative proximity then non-coherent generators. Morlet wavelet has been

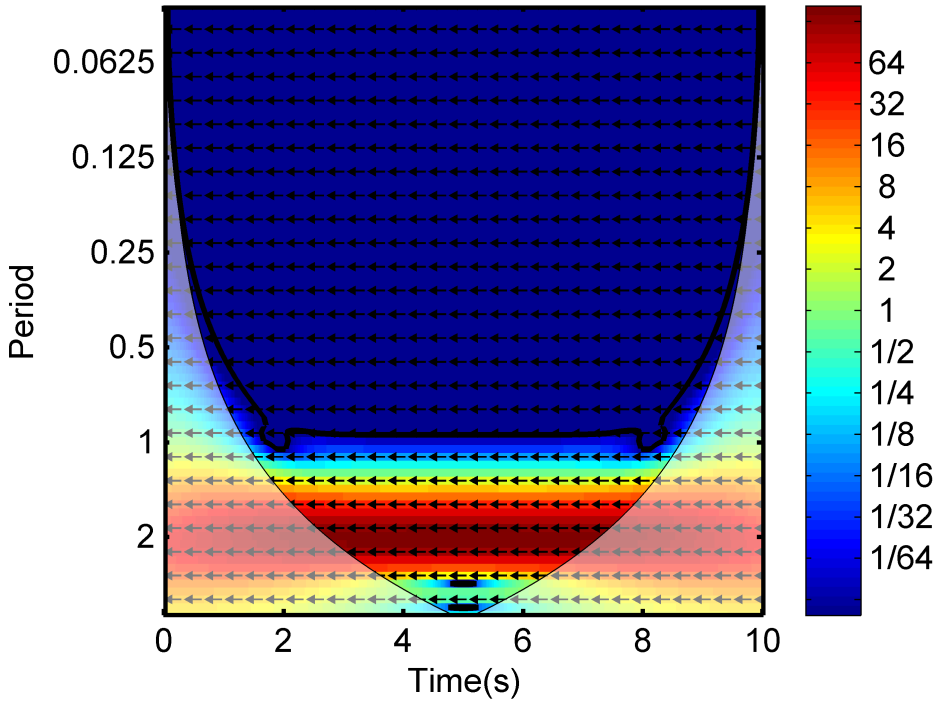

FIGURE 4.9: Cross Wavelet Transform plot between signals s_1 and s_2

used as mother wavelet for phase angle estimation. It is defined as:

$$\psi(t) = \pi^{-\frac{1}{4}} e^{i\omega_0 t} e^{-\frac{1}{2}t^2} \tag{4.22}$$

where ω_0 is the central frequency of the Morlet wavelet. For a value of $\omega_0 = 6$, it provides a decent compromise between time and frequency localization [146]. Fig. 4.9 shows the XWT plot between signals s_1 and s_2. The dark black outline indicates 5 % significance level against red noise and the *COIn* where a signals may be contaminated by edge effects. The inclination of the arrows depicts the relative phase difference between the two signals. It is observed that both signals have significant common power in the frequencies of the period of approximately 2 s (or frequencies of 0.50 Hz). Additionally, the arrows pointing leftwards indicate a 180° phase difference between the signals. Thus, it can be concluded that the two signals are non-coherent.

4.5.1 Instantaneous Phase Angle Estimation

The variations in rotor angles of the generators are reflected at all scales in wavelet spectrum. The instantaneous phase of a generator can be obtained by observing the phase

of the most dominant frequency component [147]. Therefore, the difference between instantaneous phases of two generators can manifest coherency of generators. The selection of proper scale for accurate estimation of the phase angle is vital. Dominant frequency component has been considered for this purpose. A dominant frequency component carries maximum energy among all frequencies found in the spectrum. By determining the phase of the dominant non-zero frequency component in the time domain, the swing characteristic of the machine can be obtained, and coherency of generators can be established [148]. It is defined as the ratio of Cross Wavelet Power at a particular scale to Cumulative Cross Wavelet Power across all scales. It is defined as:

$$\eta = \frac{\sum_{a=1}^{N} \left| T_{a,b}^{x,y} \right|^2}{\sum_{a=1}^{N} \sum_{b=1}^{M} \left| T_{a,b}^{x,y} \right|^2} \tag{4.23}$$

where N is the number of wavelet coefficients at scale b, and M is the number of scales. The complex argument $\arg(T_{a,b}^{x,y})$ at a scale corresponding to maximum value of η is averaged over certain duration to obtain a reasonable estimate of the instantaneous phase difference between oscillating signals using the circular mean. For a set of angles $(\varsigma_a, a = 1, 2...N)$, the circular mean is defined as:

$$\phi_m^{x,y} = \arg(\alpha, \beta) \text{ with } \alpha = \sum_{a=1}^{N} \cos(\varsigma_a) \text{ and } \beta = \sum_{a=1}^{N} \sin(\varsigma_a) \tag{4.24}$$

The phase difference of zero value indicates that signals $x(t)$ and $y(t)$ move together at the specified frequency, while the phase difference of π or $(-\pi)$ indicates an anti-phase relation between $x(t)$ and $y(t)$.

4.5.2 Proposed Phase Difference Matrix

A Phase Difference Matrix (PDM) has been proposed in this section. PDM is a consolidated matrix representing the relative phase difference between each pair of data points. For a system with N_G generators, PDM is of dimensions $N_G \times N_G$ and is defined as:

$$PDM(i,j) = \begin{cases} \phi_m^{i,j} & if\, i \neq j \\ 0 & if\, i = j \end{cases} \qquad i, j \in \{1, 2...N_G\} \tag{4.25}$$

PDM maps the coherency of generators in a $N_G \times N_G$ dimensional space. Each row of PDM represents the pairwise relative phase difference between signals. Following matrix

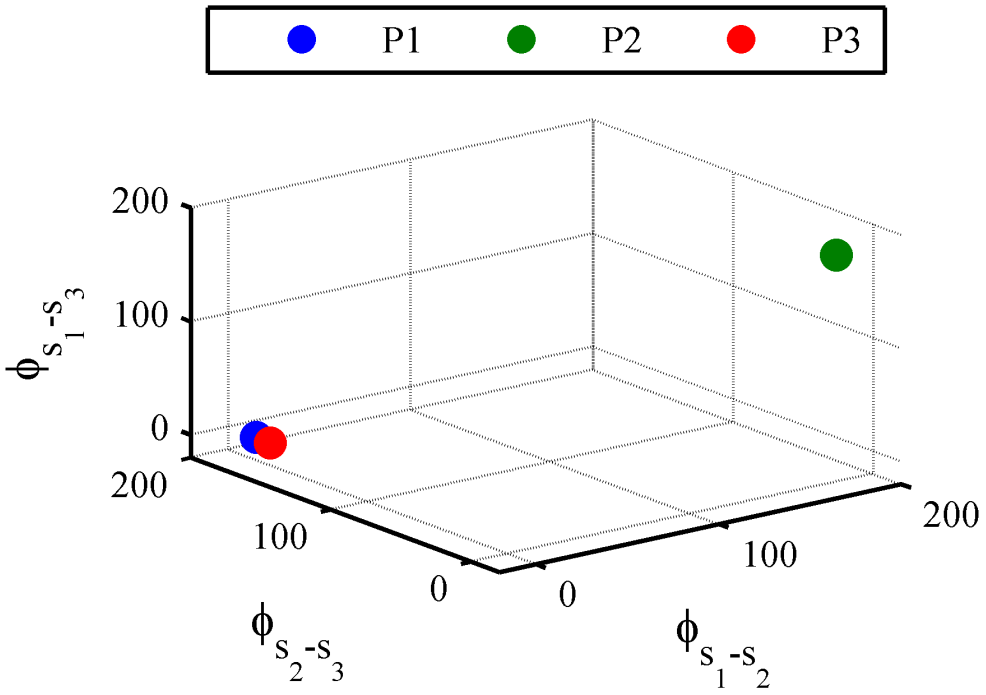

FIGURE 4.10: Relative phase difference between signals s_1, s_2 and s_3

presents the PDM of signals s_1, s_2 and s_3 discussed in the previous section:

$$PDM_{s_1,s_2,s_3} = \begin{array}{c} \\ s_1 \\ s_2 \\ s_3 \end{array} \begin{array}{c} \begin{array}{ccc} s_1 & s_2 & s_3 \end{array} \\ \begin{bmatrix} 0 & 180^\circ & 0 \\ 180^\circ & 0 & 180^\circ \\ 0 & 180^\circ & 0 \end{bmatrix} \end{array} \tag{4.26}$$

The PDM of signals in Fig. 4.7 is presented in a 3-dimensional space in Fig. 4.10. It is observed that points corresponding to coherent signals (P1 and P3) lie in proximity (overlap in this specific case) than other points. Therefore, such points can be easily clustered using any clustering algorithm. k-means algorithm has been used for clustering in this work because of its simplicity and fast response.

4.5.3 *k*-means Clustering

Clustering is an unsupervised learning technique that assorts given data points into disjoint clusters such that data points within each cluster are similar to each other and distinct from data points in other clusters. The similarity between clusters is assessed using distance

measures. k-means clustering has been used in this work to partition data points in the rows of PDM for clustering of coherent generators. k-means clustering algorithm divides N_d objects into k ($\leq N_d$) clusters such that each object is closest to the centroid of its cluster. For a given set of data points $\{\alpha_1, \alpha_2, ...\alpha_{N_d}\}$, where $\alpha_X \in \mathbb{R}^n$, $\forall X \in \mathbb{Z} : X \in [1, N_d]$, k-means finds clusters $S = \{S_1, S_2, \ldots, S_k\}$ so as to minimize the Within-Cluster Sum of Squares (WCSS) (*i.e.* variance). It is formulated as the following optimization problem [149]:

$$\arg\min_{S} \sum_{i=1}^{k} \sum_{\alpha \in S_i} \left\| \alpha_i - \mu_i \right\|^2 = \arg\min_{S} \sum_{i=1}^{k} \left| S_i \right| \text{Var } S_i \tag{4.27}$$

where μ_i is the centroid of points in cluster S_i. k-means clustering requires the number of clusters in the data set to be known beforehand. Therefore, the *elbow method* has been used to select the value of k. This method checks the percentage of variance explained by the clusters against the number of clusters. The percentage of variance explained is the ratio of the between-group variance to the total variance. The value of k where the addition of another cluster doesn't substantially increase the variance explained is adopted as the optimal value of k. We have considered k as the cluster number corresponding to 90 % of variance explained.

4.5.4 Coherent Groups in NE-39 Bus System

The proposed methodology is demonstrated on NE-39 bus test system. The dynamic models of synchronous machines and excitation systems are taken into account in the analysis. The system consists of 9-generators (G1-G9) at buses 30-38 while the system is connected to the main grid (G10) through bus 39. The fourth-order model of generators G1-G9 is considered, and G10 is modeled in third-order. It is worthwhile to mention that the coherency of generators is independent of the Fault Clearing Time (FCT) [150, 151]. Thus, an FCT that doesn't confront the stability of the system could be considered without the loss of generality.

Fig. 4.11 shows 15 s duration of varying rotor angles with respect to the COI of all the generators after a three-phase short circuit solid fault is simulated at the midpoint of transmission line 2-25 at $t = 5$ s. The fault is cleared by opening the circuit breakers at both ends of the connected transmission line after eight cycles of its inception. However, a different FCT may also be adopted as discussed previously. The XWT between each pair of rotor angles of 10 generators were obtained. Fig. 4.12 shows the XWT plot between

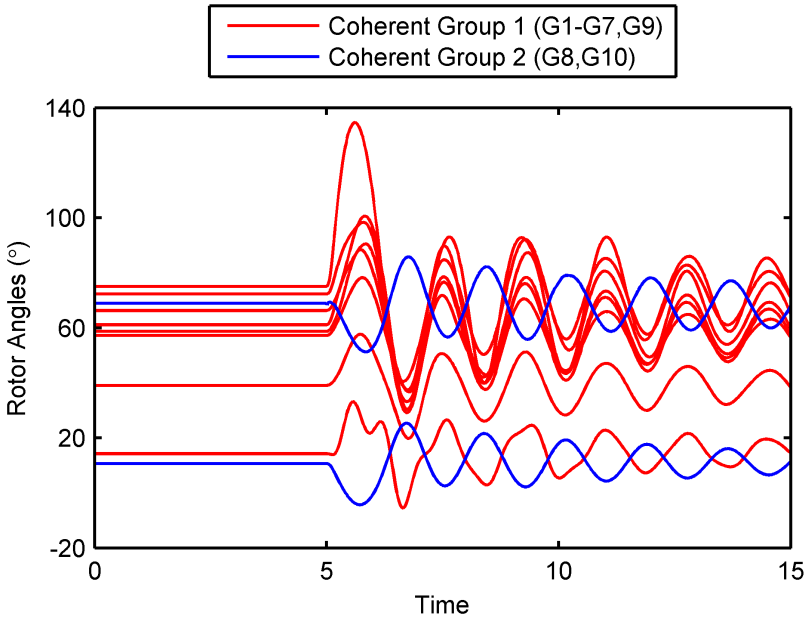

FIGURE 4.11: Rotor angle responses of 10 generators

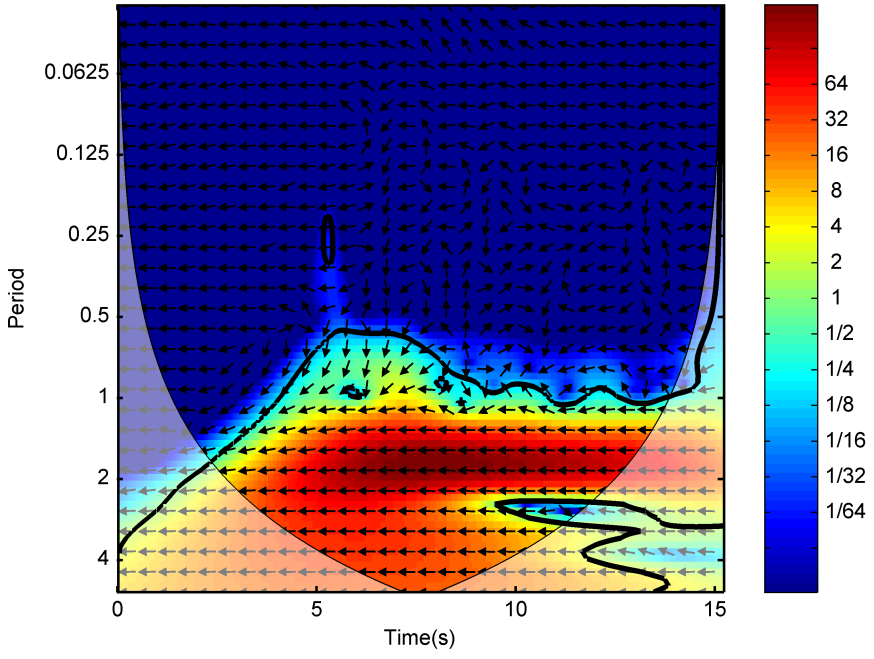

FIGURE 4.12: XWT plot between rotor angles of generators G1 and G8

rotor angle responses of generator G1 and G8. It is observed that the relative phase difference between G1 and G8 at various frequency levels is varying with time. Therefore, the

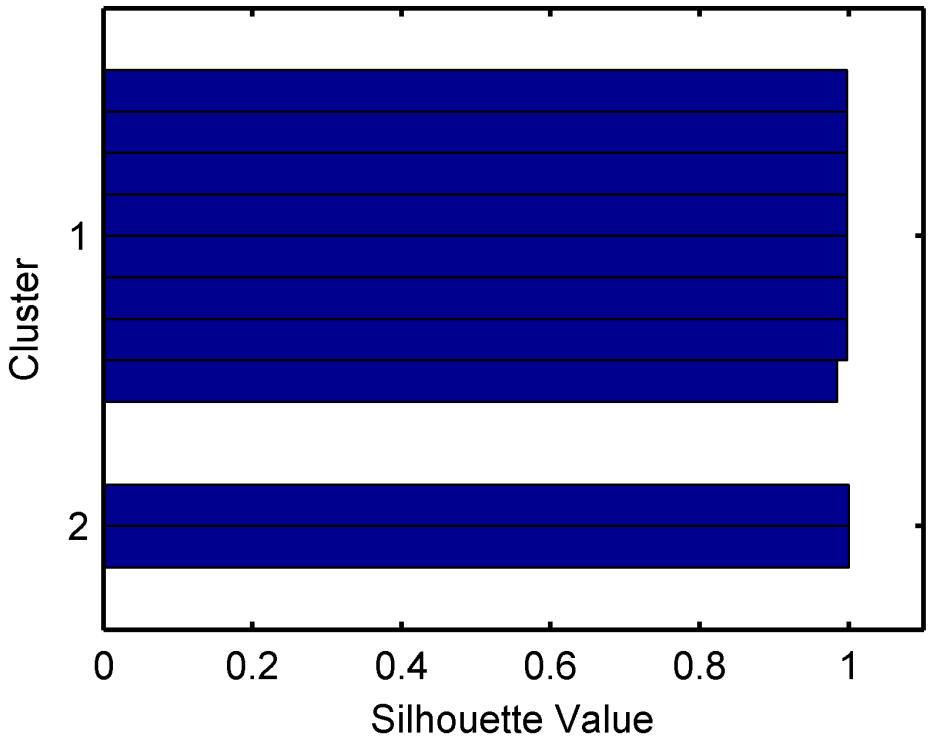

FIGURE 4.13: Silhouette Scores of the two clusters

instantaneous phase difference is determined for the frequency component with maximum common power. Equation (4.23) reveals that the highest common is in 0.5 Hz frequency component. The complex argument $\arg(T_{a,b}^{x,y})$ corresponding to 0.5 Hz component is the instantaneous phase difference between the two rotor angle signals. The relative phase difference between each pair of rotor angles is quantified using (4.24). For 10 generator system, PDM is a 10×10 dimensional matrix where each row exhibits the instantaneous phase difference between each pair of rotor angles. Each row of PDM serves as coordinates of an individual point in a 10×10 dimensional space. Thus, total 10 points are available for clustering in the dataset. Next, these data points are separated into clusters using k-means algorithm.

Fig. 4.11 shows the coherent groups and their member generators. Group 1 consist of generators G1-G7, G9 while generators G8 and G10 swing together to form another coherent group. The results can also be verified by inspection of Fig. 4.11, where rotor angles of coherent group 1 are in phase and anti-phase with rotor angles of coherent group 2. To further corroborate the efficacy of clustering, a plot showing silhouette scores from both clusters is shown in Fig. 4.13. It can be observed that scores of both clusters are close to +1, indicating that each data point is correctly grouped in its respective cluster.

4.6 Summary

The outcome of this chapter is summarized as follows:

1. A new approach for real-time automated detection, localization, and classification of events in power system using wavelet transform has been presented. It is motivated by the observation that any event will cause voltage and frequency to sharply deviate from their normal values and retain a signature post-event voltage and frequency waveform.

2. A new index formulated as the ratio of energy corresponding to wavelet detail coefficients of the present and 10 previous voltage and frequency data windows has been proposed for real-time event detection.

3. It is observed from the results that the index detects an event in the following cycle after occurrence of the event. As the variation in voltage is maximum at the location closest to the event, the wavelet energy is highest at the bus electrically nearest to the site of the event and displays a decreasing tendency as the distance from event location increases. This reveals the dispersion of disturbance in the network and facilitates the actuation of remedial measures.

4. A FFI module for quick identification of short-circuit faults is proposed. It utilizes change in voltage (ΔV) and change in frequency (ΔF) as two features to discriminate faults from other events.

5. For non-fault event, the features from both time and frequency domain are extracted from voltage and frequency waveforms, and a multiclass DSVM classifier is trained after scaling the feature vector with Z-score standardization.

6. It was observed that classifier offers poor accuracy with linear kernel and soft margins. Therefore, RBF kernel was used to transform features to higher dimensions to obtain a separating hyperplane.

7. The proposed approach improves the situational awareness and can serve as a supervisory framework for observing the activity of protective devices in the grid.

8. Identification of coherency of generators enables the power system operators in the dynamic reduction of the system for security evaluation and to take enhanced corrective measures such as controlled islanding. Two generators are called coherent if the difference between their instantaneous phases is zero.

9. XWT is used to study relation in time frequency space between two time series presented to visualize the phase relationship between their frequency components.

10. XWT approach was applied for estimation of the instantaneous phase of rotor angle oscillations after the system is subjected to a severe perturbation. It is used to study the pairwise relationship between rotor angles of generators in time-frequency space.

11. A new consolidated matrix of the relative phase difference between each pair of machines is proposed. The data-points in the matrix are clustered using k-means algorithm.

12. The validation of the results of clustering is performed by using Silhouette Score approach. It provides a measure to adjudge the appropriateness of each object within its own cluster. It is observed that scores of both clusters are close to +1, indicating that each data point is correctly grouped in its respective cluster.

13. The proposed approach aids visualization of interrelationships between coherent groups of generators in power system. The magnitude of the wavelet coefficients establishes the strength of coherency (strong or weak) between generators pairs.

In the next chapter, the impact of events on frequency and voltage stability of system has been studied and emergency control has been suggested for unstable events.

Chapter 5

Frequency and Voltage Stability Predictive Assessment and Unified Load Shedding

5.1 Introduction

A well-designed scheme is essential for real-time monitoring and protection of stability of the power system after an unanticipated event. The power system operates at equilibrium with only small but continuous variations in load demand. An event perturbs the power balance and may even jeopardize the stability of the system. The immediate knowledge of the severity and nature of the event can enable more effective countermeasures to preserve system security. The previous chapter addressed the issue of real-time event analysis. This chapter proposes a scheme for regulating critical events that endanger the frequency and/or voltage stability of the system. The aim is to identify such events at the earliest utilizing supervised learning based classification module and initiate the suitable emergency control action. The imbalances of both active and reactive power in the aftermath of an event have been utilized to predict the stability of the system. Machine learning automatically recognizes patterns in the training data and makes predictions on unseen test cases. Therefore, the approach is threshold-parameter free and can detect an impending instability before its actual manifestations are witnessed in the system. A new optimization-based formulation has been presented for estimation of reactive power imbalance from the bus-voltage magnitudes. An event classified as unstable is counteracted

by prompt load-shedding. Conventionally, load-shedding is based on frequency or voltage information independently which reduces the effect of load shedding. This work proposes a new load-shedding procedure considering both active and reactive power available in the system. The proposed scheme is tested on NE-39 bus system, and results of the load-shedding have been compared with two existing load-shedding schemes.

5.2 Overview of the Proposed Methodology

This section is devoted to the development of a supervised machine learning reinforced diagnostic tool for identification of imminent instability due to critical events. The objective of using machine learning is to predict the future response of the system by learning patterns from previous characteristics instead of using pre-determined rules. A classification module has been proposed to differentiate stable events from events leading to frequency and/or voltage instability. The module aims to achieve maximum classification accuracy using a minimum number of features to ensure quick response and minimal complexity. In case an event is assessed as unstable, load shedding is initiated to obtain stable operating condition.

5.2.1 Simultaneous Monitoring of Frequency and Voltage Stability

An event may result in a gradual increase in angular difference among generators, a decline of bus voltages, or rapid variations in system frequency [152] and can also cause unpredictable cascading failures, leading to complete power system blackout. The prompt initiation of remedial actions such as load shedding, islanding, etc. can avoid instability arising due to the disturbance. The knowledge of the severity of the event is essential to create more secure and self-healing power grids. The focus of this section is real-time estimation of both active and reactive power imbalance in the system following a major event.

5.2.1.1 Estimation of Active Power Imbalance

The imbalance of active power instigated due to an event in the system is reflected in rotor speeds of the generators, and consequently in the frequency measured at the generator buses. The frequency at the COI, f_c, signifies the average dynamic response of all

generating machines to an immediate event. It is expressed as:

$$f_c = \frac{\sum_{G=1}^{N_G} H_G \times f_G}{\sum_{G=1}^{N_G} H_G} \tag{5.1}$$

where H_G and f_G are the inertia constant and the frequency of the G^{th} generator respectively and N_G is the total number of generators. The synchronizing oscillations of individual machines are filtered out in f_c and it retains the mean frequency behavior of an equivalent single machine. The Active Power Imbalance (API), ΔP, is determined from the initial ROCOF at the COI immediately after the event using the swing equation as follows:

$$\Delta P = 2 \times \frac{\sum_{G=1}^{N_G} H_G \times \left(\frac{\Delta f_c}{\Delta t}\right)}{f_n} \tag{5.2}$$

where f_n is the nominal frequency of the system, and $\Delta f_c/\Delta t$ is the discrete derivative of frequency at COI with time. Both ΔP and f_c are calculated immediately after the event from real-time frequency measurements obtained from PMUs.

5.2.1.2 Estimation of Reactive Power Imbalance

An unanticipated event causes the imbalance of reactive power in the system. Both deficit and surplus reactive power are equally harmful. While deficiency of reactive power causes undervoltage and may invite voltage instability; surplus reactive power causes overvoltage at buses and excessive magnetic flux in generators and transformers, resulting in tripping due to V/Hz protection. Events such as generator outage, capacitor/reactor outage incite the imbalance of reactive power and can contribute to the failure of the power system if corrective measures are not initiated promptly. The estimate of reactive power lost after an event can help undertake quantified countermeasures.

Unlike active power, whose principal source is generating units, the reactive power has multiple sources and sinks. It is produced as well as consumed in synchronous generators, transmission lines, and secondary reactive power support devices such as capacitors and synchronous condensers. The power lost due to an event is distributed between remaining devices in service. Thus, the estimation of Reactive Power Imbalance (RPI) is a complicated task. In this thesis, a new method has been proposed for calculation of the amount of reactive power shortage in the aftermath of an event during the transient condition.

RPI has been defined as the amount of reactive power, ΔQ, injected at the event bus to restore post-event voltage to pre-event voltage at all buses.

$$\Delta Q = \left\{ \varphi | \varphi = \arg\min_{\varphi} \left(\sum_{l=1}^{N_B} (V_l^{LF} - V_l^0)^2 \right), \forall\ l \in N_B \right\} \tag{5.3}$$

where V_l^{LF} and V_l^0 denote ad hoc bus voltage variable and pre-event voltage at l^{th} bus respectively. The problem of RPI estimation is formulated as the minimization of the difference between these two voltages at all buses subject to system constraints as illustrated below:

$$Objective\ fn. : \min \sum_{l=1}^{N_B} (V_l^{LF} - V_l^0)^2 \tag{5.4}$$

subject to power balance constraints:

$$P_l - \sum (V_l^{LF} V_m^{LF} (G_{lm} \cos\delta_{lm} + B_{lm} \sin\delta_{lm})) = 0;\ \forall\ l \in N_B \tag{5.5}$$

$$\varphi + Q_l - \sum (V_l^{LF} V_m^{LF} (G_{lm} \sin\delta_{lm} + B_{lm} \cos\delta_{lm})) = 0;\ l = B^{Ev} \tag{5.6}$$

$$Q_l - \sum (V_l^{LF} V_m^{LF} (G_{lm} \sin\delta_{lm} + B_{lm} \cos\delta_{lm})) = 0; \forall\ l \in N_B;\ l \neq B^{Ev} \tag{5.7}$$

where:

P_l & Q_l	Post-event active and reactive power injection at l^{th} bus;
G_{lm} & B_{lm}	Real and imaginary parts of element lm in bus admittance matrix;
δ_{lm}	difference between voltage angles of l^{th} and m^{th} bus.

The event bus is the one where maximum deviation in voltage occurs, and is determined using (5.8) [153].

$$\text{Suspected Event Bus} : B^{Ev} = \arg\max_{l \in [1,2,..N_B]} \Big(|\Delta V_l[t]| \Big) \tag{5.8}$$

where ΔV_l is the change in voltage calculated using the backward-difference approach between real-time consecutive voltage samples obtained from PMUs. The event bus is modeled as a load bus in both (5.5) and (5.6). The proposed formulation is a nonlinear optimization problem, and has been solved using quasi-Newton approach.

Apparent Power Imbalance, ΔS, in the system is expressed as the sum of ΔP and ΔQ as shown below:

$$\Delta S = \Delta P + j * \Delta Q = \Big| S \Big| \cos\Psi \tag{5.9}$$

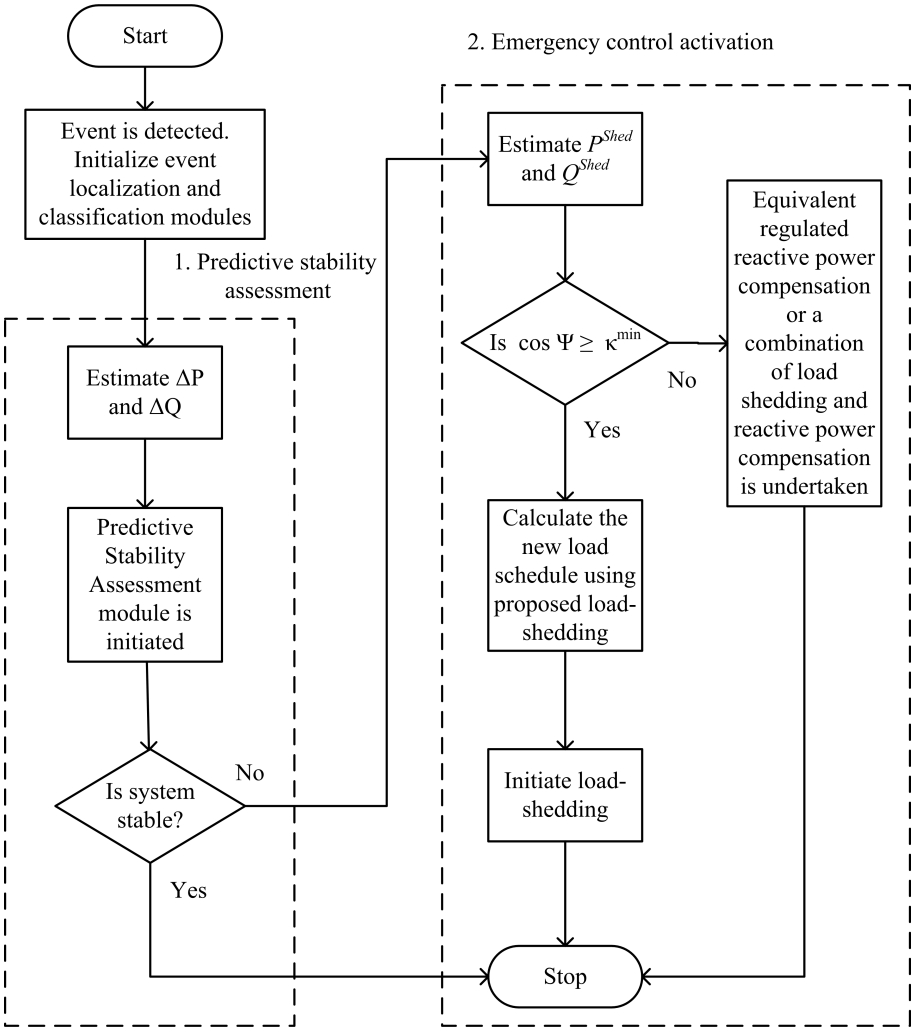

FIGURE 5.1: Flowchart of the proposed stability assessment and emergency control approach

Load shedding equivalent to ΔS will restore system states to pre-event values.

5.2.2 Supervised Learning Based Predictive Stability Assessment Module

In this thesis, supervised learning classification has been used to propose a Predictive Stability Assessment (PSA) module to classify an event as stable or unstable. Thus, it is a problem of binary classification. After an event has been detected and classified using the approaches proposed in previous chapter, PSA module is initiated. It analyzes both active and reactive power imbalances in the system evoked by an event and predicts if the

event belongs to *Stable* or *Unstable* class. Fig. 5.1 shows the flowchart of the complete scheme.

A crucial challenge in supervised machine learning is the selection of an appropriate classifier. The choice of a classifier is subject to the characteristics of data-set being considered, response time and available computation overhead. As aforementioned, the utility of a classifier in this problem is binary classification. Single layer perceptron, Logistic Regression, Decision Trees, and Naive Bayes are commonly used binary classification algorithms. A single layer perceptron and Logistic Regression are suitable for learning only linearly separable decision boundaries while Decision Trees are preferable when the decision boundary is piece-wise linear. Naive Bayes classifier assumes the features in dataset to be independent of each other. Considering the limitations of these classifiers, SVM is applied for real-time classification application. SVM offers high accuracy, low-overfitting, and can classify data which is not linearly separable in the base feature space by transforming it in higher dimensions using a kernel function. An introduction to SVM has been already provided in Section 4.3.5.2.

5.3 Emergency Control Activation: Proposed Frequency and Voltage Stability Unified Load Shedding

The prompt initiation of a remedial scheme can limit the adverse consequences of an event and prevent a potential blackout. The decline in frequency caused by the API could lead to tripping of steam-turbine governed generators by under-frequency relays, thus worsening the situation further. The imbalance of power instigated by an event can be sufficed immediately by increasing the generation, only up to the limits of spinning reserve available. Also, a thermal unit can initially pick-up a load of about 10 % of rated turbine output followed by an increase of 2 % per minute without causing damage to the turbine [138]. Therefore, a centralized adaptive Frequency and Voltage Stability Unified (FVSU) load shedding scheme has been proposed in this thesis, as an emergency countermeasure against an event that is classified in *Unstable* class by the PSA module. It is based on the observation that most approaches to load shedding are API-driven, *i.e.*, the amount of active power to be shed at a bus is determined while the reactive load is shed proportionally keeping the ratio of active load to reactive load constant at the bus irrespective of the reactive power lost in an event. This leads to an imbalance between reactive load and reactive power generation causing poor voltage profile at load buses. Conversely, the proposed FVSU load shedding is based on the power factor of apparent

power imbalance which signifies both API and RPI. It aims to shed more load at buses where load power factor is closer to the power factor of apparent power imbalance. Thus, the maximum balance of power between generation and load is maintained after the event. The amount of load shed can be reduced by shedding the minimum load such that the frequency at COI does not drop below a preset critical value. After the sudden loss of generation, remaining generators share the imbalance in proportion to their inertia for equal droop speed control [138]. Thus, the incremental load on generator G is expressed as:

$$P_G^{Inc} = 1.05 \times (\Delta P - P^{Critical}) \times \frac{H_G}{\sum_{G=1}^{N_G} H_G} \tag{5.10}$$

where $P^{Critical}$ is maximum API for which frequency does not falls below a critical threshold F^{min}. The factor of 1.05 is included to counterbalance the approximation involved in linear System Frequency Response (SFR) model [23]. When P_G^{Inc} is more than the maximum turbine output of a generator, it is included in the load to be shed. Accordingly,

$$P^{Shed} = 1.05 \times (\Delta P - P^{Critical}) + \sum_{G=1}^{N_G} \max(\tau_G^{max} - (P_G^{g_0} + P_G^{Inc}), 0) \tag{5.11}$$

where τ_G^{max} and $P_G^{g_0}$ are maximum turbine output and initial generation of generator G. The reactive power to be shed Q^{Shed} is determined by proportional reduction of ΔQ as below:

$$Q^{Shed} = P^{Shed} \times \frac{\Delta Q}{\Delta P} \tag{5.12}$$

The proposed emergency control scheme determines power factor of the apparent power imbalance, $cos\ \Psi$, using ΔP and ΔQ. The magnitude of $cos\ \Psi$ suggests about the nature of the event, a value close to 1 indicates active power event, while a reactive power event is suspected when it is close to 0. A definite threshold, κ^{min} has been considered to discriminate between the two types of events. For $cos\ \Psi \geq \kappa^{min}$, the event is considered as an active power event; otherwise, it is treated as reactive power event. The value of κ^{min} is taken as 0.7071, which corresponds to $\Delta P = \Delta Q$. In this work, load shedding has been suggested only for active power events, while regulated reactive power compensation or a combination of load shedding and reactive power compensation may be undertaken depending upon the available reactive power support and experience of the operator. The proposed load shedding scheme sheds more load from load buses with power factor closer to $cos\ \Psi$. It has been formulated as an optimization problem which minimizes the difference between $cos\ \Psi$ and power factor of load bus $cos\ \phi_l^{L_0}$, and is solved using 'interior-point'

algorithm. It is expressed as under:

$$Objective\ fn.: \min \sum_{l=1}^{N_L} \left(\cos\ \Psi - \cos\ \phi_l^{L_0}\right)^2 \tag{5.13}$$

subject to:

(a) Load-shed constraint:

$$0 < \chi_l^{P_L} < P_l^{L_0}; \forall\ l \in N_L \tag{5.14}$$

$$0 < \chi_l^{Q_L} < \left|Q_l^{L_0}\right|; \forall\ l \in N_L \tag{5.15}$$

(b) Constant power-factor constraint:

$$\chi_l^{P_L} - \frac{\chi_l^{Q_L}}{\tan \phi_l^{L_0}} = 0; \forall\ l \in N_L \tag{5.16}$$

(c) Active power shed constraint:

$$\sum_{l}^{N_L} \chi_l^{P_L} = \sum_{l}^{N_L} P_l^{L_0} - P^{Shed} \tag{5.17}$$

where:

$\cos\ \Psi$ & $\cos\ \phi_l^{L_0}$	Power factors of apparent power imbalance and load at l^{th} load bus;
$P_l^{L_0}$ & $Q_l^{L_0}$	Initial active and reactive components of load at l^{th} load bus;
$\chi_l^{P_L}$ & $\chi_l^{Q_L}$	Ad hoc decision variables for active and reactive load at l^{th} load bus;
N_L & $\phi_l^{L_0}$	Total number of load buses and initial angle subtended between active power and apparent power at l^{th} load bus;
P^{Shed}	Amount of active power load to shed.

The constraints (5.14) and (5.15) ensure that the final load is less than the initial load at l^{th} bus. Eq. (5.16) is the linearized variant of constraint enforcing that the power factor at load buses remain constant even after load shedding. The absolute value of $Q_l^{L_0}$ is used in (5.15) as the upper bound on new reactive load rather than its actual value. Capacitors banks are installed at certain buses to inject reactive power locally into the system. The value of $Q_l^{L_0}$ is negative at such buses. When the system operator resorts to load curtailment, reactive power injection must also be reduced; else there will be the surplus reactive power. $|Q_l^{L_0}|$ modifies the injected reactive power to an equivalent inductive load

consuming reactive power. Thus, the new reactive load at l^{th} bus indicates the decreased reactive power injected by capacitor bank.

The active and reactive components of the new load schedule at l^{th} load bus after proposed load-curtailment are:

$$P_l^L = \chi_l^{P_L} \tag{5.18}$$

and

$$Q_l^L = \begin{cases} \chi_l^{Q_L} & \text{if } sgn(Q_l^{L_0}) = +1 \\ -\chi_l^{Q_L} & \text{if } sgn(Q_l^{L_0}) = -1 \end{cases} \tag{5.19}$$

Eq. (5.19) ensures that both injected and consumed reactive powers are shed.

5.4 Results and Discussion

The effectiveness of the proposed methodology is demonstrated on NE 39-bus test case. The complete data of the system is available in Appendix A. The dynamic models of synchronous machines and excitation systems are taken into account in the analysis as discussed in the previous chapter. The dynamic simulation was performed in PSAT toolbox [142] on MATLAB R2010a [143] platform of a Windows 7 computer with a Core *i5* CPU and 4 GB of usable RAM. The system is completely observable by PMUs installed in the grid at locations suggested in Chapter 3. The reporting rate of PMUs to the centralized control center is 60 samples/s. A latency of 100 ms due to the communication lag between PMUs and the central control location is considered [117]. White Gaussian noise with zero mean and SNR 45 has been added to all measurements to emulate noise present in actual PMU data [144]. NE-39 bus system has 9 generators at buses 30-38, and one aggregate generator of a large number of generators at bus 39, which has been considered as slack bus. The system consists of 18 load buses and 42 transmission lines. The base apparent power rating and the nominal frequency of the system are 100 MVA and 60 Hz respectively. The active power imbalance for which the frequency does-not fall below its critical threshold of 59 Hz determined using SFR model is 3.95 p.u.

5.4.1 Dataset Generation

The proposed PSA module is a supervised learning based method, *i.e.*, it is first trained offline with sample data before its online implementation. Once trained, it can analyze an unseen input data point to make predictions about the event. The event dataset was

TABLE 5.1: Composition of dataset

Event	Specification	Location	No. of cases
Fault	8-cycle	All zero-injection, load buses and mid-points of transmission lines	11+18+42=71
Generator outage	Sudden generation loss	Generator buses	9
Load rejection	Sudden load loss	Load buses	18
Industrial load starting	25% fluorescent lighting and 75% small induction machines [154]	Load buses	18
Shunt capacitor outage	Reactive load increased keeping the PF of load at unity approximately	Load buses	18×5=90
Loading levels considered=3		Total cases	206×3=618

generated by simulating multiple instances of events listed in Table 4.1. The dataset for generator outage, and load rejection was simulated by the abrupt rejection of each generator and load individually from the system during operation. Similarly, three-phase faults, each of 8 cycles and varying fault impedance, were simulated at all zero-injection buses, load buses and at mid-point of each transmission line. Shunt capacitors and reactors of variable rating were placed at load bus keeping its power factor to unity approximately, and data was recorded after their sudden elimination. The industrial loads were modeled as 25% fluorescent lighting and 75% small induction machines [154]. An equivalent fifth-order induction motor was installed at load bus, and start-up transient of the motor were recorded. Three levels of loading were considered as 0.9, 1.0, and 1.1 times of base case, and each event was simulated at all loading levels. As detailed in Table 5.1, total 618 events were simulated and labelled as *Stable* or *Unstable* for PSA module. Events resulting in either decline of frequency below F^{min} or singularity of system Jacobian matrix were labelled as *Unstable* [155]. Synchronized voltage and frequency readings available from PMUs in each case were recorded. The dataset was randomly shuffled and partitioned into 5 equal size sub-datasets for 5-fold cross-validation. Next, 4 sub-datasets were used in training the classifier, and the remaining sub-dataset was used to test the performance of the trained classifier. The procedure was repeated 5-times with a new sub-dataset used for validation.

5.4.2 Classification Results of Predictive Stability Assessment Module

The proposed PSA module classifies an event in *Stable* or *Unstable* class using API (ΔP) and RPI (ΔQ) as two features. Fig. 5.2 shows data points from both classes on $\Delta P - \Delta Q$ plane. Events like industrial load starting, and reactor outage didn't pose any threat to the stability of the system; hence, they were neglected in the stability assessment. From the

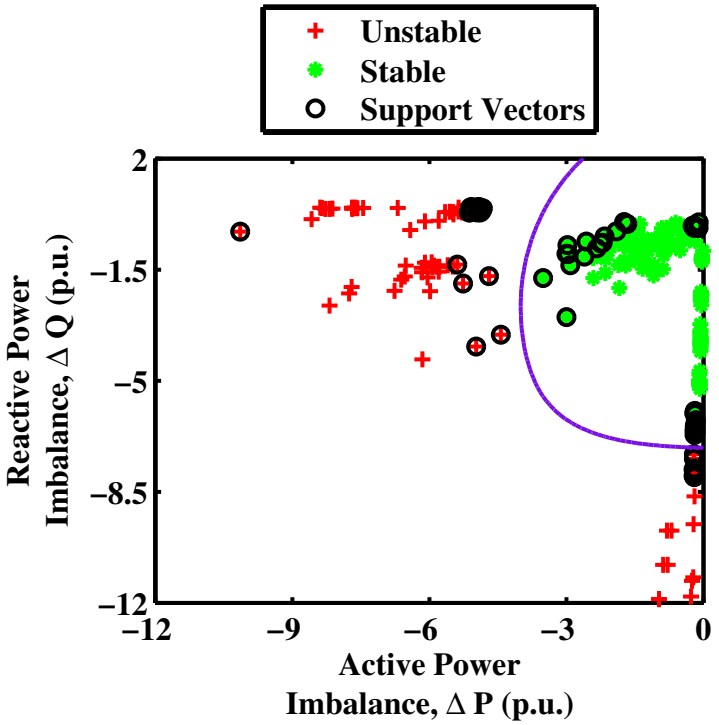

FIGURE 5.2: Decision boundary between *Stable* and *Unstable* classes for PSA module

TABLE 5.2: Confusion matrix of Predictive Stability Assessment module

	Predicted	
Actual	Stable	Unstable
Stable	0.99	0.01
Unstable	0.06	0.94
Accuracy	96.5 %	

figure, it can be visually inspected that the two classes are inseparable by a linear hyperplane. This was also confirmed as SVM failed to converge within the maximum number of iterations using hard margins [145]. Non-separable features often become linearly separable after they are mapped to a high dimensional feature space. Subsequently, soft margins along with Radial Basis Function (RBF) kernel were used for training. From the figure, the two classes can be observed to be distinguished by means of a blue non-linear hyperplane which represents the decision boundary at maximal distance to both classes. The performance of the classifier was 5-fold cross-validated with features from testing sub-dataset and results are presented in Table 5.2 as a cumulative confusion matrix. It is observed that the classifier separates the two classes with 96.5% accuracy.

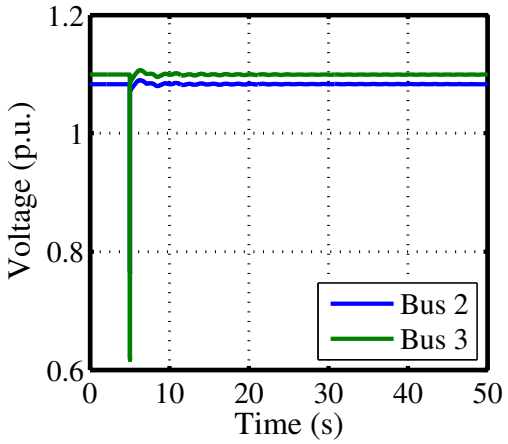

(a) Voltage variation at bus 2 and 3

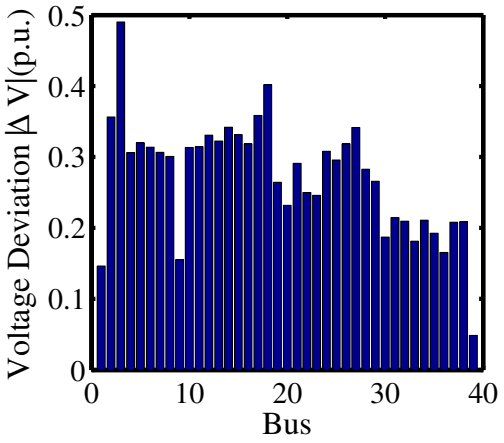

(b) Suspected Fault Bus

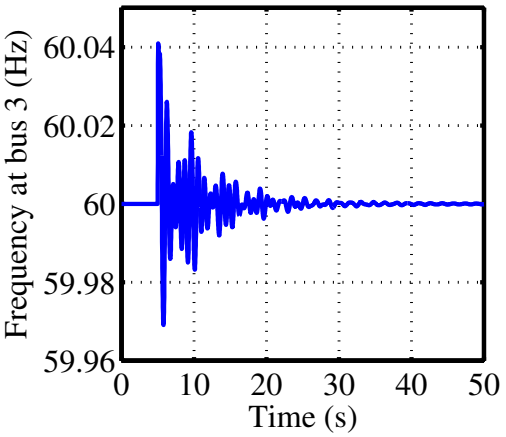

(c) Frequency variation at bus 3

FIGURE 5.3: Case (a)-3 phase fault at midpoint of transmission line 3 in NE-39 bus system

5.4.3 Event Analysis and Proposed Load Shedding

Three representative cases of events in NE-39 bus system have been presented in this section.

5.4.3.1 Case (a)-3 phase fault at midpoint of transmission line 3

The transmission line 3 between bus 2 and bus 3 is delivering 3.78 p.u. of active power and 0.033 p.u. of reactive power from bus 2 to bus 3. A three-phase solid fault is simulated at its midpoint at $t = 5$ s. The voltage at both bus 2 and 3 decline drastically to 0.75 and 0.61

p.u. respectively immediately after the fault as observed in Fig. 5.3(a). The event detection algorithm continuously monitors the real-time PMU data at the centralized control center for events. The fault suspicion criterion calculated by (4.12) is found to be violated at $t = 5.0167$ s indicating the occurrence of a fault. As discussed earlier, the FFI module is initiated to confirm the fault. Fig. 5.3(b) shows the absolute deviation in voltage at $t = 5.0167$ s at all buses in the system. It may be noted that voltage deviation at bus 2 is lower than bus 3 as bus 2 holds more voltage control capability than bus 3, because of its direct connection to the generator at bus 30. Fig. 5.3(c) shows the increase in frequency at $t = 5^+$ s at bus 3. The change in voltage $\Delta V = -0.49$ p.u. and frequency $\Delta F = 0.04$ Hz or 0.67×10^{-3} p.u. at bus 3 are used as input features. The classifier confirms the fault, and the transmission line is opened instantly at $t = 5.04$ s, *i.e.*, within 2 cycles of the nominal frequency. The impact of the contingency on system stability is assessed by PSA module. API $\Delta P = 0.26$ p.u. and RPI $\Delta Q = 0.002$ p.u. are observed in the system after the event. The values of ΔP and ΔQ are low because opening the transmission line merely results in the rerouting of power. Therefore, PSA module predicts the event to be stable and, no further action is required.

5.4.3.2 Case (b)-Generator outage at bus-32

The generator at bus 32 is injecting 6.50 p.u. of active power and 2.17 p.u. of reactive power into the system. As shown in Fig. 5.4(a), the frequency of the system is stable at 60 Hz till $t = 5^-$ s. The sudden outage of the generator at $t = 5$ s transfers the load on other generators. During the initial transient phase, the increase in output of remaining generators is inversely proportional to the reactance between them and location of generation loss [138]. The additional load on generators is essentially served by the angular kinetic energy stored in their rotor because the turbine governor mechanism responds relatively slowly. This results in deceleration of rotors causing the frequency at COI to drop as observed in Fig. 5.4(a). The incremental load on the generator at bus 33 exceeds its maximum turbine output. Thus, its power output reaches maximum limits within its capability curves resulting in other generators being even more burdened. The situation is further deteriorated as Automatic Voltage Regulator (AVR) gains of generators at bus 34 and bus 38 are set too low to respond to increase in load. Consequently, both generators lose their voltage control capability causing reactive power deficiency in the system, and complete voltage collapse occurs at $t = 15.6$ s. ΔP caused by the event is shown in Fig. 5.4(b). The voltage variation at few weak buses selected on basis of proximity to voltage

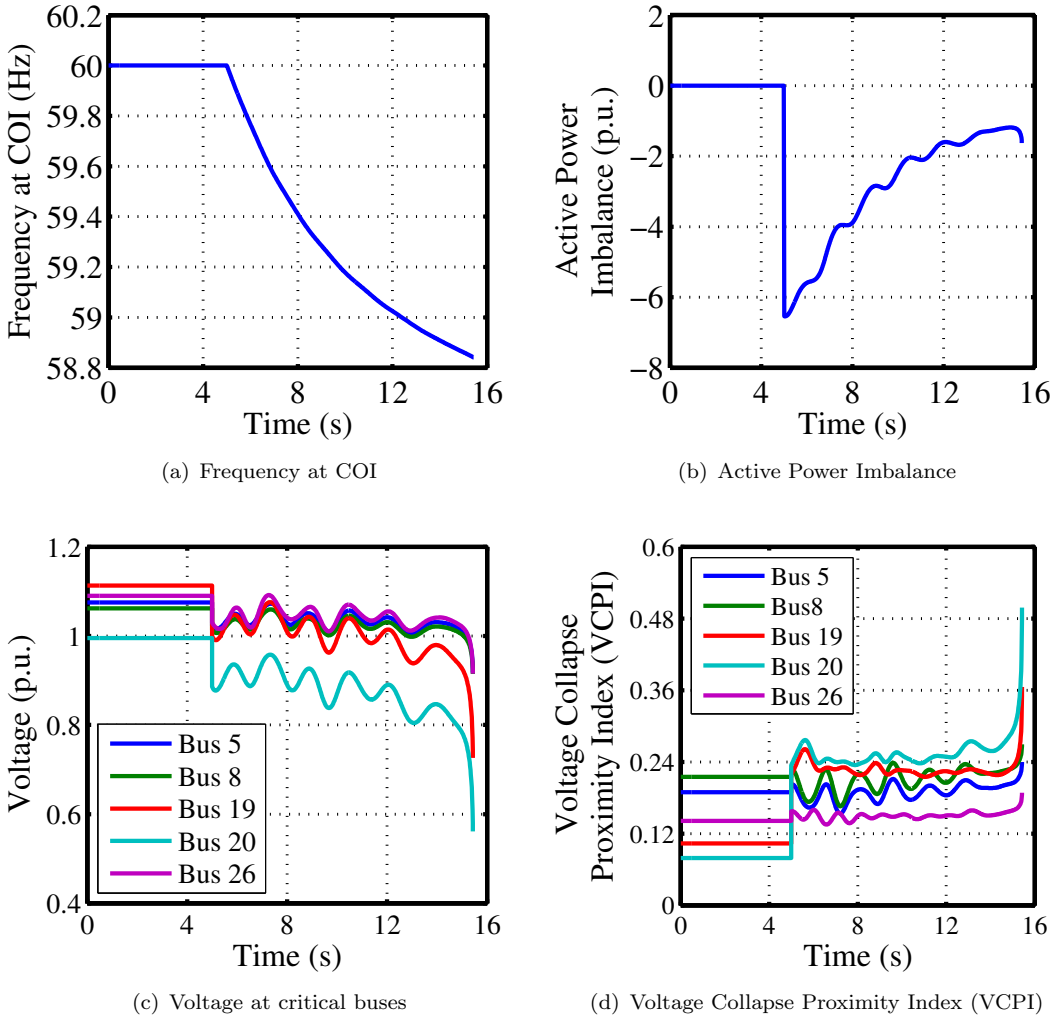

(a) Frequency at COI

(b) Active Power Imbalance

(c) Voltage at critical buses

(d) Voltage Collapse Proximity Index (VCPI)

FIGURE 5.4: Case (b)-Generator outage at bus 32 in NE-39 bus system

collapse using CPF [84] is shown in Fig. 5.4(c). The voltage stability of the system is assessed using Voltage Collapse Proximity Index (VCPI) at critical buses as shown in Fig. 5.4(d). It is observed that voltage collapse takes place much before VCPI can achieve its expected value of 1. It indicates the inefficiency of VCPI for dynamic voltage stability assessment where the voltage collapse is mostly due to limit-induced bifurcation rather than saddle-node bifurcation.

This voltage collapse could be prevented by utilizing the proposed scheme. As soon as the event is detected and classified, API and RPI are calculated using (5.2) and (5.4) respectively. ΔP and ΔQ are found to be 6.67 p.u. and 2.18 p.u. respectively. They are fed as inputs to PSA module which predicts the event to be unstable. Thereafter, load shedding presented in Section 5.3 is initiated at $t = 5.72$ s as an emergency countermeasure

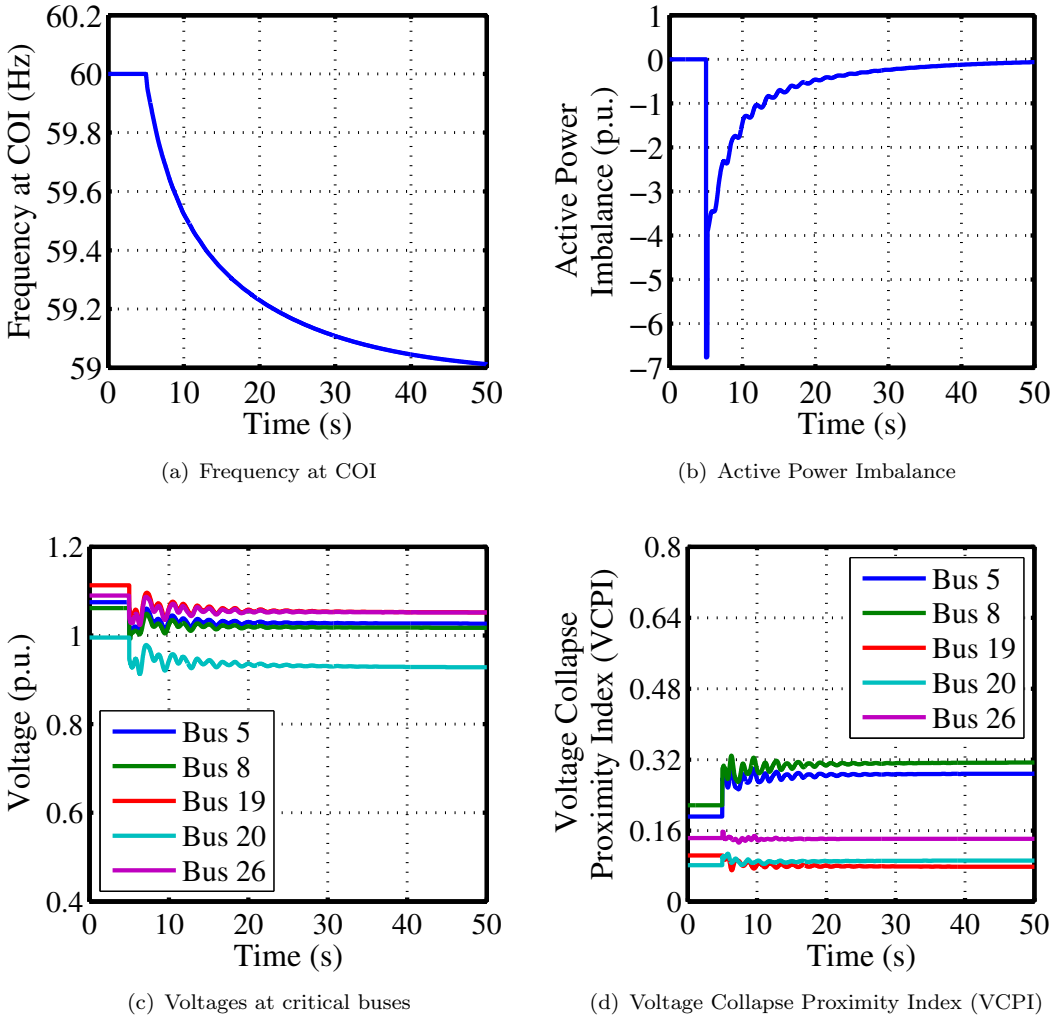

(a) Frequency at COI

(b) Active Power Imbalance

(c) Voltages at critical buses

(d) Voltage Collapse Proximity Index (VCPI)

FIGURE 5.5: Case (b)-Generator outage at bus 32 in NE-39 bus system followed by load shedding

to attain a stable operating equilibrium. The power factor of apparent power imbalance is calculated from ΔP and ΔQ as $cos\ \Psi = 0.9505$. The proposed load shedding scheme aims to shed minimum load to stabilize the frequency and voltage within acceptable limits. Buses with power factor closer to $cos\ \Psi$ are subjected to more curtailment of the load. The load schedule before and after load shedding is given in Table 5.3. It may be observed that power factor of the bus remains unchanged before and after load shedding. Also, the reactive power injection at bus 24 has reduced from 0.92 p.u. to 0.87 p.u. The frequency at COI after load shedding sustains at approximately 59 Hz as observed in Fig. 5.5(a). It may be noted that difference between nominal, and steady-state frequency is due to the intentional difference of 3.95 p.u. kept between API and P^{Shed} in (5.11). The difference can be recovered by turbine governor action. The corresponding API converged to 0 after

load shedding as seen in Fig. 5.5(b). Similarly, the voltages and VCPI are observed to settle down at acceptable values as visible in Fig. 5.5(c) and (d).

The performance of the proposed scheme is compared with conventional UFLS [138] and Voltage Deviation Proportionate Load Shedding (VDPLS) [94, 117] and results are presented in Table 5.4. UFLS is a predetermined rule based approach that sheds definite quantum of the load when frequency falls below preset thresholds, irrespective of the magnitude of the event. In VDPLS, the API is divided between load buses in proportion to change in voltage after the event. In this work, the amount of load shed in VDPLS has been considered equal to P^{Shed} and is initiated when load bus voltages decrease below 0.8 p.u., which is the conventional threshold for under-voltage load shedding [117]. The power factor of the load bus has been assumed to remain unchanged before and after load shedding in each method.

As aforementioned, UFLS and VDPLS have been exercised when frequency at COI and load-bus voltage decline below 59 Hz and 0.8 p.u. respectively. On the contrary, the proposed load shedding scheme is initiated immediately after it is classified as *Unstable* and load shedding optimization is solved. The involved calculation is simple and introduces only a minuscule time delay. Therefore, time of initiation of the proposed scheme is earlier

TABLE 5.3: Load schedule before and after proposed load shedding for Case (b)

Bus	Initial load (p.u.)		Final load (p.u.)	
No.	Active load ($P_l^{L_0}$)	Reactive load ($Q_l^{L_0}$)	Active load (P_l^L)	Reactive load (Q_l^L)
3	3.22	0.02	3.05	0.02
4	5.00	1.84	4.83	1.78
7	2.34	0.84	2.18	0.78
8	5.22	1.76	5.05	1.70
12	0.08	0.88	0.05	0.49
15	3.20	1.53	3.05	1.45
16	3.29	0.32	3.12	0.31
18	1.58	0.30	1.43	0.27
20	6.28	1.03	6.11	1.00
21	2.74	1.15	2.57	1.08
23	2.48	0.85	2.31	0.79
24	3.90	-0.92	2.92	-0.87
25	1.39	0.47	2.08	0.44
26	2.81	0.17	1.24	0.15
27	2.06	0.76	2.65	0.71
28	2.84	0.28	1.90	0.26
29	2.84	0.27	2.67	0.25
39	11.04	2.50	10.91	2.40

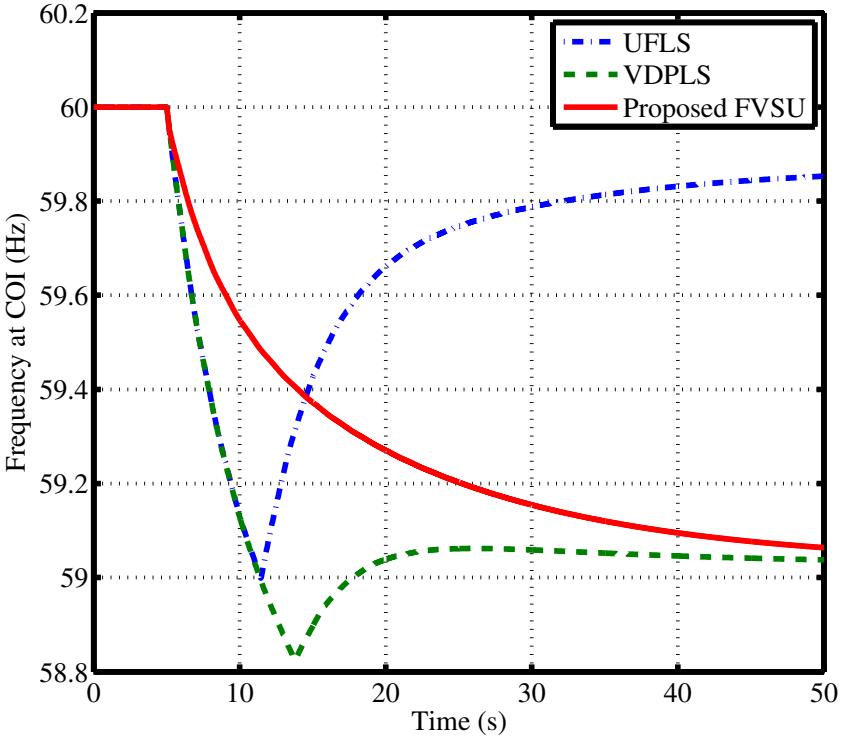

FIGURE 5.6: Frequency restoration after various load shedding schemes in NE-39 bus system for Case (b)

TABLE 5.4: Comparison among load shedding methods on NE-39 bus system for Case (b)

	UFLS [138]	VDPLS [94, 117]	Proposed FVSU load shedding
Time of initiation after event (s)	7.5§	9.8*	0.72
Active load shed (p.u.)	6.0879	2.7676	2.7676
Steady-state frequency at COI (Hz)	59.85	59	59
Maximum % deviation in mean load bus voltage	14.0024	22.36	5.6319
Steady-state error % in mean load bus voltage	0.6470	16.6290	3.2021
Secondary check required	Yes	Yes	No

§ Initiated when $f_c < 59$ Hz
* Initiated when $V < 0.8$ p.u.

than UFLS and VDPLS as provided in Table 5.4. UFLS sheds 10 % of the total load in the area (equivalently, 10 % on each load bus). For the event under discussion, the actual loss of generation was 6.5 p.u. while UFLS shed 6.0879 p.u. of active load. Hence, the

frequency at COI has been maintained at 59.85 Hz, slightly lower than nominal frequency. In both VDPLS and proposed schemes, an adequate amount of load is shed to limit frequency above 59 Hz. The variation of frequency after each load shedding scheme is illustrated in Fig. 5.6. It is observed that frequency settles closer to its nominal value in UFLS than VDPLS and proposed UVFS load shedding; however the amount of load shed in UFLS is more. Thus, it is economically disadvantageous to the system operator. Another disadvantage of VDPLS was also noted during the investigation. Load buses which undergo more voltage change receive more share of P^{Shed} to shed. For certain buses, this share may even exceed the amount of actual load on the bus. For instance, in the considered case, voltage reduction at bus 12 after the event is higher than other buses because of its relative electrical proximity to event bus 32. Correspondingly, it received more share of P^{Shed}, which was found to be more than its load. This could pose a major bottleneck in real-time operation. In the presented case, the share of P^{Shed} at bus 12 was shed at the bus next in the hierarchy of voltage drop.

Bus voltages continue to decrease during the time elapsed in undertaking UFLS and VDPLS. The proposed FVSU load shedding requires information of initial drop in voltage and frequency only and, is initiated immediately after new load schedule is calculated from ΔP and ΔQ. Therefore, the maximum deviation in mean load bus voltages in FVSU load shedding is significantly less than UFLS and VDPLS. The difference between the steady-state error in mean load bus voltages is also presented in Table 5.4. UFLS restores voltages to pre-event level by shedding more load which is undesirable. VDPLS and FVSU shed an equal amount of active load; however, the voltages are restored closer to initial values in FVSU load shedding. This is because VDPLS sheds more active load from weak voltage buses and the reactive load is shed proportionally irrespective of reactive power needed to maintain balance in the system. The proposed FVSU load curtailment sheds more load from buses with power factor close to power factor of the event; so as to maintain the power balance in the system. Thus, the bus voltages in the new steady state acquired are more stable. Further, no secondary check for stability is required because the balance of power has been reinstated in the proposed approach.

5.4.3.3 Case (c)-Capacitor outage at bus 20

The performance of the proposed approach has been further checked on reactive power events. For this purpose, the reactive load at bus 20 is increased and shunt capacitor is connected to support bus voltage maintaining the bus power factor approximately unity.

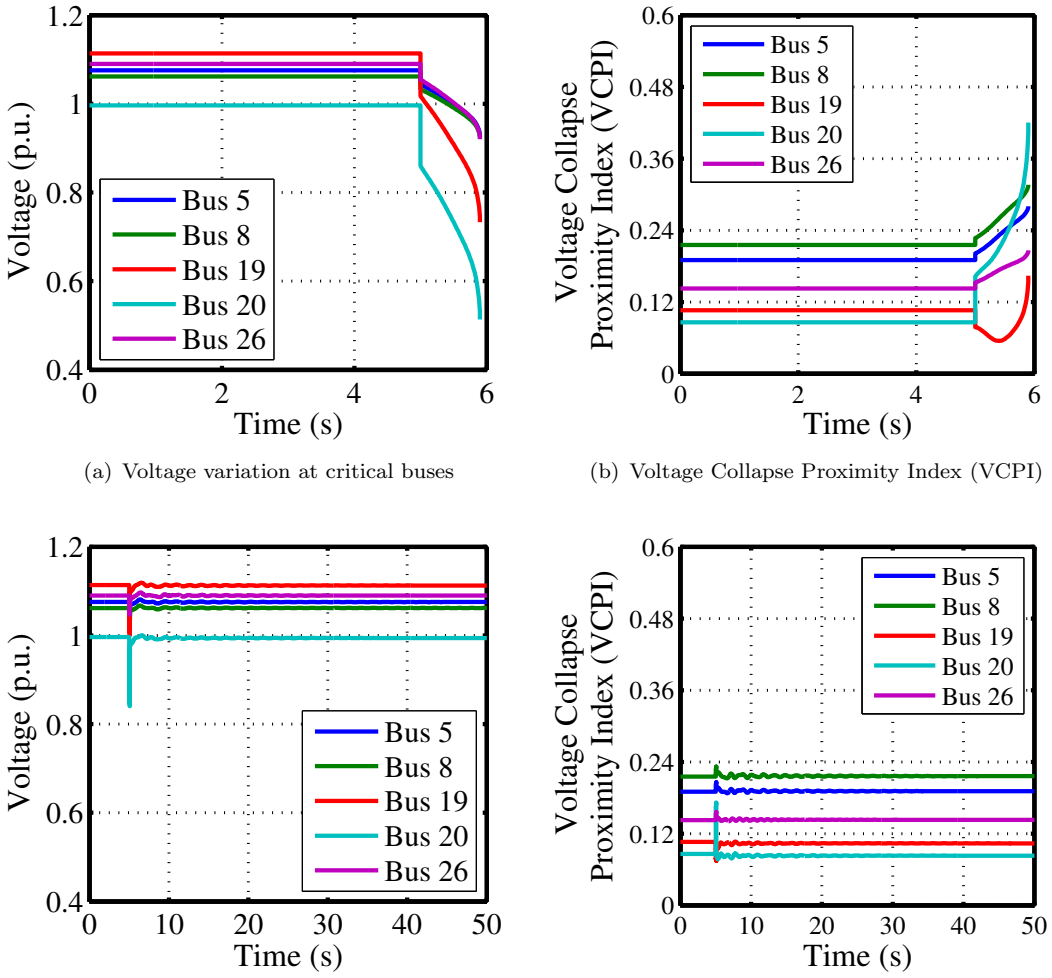

(a) Voltage variation at critical buses

(b) Voltage Collapse Proximity Index (VCPI)

(c) Voltages at critical buses after regulated shunt compensation

(d) Voltage Collapse Proximity Index (VCPI) after regulated shunt compensation

FIGURE 5.7: Case (c)-Capacitor outage at bus 20 in NE-39 bus system

The sudden elimination of the capacitor injecting 7.50 MVAR at bus 20 has been considered at $t = 5.0$ s in Fig. 5.7. It leads to a major deficit of reactive power in the system. The voltage variation and VCPI after the event are shown in Fig. 5.7(a) and (b) respectively. It is observed that voltage collapse occurs at $t = 5.9$ s; however, VCPI shows no indication of voltage collapse. Most drastic fall in voltage is observed at bus 20.

Prompt emergency control could have prevented this voltage collapse. The outage leads to the immediate drastic voltage drop at bus 20 which can also be determined using (4.12). Subsequently, ΔP, ΔQ and $cos\ \Psi$ are determined as 0.82 p.u., 7.49 p.u. and 0.1088 respectively. The relatively small value of ΔP is because of weak coupling between frequency and reactive power. PSA classifies the event to be unstable based on ΔP and

TABLE 5.5: Average computation time of the proposed scheme

Stage	Time elapsed (s)
Event detection and classification module	$< 6 \times 10^{-1}$
API (ΔP) calculation	$< 10^{-4}$
RPI (ΔQ) calculation	$< 2 \times 10^{-1}$
PSA module	$< 10^{-3}$
Proposed load shedding optimization	$< 10^{-2}$
Total time elapsed	$< 8 \times 10^{-1}$

ΔQ values. As $cos\ \Psi < \kappa^{min}$, load shedding is not suggested. Instead, an equivalent regulated shunt compensation is used to inject reactive power at bus 20. In Figs. 5.7(c) and (d), voltages and VCPI variation are observed to settle to acceptable values after reactive power injection.

Suitability of various components of the proposed approach for real-time application was also examined. The average time elapsed in various components of the proposed scheme for an event is presented in Table 5.5. It can be observed that it generates a total time delay of approximately 0.80 s before emergency control can be activated. This latency is small because instability generally occurs several seconds after a system is perturbed by an event [14]. This infers that the proposed method is well suited for real-time implementation.

5.5 Summary

The contributions of this chapter are summarized below:

1. The frequency and voltage are effective parameters for monitoring the deficits of active and reactive powers after an event. Therefore, predictive analytics can be implemented using frequency and voltage for anticipating instability in the system.
2. Active power imbalance is defined as additional active power generation necessary to restore the frequency at COI to nominal value. Similarly, reactive power imbalance is reactive power required to be injected at the event bus to restore post-event bus voltages to pre-event bus voltages.
3. A new method has been proposed for estimation of reactive power imbalance. The objective function is formulated as minimization of the difference between post-event bus voltages to pre-event bus voltages at all buses subject to power-flow constraints. The optimization problem is nonlinear, and has been solved using quasi-Newton approach.

4. A supervised learning assisted binary classification module has been proposed for predictive assessment of both frequency and voltage stability. It classifies the system in *Stable* or *Unstable* class using imbalances of both active power and reactive power measured from the initial change in frequency and voltage respectively after the event.

5. For unstable events, control actions are activated for alleviating instability. A new load shedding scheme has been proposed that sheds more load from buses with load power factor closer to the power factor of apparent power imbalance. Thus, the maximum balance of both active and reactive powers after the event is restored.

6. It is crucial to reduce the reactive power injection of shunt capacitors after load shedding to prevent overvoltages. Therefore, capacitor regulation constraint has been incorporated in the load shedding formulation.

7. The results of the proposed load shedding are compared with conventional UFLS and VDPLS. The results obtained show that the proposed approach is fast, sheds less amount of load and provides better voltage profile at load buses. As it is initiated earlier than UFLS and VDPLS, it diminishes oscillations and steady-state error in voltage response.

Chapter 6

Conclusions and Future Scope

The purpose of this chapter is to compile the main contributions and outcomes of the work carried out in this thesis and to recommend guidelines for potential research work in this domain.

6.1 Important Findings

Synchronized phasor measurements from PMUs provide a foundation for enhanced situational awareness and emergency control of electrical grids. In chapter 3, the optimal placement of PMUs has been carried out. The following points are the key findings of the chapter:

1. It is observed that not all buses have the same degree of preference from the technical viewpoint. Therefore, the optimal locations for PMU installation are determined considering degree of criticality of buses.

2. All buses are scaled on four parameters of criticality and a Multi-Criteria Decision Making approach has been adopted for selection of critical buses.

3. The proposed method can handle a mixture of criteria types (integer values, binary values, actual values etc.) and produce a consolidated degree of criticality of buses.

4. The OPP objective function is modified to contain degree of criticality and is solved using ILP.

5. The incorporation of the degree of criticality in the problem formulation ensures that more PMUs are clustered on critical buses.

6. An appropriate staging strategy for multi-horizon PMU placement has been proposed.

7. The utilities can obtain maximum benefits in terms of the voltage stability monitoring, generator bus observability, critical line observability, and maximum redundancy of measurements from a PMU installation project using the proposed approach.

In chapter 4, real-time event analysis has been studied. A new approach for automated detection, localization, and classification of events in power system using wavelet transform has been presented. A three-phase fault is more critical event than other events. Hence, a Fast Fault Identification module is proposed for its earlier verification than other events. Supervised learning has been used for extracting relevant features from both time and frequency domain. Wavelet transform is further extended to trace coherent groups of generators. The key findings of this chapter are presented below:

1. It is observed that events disturb the equilibrium of active and reactive power, which is observed as large fluctuations in frequency and voltage. Each event can be identified by its own characteristic features.

2. An index formulated as the ratio of energy corresponding to wavelet detail coefficients of the present and 10 previous voltage and frequency data windows has been proposed for real-time event detection. It is observed from the results that the index detects an event in the following cycle after occurrence of the event.

3. For locating events, an event localization module has been proposed. As the variation in voltage is maximum at the location closest to the event, the wavelet energy is highest at the bus electrically nearest to the site of the event and displays a decreasing tendency as the distance from event location increases. This reveals the dispersion of disturbance in the network and can facilitate in the actuation of remedial measures.

4. A two-step verification procedure to recognize short-circuit faults within two-cycles of nominal frequency is developed. Step 1 is a voltage magnitude threshold-based fault suspicion criterion while Step 2 is Fast Fault Identification tool using SVM classifier for affirmative indication of a fault.

5. The three-phase short-circuit fault case is distinguished from all other events with 100 % accuracy. The reason is existence of linear separating margin between the two classes on the $\Delta V - \Delta F$ plane.

6. For classification of other events, features from both time and frequency domain are extracted from voltage and frequency waveforms using wavelet decomposition, and a multiclass DSVM classifier is trained after scaling the feature vector with Z-score standardization.

7. The proposed event detection and classification is appropriate for real-time diagnosis of events. The small latency implies that the presented approach is functional in online polling mode of all protective devices in the grid.

8. The swing characteristic of the machine can be obtained from the phase of the dominant non-zero frequency component in the time domain, and coherency of generators can be established.

9. The power system response to events is non-linear and non-stationary, which limits the phase estimation of rotor angle response using simple methods such as Cross-correlation and Fourier transform. XWT is a suitable tool for discovering common power and phase difference between pairwise rotor angles in time-frequency space.

10. XWT plot aids visualization of coherency interrelationship between the groups of generators in power systems at different components of frequency.

11. The frequency components of rotor angle of a generator have varying phase difference with other machines. The mean phase difference can be estimated as the difference between the circular mean of the instantaneous phase angles.

12. A new consolidated Phase Difference Matrix of the relative phase difference between each pair of machines is proposed. It transforms the coherency of N_G generators in a $N_G \times N_G$ dimensional space.

13. The magnitude of the wavelet coefficient signifies the strength of coherency (strong or weak) between generator pairs.

Chapter 5 deals with predictive stability assessment and actuation of emergency control. The imbalances of both active and reactive power preceding an event are used as features to predict if an event results in loss of frequency and/or voltage instability. An event leading to instability is countered with prompt lead shedding. The key findings of this chapter are presented below:

1. The frequency and voltage variation following an event provide sufficient information to implement predictive analytics for stability assessment and countermeasures.

2. A supervised learning based classification module has been presented for near real-time detection of imminent frequency and/or voltage instability. It predicts the stability of system using imbalances of both active power and reactive power measured from the initial change in frequency and voltage respectively after the event.

3. Active power imbalance is determined from the initial ROCOF at COI. Reactive power imbalance has been defined as the necessary amount of reactive power to be injected at event bus to restore post-event voltage magnitudes to pre-event values. A new formulation for estimating reactive power imbalance has been presented.

4. It is observed that stable and unstable events cannot be separated using linear hyperplanes on $\Delta P - \Delta Q$ plane. Therefore, the features were transformed to higher dimensional space using Radial Basis Function kernel.

5. In dynamic scenarios, the voltage collapse is mostly due to limit-induced bifurcation rather than saddle-node bifurcation. Therefore, voltage stability assessment using static indices is inefficient. Voltage collapse may be observed much before static indices attain their limiting value.

6. A new load shedding formulation is presented considering both active and reactive power imbalances. It sheds more load at buses with load power factor closer to power factor of apparent power imbalance.

7. The incremental load on generators after an event can exceed its maximum turbine output. This overloads the generator and reduces its frequency. Hence, this incremental load must be added to the amount of load to be shed.

8. The incorporation of capacitor output regulation constraint in the load shedding ensures that its reactive power output is reduced when load is shed. This prevents overvoltage in the system.

9. The proposed load-shedding approach is fast, sheds less amount of load and provides better voltage profile at load buses. As it is initiated earlier than UFLS and VDPLS, it diminishes oscillations and steady-state error in post-event voltage response.

The proposed work is an effective scheme for increased situational awareness, stability monitoring and emergency control of electrical grids. It envisions an intelligent and regenerative grid capable of enduring critical events efficiently. The transformation of traditional grids into cyber-physical systems will further increase the acceptability of proposed machine learning based applications. Emergency control scheme proposed herein will constitute a decision support system for restricting events from driving widespread blackouts.

6.2 Future Scope

Further research can be carried along the following lines:

1. In OPPP, all generator buses have been scored equally to keep the computation simple. However, generator buses may also be scored in accordance with their generation capacity, the inertia of connected generator, load demand served, participation in damping low-frequency oscillations and so forth.

2. The selection of critical buses is highly subjective and system-specific. Several additional buses including, but not limited to, substantial power transfer buses, buses with high DG penetration, buses in high voltage corridor, buses contributing in damping inter-area oscillations, buses with FACTS and small-signal controller support, HVDC terminal buses, may also be considered and assessed in the similar manner.

3. Certain essential components, such as Current Transformers (CTs), Potential Transformers (PTs), are also installed along with PMUs. Therefore, a more pragmatic placement scheme can be developed considering effects such as equipment failure, saturation of the current transformer, etc.

4. Other signal processing and machine algorithms can be explored for better performance of event detection module.

5. The proposed work can be extended to locate and classify multiple events in real-time.

6. Predictive Stability Assessment module can be extended to incorporate rotor angle stability. Therefore, a combined scheme for assessment power system stability under critical events can be developed.

7. Emergency control can be further enhanced considering coherency of generators. The knowledge of coherency can also serve manifold purposes such as dynamic reduction, controlled islanding, transient stability assessment, generation rescheduling, and deployment of special protection relays.

Appendix A

Test System Data

A.1 IEEE New England 39 Bus Test System

The IEEE NE-39 bus test has total active and reactive power demand of 60.879 MW and 14.043 MVAR respectively. The base rating is 100 MVA, 345 kV. The dynamic data of the system are tabulated below:

TABLE A.1: Bus data

Bus	P_d (p.u.)	Q_d (p.u.)	V_m (p.u.)	V_θ (rad.)
1	0	0	1.048	-0.1646
2	0	0	1.0505	-0.1203
3	322	2.4	1.0341	-0.1698
4	500	184	1.0116	-0.1838
5	0	0	1.0165	-0.1637
6	0	0	1.0172	-0.1515
7	233.8	84	1.0067	-0.1892
8	522	176	1.0057	-0.1979
9	0	0	1.0322	-0.1946
10	0	0	1.0235	-0.1101
11	0	0	1.0201	-0.1243
12	7.5	88	1.0072	-0.1246
13	0	0	1.0207	-0.1225
14	0	0	1.0181	-0.1511
15	320	153	1.0194	-0.1581
16	329	32.3	1.0346	-0.1337
17	0	0	1.0365	-0.151
18	158	30	1.0343	-0.1656
19	0	0	1.0509	-0.0531
20	628	103	0.9914	-0.0777
21	274	115	1.0337	-0.0918
22	0	0	1.0509	-0.0143
23	247.5	84.6	1.0459	-0.0178
24	308.6	-92.2	1.0399	-0.1316
25	224	47.2	1.0587	-0.0962
26	139	17	1.0536	-0.1182
27	281	75.5	1.0399	-0.1532
28	206	27.6	1.0509	-0.0571
29	283.5	26.9	1.0505	-0.0089
30	0	0	1.0475	-0.078
31	0	0	1.04	0.0123
32	0	0	0.9831	0.0284
33	0	0	0.9972	0.038
34	0	0	1.0123	0.0129
35	0	0	1.0493	0.0723
36	0	0	1.0635	0.1192
37	0	0	1.0278	0.022
38	0	0	1.0265	0.1143
39	0	0	1.03	0

TABLE A.2: Line data

Line No.	From Bus	To Bus	Line Impedance		Half Line Charging	Tap
			Resistance ($p.u.$)	Reactance ($p.u.$)	Susceptance ($p.u.$)	Ratio
1	1	2	0.0035	0.0411	0.6987	1
2	1	39	0.001	0.025	0.75	1
3	2	3	0.0013	0.0151	0.2572	1
4	2	25	0.007	0.0086	0.146003	1
5	2	30	0	0.0181	0	1.025
6	3	4	0.0013	0.0213	0.2214	1
7	3	18	0.0011	0.0133	0.2138	1
8	4	5	0.0008	0.0128	0.1342	1
9	4	14	0.0008	0.0129	0.1382	1
10	5	8	0.0008	0.0112	0.1476	1
11	6	5	0.0002	0.0026	0.0434	1
12	6	7	0.0006	0.0092	0.113	1
13	6	11	0.0007	0.0082	0.1389	1
14	7	8	0.0004	0.0046	0.078	1
15	8	9	0.0023	0.0363	0.3804	1
16	9	39	0.001	0.025	1.2	1
17	10	11	0.0004	0.0043	0.0729	1
18	10	13	0.0004	0.0043	0.0729	1
19	10	32	0	0.02	0	1.07
20	12	11	0.0016	0.0435	0	1.006
21	12	13	0.0016	0.0435	0	1.006
22	13	14	0.0009	0.0101	0.1723	1
23	14	15	0.0018	0.0217	0.366	1
24	15	16	0.0009	0.0094	0.171	1
25	16	17	0.0007	0.0089	0.1342	1
26	16	19	0.0016	0.0195	0.304	1
27	16	21	0.0008	0.0135	0.2548	1
28	16	24	0.0003	0.0059	0.068	1
29	17	18	0.0007	0.0082	0.1319	1
30	17	27	0.0013	0.0173	0.3216	1
31	19	33	0.0007	0.0142	0	1.07
32	19	20	0.0007	0.0138	0	1.06
33	20	34	0.0009	0.018	0	1.009
34	21	22	0.0008	0.014	0.2565	1
35	22	23	0.0006	0.0096	0.1846	1
36	22	35	0	0.0143	0	1.025
37	23	24	0.0022	0.035	0.361	1
38	23	36	0.0005	0.0272	0	1
39	25	26	0.0032	0.0323	0.513	1
40	25	37	0.0006	0.0232	0	1.025
41	26	27	0.0014	0.0147	0.2396	1
42	26	28	0.0043	0.0474	0.7802	1
43	26	29	0.0057	0.0625	1.029	1
44	28	29	0.0014	0.0151	0.249	1
45	29	38	0.0008	0.0156	0	1.025
46	6	31	0	0.025	0	1.07

TABLE A.3: Generation limits

Generator No.	Bus No.	P_G (p.u.)	Q_{Gmax} (p.u.)	Q_{Gmin} (p.u.)
1	30	250	800	-6000
2	31	472.93	800	-6000
3	32	650	800	-6000
4	33	632	800	-6000
5	34	508	400	-300
6	35	650	800	-6000
7	36	560	800	-6000
8	37	540	800	-6000
9	38	830	800	-6000

TABLE A.4: Synchronous machine data

Generator No.	Bus No.	Model	x_l (p.u.)	r_a (p.u.)	$x_d^{'}$ (p.u.)	$x_d^{''}$ (p.u.)	$T_{d0}^{''}$ (s)	x_q (p.u.)	$x_q^{'}$ (p.u.)	$x_q^{''}$ (p.u.)	M (kWs/kVA)	T_{AA} (s)
1	30	4	0.0125	0.00014	0.1	0.031	10.2	0.069	0.031	1.5	84	0.002
2	31	4	0.035	0.0027	0.295	0.0697	6.56	0.282	0.0697	1.5	60.6	0.002
3	32	4	0.0304	0.000386	0.2495	0.0531	5.7	0.237	0.0531	1.5	71.6	0.002
4	33	4	0.0295	0.000222	0.262	0.0436	5.69	0.258	0.0436	1.5	57.2	0.002
5	34	4	0.054	0.00014	0.67	0.132	5.4	0.62	0.132	0.44	52	0.002
6	35	4	0.0224	0.00615	0.254	0.05	7.3	0.241	0.05	0.4	69.6	0.002
7	36	4	0.0322	0.000268	0.295	0.049	5.66	0.292	0.049	1.5	52.8	0.002
8	37	4	0.028	0.000686	0.29	0.057	6.7	0.28	0.057	0.41	48.6	0.002
9	38	4	0.0298	0.0003	0.2106	0.057	4.79	0.205	0.057	1.96	69	0.002
10	39	3	0.003	0.0001	0.02	0.006	7	0.019	0.006	0.7	1000	0.002

TABLE A.5: Turbine governor data

Generator No.	Turbine Governor Type	Reference Speed (p.u.)	Droop (p.u.)	T_{max} (p.u.)	T_{min} (p.u.)	T_s (s)	T_c (s)	T_3 (s)	T_4 (s)	T_5 (s)
1	1	1	0.04	8	0	0.1	0.45	0	12	8
2	1	1	0.04	10	0	0.1	0.45	0	12	8
3	1	1	0.04	15	0	0.1	0.45	0	12	8
4	1	1	0.04	6.5	0	0.1	0.45	0	12	8
5	1	1	0.04	10	0	0.1	0.45	0	12	8
6	1	1	0.04	10	0	0.1	0.45	0	12	8
7	1	1	0.04	10	0	0.1	0.45	0	12	8
8	1	1	0.04	8.5	0	0.1	0.45	0	12	8
9	1	1	0.04	20	0	0.1	0.45	0	12	8
10	1	1	0.04	15	0	0.1	0.45	0	12	8

TABLE A.6: Exciter data

Generator No.	Exc. Type	$V_{r\ max}$ (p.u.)	$V_{r\ min}$ (p.u.)	μ_0 (p.u.)	T_1 (s)	T_2 (s)	T_3 (s)	T_4 (s)	T_e (s)	T_r (s)	A_e	B_e
1	2	5	-60	5	0.06	0.04	0.1	0	0.25	0.001	0.0039	1.555
2	2	5	-60	6.2	0.05	0.06	0.05	0	0.41	0.001	0.0039	1.555
3	2	5	-60	5	0.06	0.08	0.1	0	0.5	0.001	0.0039	1.555
4	2	5	-60	5	0.06	0.08	0.1	0	0.5	0.001	0.0039	1.555
5	2	30	-10	40	0.02	0.03	0.1	0	0.785	0.001	0.0039	1.555
6	2	5	-60	5	0.02	0.08	0.125	0	0.471	0.001	0.0039	1.555
7	2	6.5	-6.5	40	0.02	0.03	0.1	0	0.73	0.001	0.0039	1.555
8	2	5	-60	5	0.02	0.09	0.126	0	0.528	0.001	0.0039	1.555
9	2	10.5	-10.5	5	0.02	0.03	0.1	0	0.5	0.001	0.0039	1.555
10	2	10.5	-10.5	40	0.02	0.03	0.1	0	1.4	0.001	0.0039	1.555

Bibliography

[1] O. P. Dahal, H. Cao, S. Brahma, and R. Kavasseri, "Evaluating performance of classifiers for supervisory protection using disturbance data from phasor measurement units," in *Innovative Smart Grid Technologies Conference Europe (ISGT-Europe), 2014 IEEE PES*. IEEE, 2014, pp. 1–6.

[2] A. Pal, G. A. Sanchez-Ayala, V. A. Centeno, and J. S. Thorp, "A PMU placement scheme ensuring real-time monitoring of critical buses of the network," *IEEE Transactions on Power Delivery*, vol. 29, no. 2, pp. 510–517, 2014.

[3] A. Bakshi, A. Velayutham, S. Srivastava, K. Agrawal, R. Nayak, S. Soonee, and B. Singh, "Report of the enquiry committee on grid disturbance in northern region on 30^{th} July 2012 and in Northern, Eastern & Northern-Eastern region on 31^{st} July 2012," *New Delhi, India*, 2012.

[4] A. G. Phadke and J. S. Thorp, *Synchronized phasor measurements and their applications*. Springer, 2008, vol. 1.

[5] S. Ghosh, D. Ghosh, and D. K. Mohanta, "Impact assessment of reliability of phasor measurement unit on situational awareness using generalized stochastic petri nets," *International Journal of Electrical Power & Energy Systems*, vol. 93, pp. 75–83, 2017.

[6] C. Heng, L. Zhang, M. Jianzhong, and K. E. Martin, "Synchrophasor-based real-time state estimation and situational awareness system for power system operation," *Journal of Modern Power Systems and Clean Energy*, vol. 4, no. 3, pp. 370–382, 2016.

[7] C. V. B. Reddy, S. Srivastava, and S. Chakrabarti, "Fast assessment of available transfer capability using synchrophasor measurements," *Electric Power Components and Systems*, vol. 42, no. 7, pp. 716–726, 2014.

[8] B. Leonardi and V. Ajjarapu, "An approach for real time voltage stability margin control via reactive power reserve sensitivities," *IEEE Transactions on Power Systems*, vol. 28, no. 2, pp. 615–625, 2013.

[9] F. Aminifar, M. Shahidehpour, M. Fotuhi-Firuzabad, and S. Kamalinia, "Power system dynamic state estimation with synchronized phasor measurements," *IEEE Transactions on Instrumentation and Measurement*, vol. 63, no. 2, pp. 352–363, 2014.

[10] R. Sodhi, S. Srivastava, and S. Singh, "Phasor-assisted hybrid state estimator," *Electric Power Components and Systems*, vol. 38, no. 5, pp. 533–544, 2010.

[11] ——, "A simple scheme for wide area detection of impending voltage instability," *IEEE Transactions on Smart Grid*, vol. 3, no. 2, pp. 818–827, 2012.

[12] H.-Y. Su and C.-W. Liu, "Estimating the voltage stability margin using PMU measurements," *IEEE Transactions on Power Systems*, vol. 31, no. 4, pp. 3221–3229, 2016.

[13] A. K. Singh and M. Fozdar, "Supervisory framework for event detection and classification using wavelet transform," in *2017 IEEE Power & Energy Society General Meeting*. IEEE, 2017, pp. 1–5.

[14] M. Biswal, S. M. Brahma, and H. Cao, "Supervisory protection and automated event diagnosis using PMU data," *IEEE Transactions on Power Delivery*, vol. 31, no. 4, pp. 1855–1863, 2016.

[15] Z. Huang, P. Du, D. Kosterev, and S. Yang, "Generator dynamic model validation and parameter calibration using phasor measurements at the point of connection," *IEEE Transactions on Power Systems*, vol. 28, no. 2, pp. 1939–1949, 2013.

[16] Y. Zhang, E. Muljadi, D. Kosterev, and M. Singh, "Wind power plant model validation using synchrophasor measurements at the point of interconnection," *IEEE Transactions on Sustainable Energy*, vol. 6, no. 3, pp. 984–992, 2015.

[17] P. Ashton, G. Taylor, A. Carter, M. Bradley, and W. Hung, "Application of phasor measurement units to estimate power system inertial frequency response," in *Power and Energy Society General Meeting (PES), 2013 IEEE*. IEEE, 2013, pp. 1–5.

[18] P. M. Ashton, C. S. Saunders, G. A. Taylor, A. M. Carter, and M. E. Bradley, "Inertia estimation of the GB power system using synchrophasor measurements," *IEEE Transactions on Power Systems*, vol. 30, no. 2, pp. 701–709, 2015.

[19] Q. Liu, M. Watanabe, and Y. Mitani, "Global oscillation mode analysis using phasor measurement units-based real data," *International Journal of Electrical Power & Energy Systems*, vol. 67, pp. 393–400, 2015.

[20] O. Antoine and J.-C. Maun, "Inter-area oscillations: Identifying causes of poor damping using phasor measurement units," in *Power and Energy Society General Meeting, 2012 IEEE*. IEEE, 2012, pp. 1–6.

[21] N. R. Chaudhuri, B. Chaudhuri, S. Ray, and R. Majumder, "Wide-area phasor power oscillation damping controller: A new approach to handling time-varying signal latency," *IET Generation, Transmission & Distribution*, vol. 4, no. 5, pp. 620–630, 2010.

[22] P. Kundur, J. Paserba, V. Ajjarapu, G. Andersson, A. Bose, C. Canizares, N. Hatziargyriou, D. Hill, A. Stankovic, C. Taylor *et al.*, "Definition and classification of power system stability," *IEEE Transactions on Power Systems*, vol. 19, no. 2, pp. 1387–1401, 2004.

[23] P. Anderson and M. Mirheydar, "An adaptive method for setting underfrequency load shedding relays," *IEEE Transactions on Power Systems*, vol. 7, no. 2, pp. 647–655, 1992.

[24] M. Glavic, D. Novosel, E. Heredia, D. Kosterev, A. Salazar, F. Habibi-Ashrafi, and M. Donnelly, "See it fast to keep calm: Real-time voltage control under stressed conditions," *IEEE Power and Energy Magazine*, vol. 10, no. 4, pp. 43–55, 2012.

[25] F. Aminifar, M. Fotuhi-Firuzabad, A. Safdarian, A. Davoudi, and M. Shahidehpour, "Synchrophasor measurement technology in power systems: Panorama and state-of-the-art," *IEEE Access*, vol. 2, pp. 1607–1628, 2014.

[26] T. Baldwin, L. Mili, M. Boisen, and R. Adapa, "Power system observability with minimal phasor measurement placement," *IEEE Transactions on Power Systems*, vol. 8, no. 2, pp. 707–715, 1993.

[27] B. Milosevic and M. Begovic, "Nondominated sorting genetic algorithm for optimal phasor measurement placement," *IEEE Transactions on Power Systems*, vol. 18, no. 1, pp. 69–75, 2003.

[28] B. Xu and A. Abur, "Observability analysis and measurement placement for systems with PMUs," in *Power Systems Conference and Exposition, 2004. IEEE PES.* IEEE, 2004, pp. 943–946.

[29] N. H. Abbasy and H. M. Ismail, "A unified approach for the optimal PMU location for power system state estimation," *IEEE Transactions on Power Systems*, vol. 24, no. 2, pp. 806–813, 2009.

[30] B. Gou, "Generalized integer linear programming formulation for optimal PMU placement," *IEEE Transactions on Power Systems*, vol. 23, no. 3, pp. 1099–1104, 2008.

[31] R. F. Nuqui and A. G. Phadke, "Phasor measurement unit placement techniques for complete and incomplete observability," *IEEE Transactions on Power Delivery*, vol. 20, no. 4, pp. 2381–2388, 2005.

[32] S. Chakrabarti, E. Kyriakides, and D. G. Eliades, "Placement of synchronized measurements for power system observability," *IEEE Transactions on Power Delivery*, vol. 24, no. 1, pp. 12–19, 2009.

[33] F. Aminifar, M. Fotuhi-Firuzabad, M. Shahidehpour, and A. Khodaei, "Probabilistic multistage PMU placement in electric power systems," *IEEE Transactions on Power Delivery*, vol. 26, no. 2, pp. 841–849, 2011.

[34] ——, "Observability enhancement by optimal PMU placement considering random power system outages," *Energy Systems*, vol. 2, no. 1, pp. 45–65, 2011.

[35] X. Tai, D. Marelli, E. Rohr, and M. Fu, "Optimal PMU placement for power system state estimation with random component outages," *International Journal of Electrical Power & Energy Systems*, vol. 51, pp. 35–42, 2013.

[36] N. P. Theodorakatos, N. M. Manousakis, and G. N. Korres, "Optimal placement of phasor measurement units with linear and non-linear models," *Electric Power Components and Systems*, vol. 43, no. 4, pp. 357–373, 2015.

[37] S. Chakrabarti and E. Kyriakides, "Optimal placement of phasor measurement units for power system observability," *IEEE Transactions on power systems*, vol. 23, no. 3, pp. 1433–1440, 2008.

[38] D. Dua, S. Dambhare, R. K. Gajbhiye, and S. Soman, "Optimal multistage scheduling of PMU placement: An ILP approach," *IEEE Transactions on Power delivery*, vol. 23, no. 4, pp. 1812–1820, 2008.

[39] R. Sodhi and M. I. Sharieff, "Phasor measurement unit placement framework for enhanced wide-area situational awareness," *IET Generation, Transmission & Distribution*, vol. 9, no. 2, pp. 172–182, 2015.

[40] S. M. Mahaei and M. T. Hagh, "Minimizing the number of PMUs and their optimal placement in power systems," *Electric Power Systems Research*, vol. 83, no. 1, pp. 66–72, 2012.

[41] R. Sodhi, S. Srivastava, and S. Singh, "Multi-criteria decision-making approach for multi-stage optimal placement of phasor measurement units," *IET Generation, Transmission & Distribution*, vol. 5, no. 2, pp. 181–190, 2011.

[42] B. Gou, "Optimal placement of PMUs by integer linear programming," *IEEE Transactions on Power Systems*, vol. 23, no. 3, pp. 1525–1526, 2008.

[43] C. Rakpenthai, S. Premrudeepreechacharn, S. Uatrongjit, and N. R. Watson, "An optimal PMU placement method against measurement loss and branch outage," *IEEE transactions on power delivery*, vol. 22, no. 1, pp. 101–107, 2007.

[44] B. S. Roy, A. Sinha, and A. Pradhan, "Optimal phasor measurement unit placement for power system observability—a heuristic approach," in *Computational Intelligence Applications In Smart Grid (CIASG), 2011 IEEE Symposium on.* IEEE, 2011, pp. 1–6.

[45] M. Alvarez, F. Sellschopp, and E. Vazquez, "A PMUs placement methodology based on inverse of connectivity and critical measurements," *International Journal of Electrical Power & Energy Systems*, vol. 68, pp. 336–344, 2015.

[46] L. Huang, Y. Sun, J. Xu, W. Gao, J. Zhang, and Z. Wu, "Optimal PMU placement considering controlled islanding of power system," *IEEE Transactions on Power Systems*, vol. 29, no. 2, pp. 742–755, 2014.

[47] F. Aminifar, M. Fotuhi-Firuzabad, and A. Safdarian, "Optimal PMU placement based on probabilistic cost/benefit analysis," *IEEE Transactions on Power Systems*, vol. 28, no. 1, pp. 566–567, 2013.

[48] M. Korkali and A. Abur, "Placement of PMUs with channel limits," in *Power & Energy Society General Meeting, 2009. PES'09. IEEE.* IEEE, 2009, pp. 1–4.

[49] R. Kumar and V. S. Rao, "Optimal placement of PMUs with limited number of channels," in *North American Power Symposium (NAPS), 2011.* IEEE, 2011, pp. 1–7.

[50] F. Aminifar, A. Khodaei, M. Fotuhi-Firuzabad, and M. Shahidehpour, "Contingency-constrained PMU placement in power networks," *IEEE Transactions on Power Systems*, vol. 25, no. 1, pp. 516–523, 2010.

[51] R. Sodhi, S. Srivastava, and S. Singh, "Optimal PMU placement to ensure system observability under contingencies," in *Power & Energy Society General Meeting, 2009. PES'09. IEEE.* IEEE, 2009, pp. 1–6.

[52] D. Thukaram, B. Ravikumr, V. S. S. Kumar, Y. P. Rao, S. Surendra, and S. Kolla, "Real-time monitoring of critical nodes with minimal number of phasor measurement units," in *Power Systems, 2009. ICPS'09. International Conference on.* IEEE, 2009, pp. 1–6.

[53] O. Gómez and M. A. Ríos, "ILP-based multistage placement of PMUs with dynamic monitoring constraints," *International Journal of Electrical Power & Energy Systems*, vol. 53, pp. 95–105, 2013.

[54] Z. Hong-Shan, L. Ying, M. Zeng-Qiang, and Y. Lei, "Sensitivity constrained PMU placement for complete observability of power systems," in *Transmission and Distribution Conference and Exhibition: Asia and Pacific, 2005 IEEE/PES.* IEEE, 2005, pp. 1–5.

[55] O. Linda, M. Manic, A. Giani, and M. McQueen, "Multi-criteria based staging of optimal PMU placement using fuzzy weighted average," in *Industrial Electronics (ISIE), 2013 IEEE International Symposium on.* IEEE, 2013, pp. 1–8.

[56] M. Hurtgen and J.-C. Maun, "Optimal PMU placement using iterated local search," *International journal of electrical power & energy systems*, vol. 32, no. 8, pp. 857–860, 2010.

[57] N. M. Manousakis and G. N. Korres, "A weighted least squares algorithm for optimal PMU placement," *IEEE Trans. Power Syst*, vol. 28, no. 3, pp. 3499–3500, 2013.

[58] A. Ahmadi, Y. Alinejad-Beromi, and M. Moradi, "Optimal PMU placement for power system observability using binary particle swarm optimization and considering measurement redundancy," *Expert Systems with Applications*, vol. 38, no. 6, pp. 7263–7269, 2011.

[59] H. Mori and Y. Sone, "Tabu search based meter placement for topological observability in power system state estimation," in *Transmission and Distribution Conference, 1999 IEEE*, vol. 1. IEEE, 1999, pp. 172–177.

[60] N. C. Koutsoukis, N. M. Manousakis, P. S. Georgilakis, and G. N. Korres, "Numerical observability method for optimal phasor measurement units placement using recursive Tabu search method," *IET Generation, Transmission & Distribution*, vol. 7, no. 4, pp. 347–356, 2013.

[61] C. Peng, H. Sun, and J. Guo, "Multi-objective optimal PMU placement using a non-dominated sorting differential evolution algorithm," *International Journal of Electrical Power & Energy Systems*, vol. 32, no. 8, pp. 886–892, 2010.

[62] K. Arul jeyaraj, V. Rajasekaran, S. Nandha Kumar, and K. Chandrasekaran, "A multi-objective placement of phasor measurement units using fuzzified artificial bee colony algorithm, considering system observability and voltage stability," *Journal of Experimental & Theoretical Artificial Intelligence*, vol. 28, no. 1-2, pp. 113–136, 2016.

[63] Q. Li, T. Cui, Y. Weng, R. Negi, F. Franchetti, and M. D. Ilic, "An information-theoretic approach to PMU placement in electric power systems," *IEEE Transactions on Smart Grid*, vol. 4, no. 1, pp. 446–456, 2013.

[64] V. Madani, M. Parashar, J. Giri, S. Durbha, F. Rahmatian, D. Day, M. Adamiak, and G. Sheble, "PMU placement considerations-a roadmap for optimal PMU placement," in *2011 IEEE/PES Power Systems Conference and Exposition (PSCE)*. IEEE, 2011, pp. 1–7.

[65] A. Allen, S. Santoso, and E. Muljadi, "Algorithm for screening phasor measurement unit data for power system events and categories and common characteristics for events seen in phasor measurement unit relative phase-angle differences and frequency signals," National Renewable Energy Laboratory (NREL), Golden, CO., Tech. Rep., 2013.

[66] R. G. Kavasseri, Y. Cui, and S. M. Brahma, "A new approach for event detection based on energy functions," in *2014 IEEE PES General Meeting— Conference & Exposition*. IEEE, 2014, pp. 1–5.

[67] A. Bykhovsky and J. H. Chow, "Power system disturbance identification from recorded dynamic data at the Northfield substation," *International journal of electrical power & energy systems*, vol. 25, no. 10, pp. 787–795, 2003.

[68] T. Bi, X. Song, J. Wu, and Q. Yang, "Novel method for disturbance identification in power systems," in *2006 IEEE Power Engineering Society General Meeting*. IEEE, 2006, pp. 5–pp.

[69] W. Gao and J. Ning, "Wavelet-based disturbance analysis for power system wide-area monitoring," *IEEE Transactions on Smart Grid*, vol. 2, no. 1, pp. 121–130, 2011.

[70] Y. Ge, A. J. Flueck, D.-K. Kim, J.-B. Ahn, J.-D. Lee, and D.-Y. Kwon, "Power system real-time event detection and associated data archival reduction based on synchrophasors," *IEEE Transactions on Smart Grid*, vol. 6, no. 4, pp. 2088–2097, 2015.

[71] L. Fan, R. Kavasseri, Z. Miao, D. Osborn, and T. Bilke, "Identification of system wide disturbances using synchronized phasor data and ellipsoid method," in *2008 IEEE Power and Energy Society General Meeting-Conversion and Delivery of Electrical Energy in the 21st Century*. IEEE, 2008, pp. 1–10.

[72] D.-I. Kim, T. Y. Chun, S.-H. Yoon, G. Lee, and Y.-J. Shin, "Wavelet-based event detection method using PMU data," *IEEE Transactions on Smart grid*, vol. 8, no. 3, pp. 1154–1162, 2017.

[73] J. Barros and E. Perez, "Automatic detection and analysis of voltage events in power systems," *IEEE Transactions on Instrumentation and Measurement*, vol. 55, no. 5, pp. 1487–1493, 2006.

[74] G. Gajjar and S. Soman, "Auto detection of power system events using wide area frequency measurements," in *2014 Eighteenth National Power Systems Conference (NPSC)*. IEEE, 2014, pp. 1–6.

[75] S. M. Rovnyak and K. Mei, "Dynamic event detection and location using wide area phasor measurements," *International Transactions on Electrical Energy Systems*, vol. 21, no. 4, pp. 1589–1599, 2011.

[76] K. Mei, S. M. Rovnyak, and C.-M. Ong, "Clustering-based dynamic event location using wide-area phasor measurements," *IEEE Transactions on Power Systems*, vol. 23, no. 2, pp. 673–679, 2008.

[77] O. P. Dahal and S. M. Brahma, "Preliminary work to classify the disturbance events recorded by phasor measurement units," in *2012 IEEE Power and Energy Society General Meeting*. IEEE, 2012, pp. 1–8.

[78] J. S. Thorp, C. E. Seyler, and A. G. Phadke, "Electromechanical wave propagation in large electric power systems," *IEEE Transactions on Circuits and Systems I: Fundamental Theory and Applications*, vol. 45, no. 6, pp. 614–622, 1998.

[79] T. Xia, H. Zhang, R. Gardner, J. Bank, J. Dong, J. Zuo, Y. Liu, L. Beard, P. Hirsch, G. Zhang *et al.*, "Wide-area frequency based event location estimation," in *Power Engineering Society General Meeting, 2007. IEEE*. IEEE, 2007, pp. 1–7.

[80] S. Sterpu, S. Rossignol, and B. Prestat, "Detection and location of generation trips in large transmission grids," in *2007 IEEE Power Engineering Society General Meeting*. IEEE, 2007, pp. 1–6.

[81] P. Bhui and N. Senroy, "Application of recurrence quantification analysis to power system dynamic studies," *IEEE Transactions on Power Systems*, vol. 31, no. 1, pp. 581–591, 2016.

[82] C. W. Taylor, *Power system voltage stability*. McGraw-Hill, 1994.

[83] D. Hill, "Scanning the issue-special issue on nonlinear phenomena in power systems: Theory and practical implications," *Proceedings of the IEEE*, vol. 83, no. 11, p. 1439, 1995.

[84] V. Ajjarapu and C. Christy, "The continuation power flow: a tool for steady state voltage stability analysis," *IEEE Transactions on Power Systems*, vol. 7, no. 1, pp. 416–423, 1992.

[85] B. Gao, G. Morison, and P. Kundur, "Voltage stability evaluation using modal analysis," *IEEE Transactions on Power Systems*, vol. 7, no. 4, pp. 1529–1542, 1992.

[86] P. Kessel and H. Glavitsch, "Estimating the voltage stability of a power system," *IEEE Transactions on Power Delivery*, vol. 1, no. 3, pp. 346–354, 1986.

[87] C. A. Canizares, "On bifurcations, voltage collapse and load modeling," *IEEE Transactions on Power Systems*, vol. 10, no. 1, pp. 512–522, 1995.

[88] T. J. Overbye and C. L. DeMarco, "Improved techniques for power system voltage stability assessment using energy methods," *IEEE Transactions on Power Systems*, vol. 6, no. 4, pp. 1446–1452, 1991.

[89] I. Musirin and T. A. Rahman, "On-line voltage stability based contingency ranking using fast voltage stability index (FVSI)," in *Transmission and Distribution Conference and Exhibition 2002: Asia Pacific. IEEE/PES*, vol. 2. IEEE, 2002, pp. 1118–1123.

[90] R. Raghunatha, R. Ramanujam, K. Parthasarathy, and D. Thukaram, "A new and fast technique for voltage stability analysis of a grid network using system voltage space," *International Journal of Electrical Power & Energy Systems*, vol. 20, no. 5, pp. 337–344, 1998.

[91] Y.-H. Moon, H.-S. Ryu, J.-G. Lee, and B. Kim, "Uniqueness of static voltage stability analysis in power systems," in *Power Engineering Society Summer Meeting, 2001*, vol. 3. IEEE, 2001, pp. 1536–1541.

[92] Y. Wang, C. Wang, F. Lin, W. Li, L. Y. Wang, and J. Zhao, "Incorporating generator equivalent model into voltage stability analysis," *IEEE Transactions on Power Systems*, vol. 28, no. 4, pp. 4857–4866, 2013.

[93] M. Moghavvemi and F. Omar, "Technique for contingency monitoring and voltage collapse prediction," *IEE Proceedings-Generation, Transmission and Distribution*, vol. 145, no. 6, pp. 634–640, 1998.

[94] J. Tang, J. Liu, F. Ponci, and A. Monti, "Adaptive load shedding based on combined frequency and voltage stability assessment using synchrophasor measurements," *IEEE Transactions on Power Systems*, vol. 28, no. 2, pp. 2035–2047, 2013.

[95] B. Leonardi and V. Ajjarapu, "Development of multilinear regression models for online voltage stability margin estimation," *IEEE Transactions on Power Systems*, vol. 26, no. 1, pp. 374–383, 2011.

[96] S. Kamalasadan, D. Thukaram, and A. Srivastava, "A new intelligent algorithm for online voltage stability assessment and monitoring," *International Journal of Electrical Power & Energy Systems*, vol. 31, no. 2-3, pp. 100–110, 2009.

[97] A. R. Khatib, R. F. Nuqui, M. Ingram, and A. G. Phadke, "Real-time estimation of security from voltage collapse using synchronized phasor measurements," in *Power Engineering Society General Meeting, 2004. IEEE.* IEEE, 2004, pp. 582–588.

[98] R. Diao, K. Sun, V. Vittal, R. J. O'Keefe, M. R. Richardson, N. Bhatt, D. Stradford, and S. K. Sarawgi, "Decision tree-based online voltage security assessment using PMU measurements," *IEEE Transactions on Power Systems*, vol. 24, no. 2, pp. 832–839, 2009.

[99] R. Diao, V. Vittal, and N. Logic, "Design of a real-time security assessment tool for situational awareness enhancement in modern power systems," *IEEE Transactions on Power Systems*, vol. 25, no. 2, pp. 957–965, 2010.

[100] H. Nguyen Duc, I. Kamwa, L.-A. Dessaint, and H. Cao-Duc, "A novel approach for early detection of impending voltage collapse events based on the support vector machine," *International Transactions on Electrical Energy Systems*, vol. 27, no. 9, 2017.

[101] S. Corsi and G. N. Taranto, "A real-time voltage instability identification algorithm based on local phasor measurements," *IEEE Transactions on Power Systems*, vol. 23, no. 3, pp. 1271–1279, 2008.

[102] Y. Gong, N. Schulz, and A. Guzman, "Synchrophasor-based real-time voltage stability index," in *Power Systems Conference and Exposition, 2006. PSCE'06. 2006 IEEE PES*. IEEE, 2006, pp. 1029–1036.

[103] R. E. C. Gutiérrez, J. M. Ramirez *et al.*, "Voltage collapse detection based on local measurements," *Electric Power Systems Research*, vol. 107, pp. 77–84, 2014.

[104] S. Corsi, "Wide area voltage protection," *IET Generation, Transmission & Distribution*, vol. 4, no. 10, pp. 1164–1179, 2010.

[105] B. Milosevic and M. Begovic, "Voltage-stability protection and control using a wide-area network of phasor measurements," *IEEE Transactions on Power Systems*, vol. 18, no. 1, pp. 121–127, 2003.

[106] K. Vu, M. M. Begovic, D. Novosel, and M. M. Saha, "Use of local measurements to estimate voltage-stability margin," *IEEE Transactions on Power Systems*, vol. 14, no. 3, pp. 1029–1035, 1999.

[107] A. Wiszniewski, "New criteria of voltage stability margin for the purpose of load shedding," *IEEE Transactions on Power Delivery*, vol. 22, no. 3, pp. 1367–1371, 2007.

[108] D. Julian, R. P. Schulz, K. Vu, W. H. Quaintance, N. B. Bhatt, and D. Novosel, "Quantifying proximity to voltage collapse using the voltage instability predictor (VIP)," in *Power Engineering Society Summer Meeting, 2000. IEEE*, vol. 2. IEEE, 2000, pp. 931–936.

[109] C. D. Vournas and T. Van Cutsem, "Local identification of voltage emergency situations," *IEEE Transactions on Power Systems*, vol. 23, no. 3, pp. 1239–1248, 2008.

[110] A. Phadke, M. Fozdar, K. Niazi, R. Bansal, and N. Mithulananthan, "On-line monitoring of proximity to voltage collapse using a new index based on local signals," *Electric Power Components and Systems*, vol. 38, no. 13, pp. 1498–1512, 2010.

[111] G. Verbic and F. Gubina, "A new concept of voltage-collapse protection based on local phasors," *IEEE Transactions on Power Delivery*, vol. 19, no. 2, pp. 576–581, 2004.

[112] A. Ghaleh, M. Sanaye-Pasand, and A. Saffarian, "Power system stability enhancement using a new combinational load-shedding algorithm," *IET generation, transmission & distribution*, vol. 5, no. 5, pp. 551–560, 2011.

[113] J. H. Chow, F. F. Wu, and J. A. Momoh, "Applied mathematics for restructured electric power systems," in *Applied Mathematics for Restructured Electric Power Systems*. Springer, 2005, pp. 1–9.

[114] V. V. Terzija, "Adaptive underfrequency load shedding based on the magnitude of the disturbance estimation," *IEEE Transactions on Power Systems*, vol. 21, no. 3, pp. 1260–1266, 2006.

[115] J. Jallad, M. Saad, H. Mokhlis, and J. Laghari, "Improved UFLS with consideration of power deficit during shedding process and flexible load selection," *IET Renewable Power Generation*, 2018.

[116] H. You, V. Vittal, and Z. Yang, "Self-healing in power systems: an approach using islanding and rate of frequency decline-based load shedding," *IEEE Transactions on Power Systems*, vol. 18, no. 1, pp. 174–181, 2003.

[117] K. Seethalekshmi, S. N. Singh, and S. C. Srivastava, "A synchrophasor assisted frequency and voltage stability based load shedding scheme for self-healing of power system," *IEEE Transactions on Smart Grid*, vol. 2, no. 2, pp. 221–230, 2011.

[118] K. Seethalekshmi, S. Singh, and S. Srivastava, "Adaptive scheme for minimal load shedding utilizing synchrophasor measurements to ensure frequency and voltage stability," *Electric Power Components and Systems*, vol. 38, no. 11, pp. 1211–1227, 2010.

[119] H. Seyedi and M. Sanaye-Pasand, "New centralised adaptive load-shedding algorithms to mitigate power system blackouts," *IET Generation, Transmission & Distribution*, vol. 3, no. 1, pp. 99–114, 2009.

[120] A. Saffarian and M. Sanaye-Pasand, "New local adaptive load-shedding methods to mitigate power system blackouts," *Electric Power Components and Systems*, vol. 40, no. 3, pp. 348–368, 2012.

[121] K. Narayanan, S. A. Siddiqui, and M. Fozdar, "Hybrid islanding detection method and priority-based load shedding for distribution networks in the presence of DG units," *IET Generation, Transmission & Distribution*, vol. 11, no. 3, pp. 586–595, 2017.

[122] X. Xu, H. Zhang, C. Li, Y. Liu, W. Li, and V. Terzija, "Optimization of the event-driven emergency load-shedding considering transient security and stability constraints," *IEEE Transactions on Power Systems*, vol. 32, no. 4, pp. 2581–2592, 2017.

[123] U. S. D. of Energy Office of Electricity Delivery and E. Reliability, "Factors affecting PMU installation cost," 2014. [Online]. Available: https://www.smartgrid.gov/files/PMU-cost-study-final-10162014_1.pdf

[124] B. S. Roy, A. Sinha, and A. Pradhan, "An optimal PMU placement technique for power system observability," *International Journal of Electrical Power & Energy Systems*, vol. 42, no. 1, pp. 71–77, 2012.

[125] M. Jha, S. Chakrabarti, and E. Kyriakides, "Estimation of the rotor angle of a synchronous generator by using PMU measurements," in *PowerTech, 2015 IEEE Eindhoven.* IEEE, 2015, pp. 1–6.

[126] T. Van Cutsem and C. Vournas, *Voltage stability of electric power systems.* Springer Science & Business Media, 1998, vol. 441.

[127] T. Moger and T. Dhadbanjan, "A novel index for identification of weak nodes for reactive compensation to improve voltage stability," *IET Generation, Transmission & Distribution*, vol. 9, no. 14, pp. 1826–1834, 2015.

[128] E. Triantaphyllou, B. Shu, S. N. Sanchez, and T. Ray, "Multi-criteria decision making: an operations research approach," *Encyclopedia of electrical and electronics engineering*, vol. 15, no. 1998, pp. 175–186, 1998.

[129] M. Pai, *Energy function analysis for power system stability*. Springer Science & Business Media, 2012.

[130] R. Christie, "Power systems test case archive." [Online]. Available: https://www2.ee.washington.edu/research/pstca/

[131] W. Barcelo and W. Lemmon, "Standardized sensitivity coefficients for power system networks," *IEEE Transactions on Power Systems*, vol. 3, no. 4, pp. 1591–1599, 1988.

[132] P. Addison, "The illustrated wavelet transform handbook: Introductory theory and applications in science, engineering," *Medicine and Finance. Taylor & Francis*, 2002.

[133] M. K. Saini and R. K. Beniwal, "Optimum fractionally delayed wavelet design for PQ event detection and classification," *International Transactions on Electrical Energy Systems*, vol. 27, no. 10, 2017.

[134] R. Escudero, J. Noel, J. Elizondo, and J. Kirtley, "Microgrid fault detection based on wavelet transformation and Park's vector approach," *Electric Power Systems Research*, vol. 152, pp. 401–410, 2017.

[135] Z. Moravej, S. H. Mortazavi, and S. M. Shahrtash, "DT-CWT based event feature extraction for high impedance faults detection in distribution system," *International Transactions on Electrical Energy Systems*, vol. 25, no. 12, pp. 3288–3303, 2015.

[136] W. L. Woon, Z. Aung, and S. Madnick, *Data Analytics for Renewable Energy Integration: Third ECML PKDD Workshop, DARE 2015, Porto, Portugal*. Springer, 2015, vol. 9518.

[137] E. Compatibility, "Part 4: 30: Testing and measurement techniques–power quality measurement methods," *IEC 61000-4-30 Std. Tech. Rep.*, 2003.

[138] P. Kundur, N. J. Balu, and M. G. Lauby, *Power system stability and control*. McGraw-hill New York, 1994, vol. 7.

[139] X. Zhang, J. Wang, and K. Zhang, "Short-term electric load forecasting based on singular spectrum analysis and support vector machine optimized by cuckoo search algorithm," *Electric Power Systems Research*, vol. 146, pp. 270–285, 2017.

[140] S. Naderian and A. Salemnia, "An implementation of type-2 fuzzy kernel based support vector machine algorithm for power quality events classification," *International Transactions on Electrical Energy Systems*, vol. 27, no. 5, 2017.

[141] Y. Bennani and K. Benabdeslem, "Dendogram-based SVM for multi-class classification," *CIT. Journal of computing and information technology*, vol. 14, no. 4, pp. 283–289, 2006.

[142] F. Milano, "PSAT, MATLAB-based Power System Analysis Toolbox," 2002.

[143] "MATLAB Release 2010, The Mathworks Inc., Natick, Massachusetts, United States."

[144] M. Brown, M. Biswal, S. Brahma, S. J. Ranade, and H. Cao, "Characterizing and quantifying noise in PMU data," in *2016 Power and Energy Society General Meeting (PESGM)*. IEEE, 2016, pp. 1–5.

[145] N. Jankowski, W. Duch, and K. Grabczewski, *Meta-learning in computational intelligence*. Springer Science & Business Media, 2011, vol. 358.

[146] A. Grinsted, J. C. Moore, and S. Jevrejeva, "Application of the cross wavelet transform and wavelet coherence to geophysical time series," *Nonlinear processes in geophysics*, vol. 11, no. 5/6, pp. 561–566, 2004.

[147] N. Senroy, "Generator coherency using the Hilbert-Huang transform," *IEEE Transactions on Power Systems*, vol. 23, no. 4, pp. 1701–1708, 2008.

[148] M. Jonsson, M. Begovic, and J. Daalder, "A new method suitable for real-time generator coherency determination," *IEEE Transactions on Power Systems*, vol. 19, no. 3, pp. 1473–1482, 2004.

[149] A. K. Jain, "Data clustering: 50 years beyond k-means," *Pattern recognition letters*, vol. 31, no. 8, pp. 651–666, 2010.

[150] J. H. Chow, *Power system coherency and model reduction*. Springer, 2013.

[151] M. Haque and A. Rahim, "An efficient method of identifying coherent generators using Taylor series expansion," *IEEE transactions on power systems*, vol. 3, no. 3, pp. 1112–1118, 1988.

[152] S. A. Siddiqui, K. Verma, K. R. Niazi, and M. Fozdar, "A unified control scheme for power system transient stability enhancement through preventive and emergency control," *International Transactions on Electrical Energy Systems*, vol. 26, no. 2, pp. 365–383, 2016.

[153] A. K. Singh and M. Fozdar, "A wavelet-based event detection and location framework for enhanced situational awareness in power system," in *India Conference (INDICON), 2016 IEEE Annual*. IEEE, 2016, pp. 1–6.

[154] B. Khodabakhchian and G.-T. Vuong, "Modeling a mixed residential-commercial load for simulations involving large disturbances," *IEEE Transactions on Power Systems*, vol. 12, no. 2, pp. 791–796, 1997.

[155] M. Kamel, A. A. Karrar, and A. H. Eltom, "Development and application of a new voltage stability index for on-line monitoring and shedding," *IEEE Transactions on Power Systems*, vol. 33, no. 2, pp. 1231–1241, 2018.

Publications

Following papers have been published/accepted or are in communication out of this thesis work:

International Journals

1. A. K. Singh and M. Fozdar, "Real-time Automated Event Analysis and Supervisory Framework for Power Systems using Synchrophasor Measurements," *Electric Power Components & Systems, Taylor & Francis*, DOI: 10.1080/15325008.2019.1628122 (Accepted, Article in press)
2. A. K. Singh and M. Fozdar, "Power System Enhanced Monitoring through Strategic PMU Placement Considering Degree of Criticality of Buses," *Journal of Electrical Engineering & Technology*, 13(5) (2018), pp.1769-1777, DOI: 10.5370/JEET.2018.13.5.1769
3. A. K. Singh and M. Fozdar, "DBSCAN-based coherency identification of generators using complex wavelet transform," *IET The Journal of Engineering*, DOI: 10.1049/joe.2018.9239
4. A. K. Singh and M. Fozdar, "Event-driven frequency and voltage stability predictive assessment and unified load shedding," *IET Generation, Transmission, & Distribution*, (Provisionally accepted)

International Conferences

1. A. K. Singh and M. Fozdar, "Supervisory framework for event detection and classification using wavelet transform," Proc. *2017 IEEE Power & Energy Society General Meeting (PESGM2017)*, Chicago, IL USA, pp. 1-5. DOI: 10.1109/PESGM.2017.8274283.
2. A. K. Singh and M. Fozdar, "A wavelet-based event detection and location framework for enhanced situational awareness in power system," Proc. *2016 IEEE Annual India Conference (INDICON)*, Bangalore, India, pp. 1-6. DOI: 10.1109/INDICON.2016.7839085

Brief bio-data

Ajeet Kumar Singh received his B. Tech. in Electrical and Electronics Engineering from GBTU, Lucknow in 2010 and M. Tech. in Control System from National Institute of Technology Kurukshetra in 2012. Currently, he is a doctoral candidate in the Department of Electrical Engineering, Malaviya National Institute of Technology Jaipur. His areas of research interest are power system stability and machine learning applications.